

**INVESTIGATION OF YOUNG NEUTRON  
STAR POPULATIONS WITH FALLBACK  
DISK MODEL**

by

**Onur Benli**

Submitted to the Graduate School of Engineering and Natural Sciences

in partial fulfillment of

the requirements for the degree of

Doctor of Philosophy

Sabanci University

Spring 2016

INVESTIGATION OF YOUNG NEUTRON STAR POPULATIONS  
WITH FALLBACK DISK MODEL

APPROVED BY

Assoc. Prof. Dr. Ünal Ertan  
(Thesis Supervisor)



Prof. Dr. Mehmet Ali Alpar



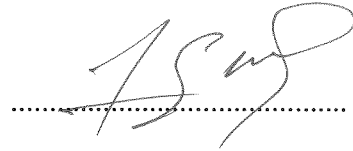
Prof. Dr. Kazım Yavuz Ekşi



Asst. Prof. Dr. Murat Kaya



Assoc. Prof. Dr. Hakan Erkut



DATE OF APPROVAL

24.06.2016



© Onur Benli 2016

All Rights Reserved

# INVESTIGATION OF YOUNG NEUTRON STAR POPULATIONS WITH FALLBACK DISK MODEL

Onur Benli

Physics, Doctor of Philosophy Thesis, 2016

Thesis Supervisor: Assoc. Prof. Dr. Ünal Ertan

## Abstract

Young isolated neutron stars manifest themselves as members of different populations, namely anomalous X-ray pulsars (AXPs), soft gamma repeaters (SGRs), dim isolated neutron stars (XDINs), rotating radio transients (RRATs), central compact objects (CCOs) and the so-called “high-magnetic-field” radio pulsars (HBRPs). In this thesis, we have investigated the long-term evolution, short-term X-ray enhancement/outburst, optical and infra-red disk emission properties and the radio properties of members of different young neutron star populations in the frame of the fallback disk model. (i) We have first investigated the X-ray enhancement and the long-term evolution of the recently discovered second “low-B magnetar” Swift J1822.3–1606. The model could produce the observed long-term source properties ( $P$ ,  $\dot{P}$ ,  $L_x$ ) simultaneously. During a soft gamma burst episode, the inner disk matter is pushed back to larger radii, forming a density gradient at the inner disk. Subsequent relaxation of the inner disk could account for the observed X-ray enhancement light curve of Swift J1822.3–1606. (ii) We have analysed the long-term evolution and the X-ray outburst light curve of a typical AXP/SGR source, SGR 0501+4516, with the similar technique applied to Swift J1822.3–1606. We have further shown that the optical/infrared data of SGR 0501+4516 are in good agreement with the emission from an irradiated fallback disk. In two separate works, we have applied the fallback disk model to (iii) six XDIN and (iv) twelve AXP/SGR sources with relatively well constrained X-ray luminosity and rotational properties. We have found that the individual source properties ( $P$ ,  $\dot{P}$ ,  $L_x$ ) of AXP/SGRs and XDINs could be obtained with similar basic disk parameters. Our results showed that the XDINs have gone through an accretion epoch in the past, while most of the AXP/SGRs are evolving in the accretion phase at present.

# GENÇ NÖTRON YILDIZI SINIFLARININ YIĞILMA DİSKLERİ İLE İNCELENMESİ

Onur Benli

Fizik, Doktora Tezi, 2016

Tez Danışmanı: Doç. Dr. Ünal Ertan

## Özet

İzole genç nötron yıldızları farklı popülasyonlar halinde karşımıza çıkarlar. Bunlar, anormal X-ışını kaynakları (AXPs), gama ışını tekrarlayıcıları (SGRs), sönük izole kaynaklar (XDINs), merkezi yoğun cisimler (CCOs), geçici dönen radyo kaynakları (RRATs) ve “yüksek manyetik alanlı” radyo pulsarları (HBRPs) olarak adlandırılmıştır. Bu tezde, farklı genç nötron yıldızı sınıflarının, uzun süreli evrimlerini, kısa süreli X-ışını parlamalarını, optik ve kızılötesi disk ışınması özelliklerini ve radyo özelliklerini kalıntı disk modeli ile inceledik. (i) İlk olarak, yakın zamanda keşfedilen “düşük manyetik alanlı magnetar” Swift J1822.3–1606’nın uzun süreli evrimini ve kısa süreli X-ışını parlaması ışık eğrisini inceledik. Kullandığımız model, kaynağın uzun-dönem gözlemsel özelliklerini ( $P$ ,  $\dot{P}$ ,  $L_x$ ) eş zamanlı olarak üretebilmektedir. Gama ışını parlaması sırasında, iç diskteki maddenin dışarıya doğru itilmiş olduğunu ve iç diskte bir yüzey yoğunluk gradyeninin oluştuğunu varsaymaktayız. İç diskte birikmiş bu maddenin, nötron yıldızının yüzeyine doğru akmasının gözlenen X-ışını parlama verilerini açıklayabildiğini gösterdik. (ii) Bu kaynağın incelenmesi sırasında kullanılan tekniklerin benzerini, daha sonra, tipik bir AXP/SGR kaynağı olan SGR 0501+4516’nın uzun süreli evrimini ve kısa süreli X-ışını parlamasını açıklamak için kullandık ve gözlemler ile örtüşen sonuçlar elde ettik. Ayrıca, kaynağın optik/kızılötesi verilerinin, ısıtılmalı bir diskten yayılan ışınma profili ile uyum içinde olduğunu gösterdik. İki ayrı çalışmada, (iii) altı tane XDIN kaynağını ve (iv) X-ışını ışınma gücü ve dönme özellikleri iyi ölçülebilmemiş on iki tane AXP/SGR kaynağını kalıntı disk modeli ile inceledik. AXP/SGR ve XDIN’lerin özelliklerinin ( $P$ ,  $\dot{P}$ ,  $L_x$ ), benzer temel disk parametreleri kullanılarak, kaynak bazında açıklanabildiğini gösterdik. Elde ettiğimiz sonuçlara göre XDIN’lerin hepsi daha önce kütle aktarım fazından geçmiş olup, şu an son pervane evresindedirler. AXP/SGR’lerin büyük bir kısmı ise halen kütle aktarım fazında bulunmaktadır.

## ACKNOWLEDGEMENTS

Firstly, I would like to express my sincere gratitude to my gracious advisor Assoc. Prof. Ünal Ertan for the continuous support of my doctoral study, for his patience and motivation. His guidance helped me in all the time of research and writing of this thesis. Besides my advisor, I would like to thank my thesis committee, K. Yavuz Ekşi, M. Hakan Erkut, Murat Kaya and especially M. Ali Alpar for their insightful comments and questions which encouraged me to improve my research. I acknowledge support from the Scientific and Technological Research Council of Turkey (TUBİTAK) through grants 110T243 and 113F166. I am deeply thankful to each family members for their permanent support and trust. I should also thank my friends and colleagues whose existence rendered the life in SU Campus bearable for me. Finally, I thank the special woman, Bilgen, who entered my life and became my wife. She always there for me in good times and bad days.

# Contents

<b>ABSTRACT</b>	<b>iii</b>
<b>ÖZET</b>	<b>iv</b>
<b>ACKNOWLEDGEMENTS</b>	<b>v</b>
<b>LIST OF ABBREVIATIONS</b>	<b>xv</b>
<b>1 INTRODUCTION</b>	<b>1</b>
1.1 X-ray Enhancement and Long-term Evolution of SWIFT J1822.3–1606 . . . . .	16
1.2 Long-term Evolution, X-ray Outburst and Optical/IR emission of SGR 0501+4516 . . . . .	16
1.3 Long-term Evolution of Dim Isolated Neutron Stars . . . . .	17
1.4 Long-term Evolution of Anomalous X-ray Pulsars and Soft Gamma Re- peaters . . . . .	18
<b>2 X-RAY ENHANCEMENT AND LONG-TERM EVOLUTION OF SWIFT J1822.3–1606</b>	<b>19</b>
2.1 Introduction . . . . .	20
2.2 Long-term Evolution of Swift J1822.3-1606 . . . . .	21
2.3 X-ray Enhancement of Swift J1822.3-1606 . . . . .	27
2.4 Discussion and Conclusion . . . . .	30
<b>3 LONG-TERM EVOLUTION, X-RAY OUTBURST AND OPTICAL/IR EMISSION OF SGR 0501+4516</b>	<b>33</b>
3.1 Introduction . . . . .	34
3.2 Long-Term Evolution of SGR 0501+4516 . . . . .	34
3.3 X-ray Outburst of SGR 0501+4516 . . . . .	37
3.4 CONCLUSIONS . . . . .	43

---

<b>4</b>	<b>LONG-TERM EVOLUTION OF DIM ISOLATED NEUTRON STARS</b>	<b>44</b>
4.1	Introduction . . . . .	45
4.2	Model . . . . .	47
4.3	Results . . . . .	50
4.4	Discussion and Conclusion . . . . .	59
<b>5</b>	<b>LONG-TERM EVOLUTION OF ANOMALOUS X-RAY PULSARS AND SOFT GAMMA REPEATERS</b>	<b>62</b>
5.1	Introduction . . . . .	63
5.2	Description of the model . . . . .	63
5.2.1	Long-term Evolutionary Phases of a Neutron Star with a Fallback disc . . . . .	67
5.3	Source Properties . . . . .	69
5.4	Results . . . . .	78
5.5	Discussion and Conclusions . . . . .	79
<b>6</b>	<b>SUMMARY AND CONCLUSION</b>	<b>82</b>
	<b>BIBLIOGRAPHY</b>	<b>94</b>

## List of Figures

- 1.1 Period–period derivative diagram ( $P - \dot{P}$  diagram) of isolated neutron stars. Radio pulsars are indicated by dots. The pulsars that are clustered at the bottom-left are millisecond pulsars. Each distinct population is represented by different shaped and coloured points described on the top-left of the figure. The two parallel lines show the upper and lower bounds of the radio pulsar death valley from Chen & Ruderman (1993). The data were taken from ATNF pulsar catalogue (1) and McGill Magnetar catalogue (2). (1) <http://www.atnf.csiro.au/people/pulsar/psrcat/> (2) <http://www.physics.mcgill.ca/pulsar/magnetar/main.html> . . . . . 6
- 1.2 A sample model curve that shows three basic evolutionary episodes of a neutron star-fallback disk system. For this illustrative model,  $B_0 = 2 \times 10^{12}$  G,  $M_d = 5.7 \times 10^{-4} M_\odot$ ,  $P_0 = 75$  ms and  $T_p = 150$  K. Durations of initial propeller phase (blue region), accretion phase (white region) and final propeller phases (green region) depend on the initial conditions. To reach the long periods of several seconds, a source should pass through the accretion phase. The initial propeller phase, which could be experienced by a fraction of the sources, has not a significant effect on the properties achieved in the accretion and final propeller phases (see the text for details). . . . . 14

- 2.1 Long-term luminosity, period and period derivative evolution of the model sources. The values of  $M_d$  and  $B_0$  employed in the models are given in the middle panel in units  $10^{-6} M_\odot$  and  $10^{12}$  G respectively. Horizontal lines in the top panel show the observational error bars of  $L$  (Scholz et al., 2012). For these models,  $C = 1 \times 10^{-4}$  except for the dashed (black) line which has  $C = 7 \times 10^{-4}$  and represents the evolution with minimum  $B_0$ . In the bottom panel, horizontal lines show the range of  $\dot{P}$  for Swift J1822.3–1606 adopted in the present work. The model sources with  $B_0$  values 0.58 and  $1.00 \times 10^{12}$  G could represent the evolution of Swift J1822.3–1606 if the source is not in the accretion phase in quiescence. The points A and B seen in the bottom panel are for a discussion of possibilities for the source properties in quiescence (see the text for explanation). . . . . 22
- 2.2 Evolution of an illustrative model source which could acquire the properties of Swift J1822.3–1606 simultaneously if the source is in the long-term accretion phase at present in the quiescent state. The values of  $M_d$  and  $B_0$  are given in the figure in units of  $10^{-6} M_\odot$  and  $10^{12}$  G respectively. For these models we take  $C = 3 \times 10^{-4}$ . . . . . 23
- 2.3 X-ray enhancement data of Swift J1822.3–1606. The data is taken from Rea et al. (2012) and . The luminosity is given on the right axis, assuming a distance of 1.6 kpc. Values of the parameters  $T_{\text{crit}}$  and  $C$  are given in the figure. For both models  $\alpha_{\text{hot}} = 0.1$ ,  $\alpha_{\text{cold}} = 0.045$  and  $B_0 = 1 \times 10^{12}$  G. The abrupt decrease seen in the model curves are produced when the innermost disk enters the cold viscosity state (see the text for explanation). The accretion luminosity (dot-dashed line) and the level of cooling luminosity taken in the models (horizontal line) are also given separately in the figure. . . . . 28

- 3.1 Illustrative model curves that can represent the long-term evolution of SGR 0501+4516. The model sources are still accreting at present. The dipole field strength  $B_0 \simeq 1.4 \times 10^{12}$  G for both models. The disc masses in solar mass and the values of the irradiation parameter  $C$  are given in the bottom panel. Horizontal dotted lines show the properties of SGR 0501+4516. The lower and upper limits in the luminosity correspond to distances of  $\sim 1.5$  and 5 kpc. . . . . 36
- 3.2 Model curves with the same parameters as those of the dashed curve in Fig. 3.1, but with different initial periods ( $P_0$ ) given in the bottom panel. It is seen that the model results are not sensitive to  $P_0$  if  $P_0 \gtrsim 60$  ms. For lower values of  $P_0$ , the sources cannot enter the light cylinder and are likely to evolve as radio pulsars that cannot reach the properties of SGR 0501+4516. . . . . 38
- 3.3 Optical/IR emission of SGR 0501+4516. The blue boxes show the model predictions of an irradiated fallback disc in four different energy bands.  $\dot{M}_{\text{in}} = 1.4 \times 10^{14}$  g s $^{-1}$ , disc inclination angle is  $\sim 70^\circ$  and irradiation efficiency  $C = 10^{-4}$ . For the bands  $g'$  and  $u'$  the data show  $3\sigma$  upper limits. . . . . 39
- 3.4 X-ray outburst decay lightcurve of SGR 0501+4516. The unabsorbed 0.5–10 keV flux data points are from XMM-Newton observations. The first five data points are taken from Rea et al. (2009) and the sixth data point is taken from Camero et al. (2014). The X-ray luminosity is calculated assuming a distance of 5 kpc. The horizontal error bar of the first data point denotes the time interval of observation. . . . . 41
- 3.5 The same as Fig. 3.4, but for a source distance of 1.5 kpc. This model curve is obtained with the irradiation efficiency  $C = 7 \times 10^{-4}$ . Smaller irradiation efficiencies do not give reasonable fits for this particular distance. 42
- 4.1 Total luminosity, period and period derivative evolution of the model sources with different magnetic dipole fields. For all model sources  $M_{\text{d}} = 3 \times 10^{-6} M_{\odot}$ . The magnitudes of the magnetic dipole field on the pole of the star,  $B_0$ , are given in units of  $10^{12}$  G in the top panel (see the text for a discussion). . . . . 53

- 4.2 The luminosity, period and period derivative evolution of the model sources with different initial disk masses. The magnetic dipole field is the same ( $B_0 = 1.2 \times 10^{12}$  G) for all sources. The disk masses are given in units of  $10^{-6}M_\odot$  in the top panel. . . . . 54
- 4.3 The model curves that can simultaneously produce the luminosity, period and period derivative of the six XDINs. For each source, we determined the ranges of  $M_d$  and  $B_0$  that can produce the source properties (see Table 4.1). Here, we show illustrative model curves that can represent the long-term evolution of these XDINs. The values of  $B_0$  and  $M_d$  used in the models are given in the top panel in units of  $10^{12}$  G and  $10^{-6}M_\odot$  respectively. . . . . 57
- 4.4 Magnetic dipole field strength on the pole of the neutron star versus period distribution for six XDINs. The two parallel lines (green and blue) show the upper and lower bounds of the radio pulsar death valley from Chen & Ruderman (1993). Crosses are the  $B_0$  values inferred from the dipole torque formula. Vertical bars show the ranges of  $B_0$  that can produce the properties of the sources in the fallback disk model (see Figure 4.3). It is seen that all these sources remain below the lower boundary of the death valley (death line) indicating that these XDINs cannot be normal radio pulsars, if they are evolving with fallback disks. . . . . 58
- 5.1 A sample model curve that shows three basic evolutionary episodes of a neutron star-fallback disk system. For this illustrative model,  $B_0 = 2 \times 10^{12}$  G,  $M_d = 5.7 \times 10^{-4} M_\odot$ ,  $P_0 = 75$  ms and  $T_p = 150$  K. Durations of initial propeller phase (blue region), accretion phase (white region) and final propeller phases (green region) depend on the initial conditions. To reach the long periods of several seconds, a source should pass through the accretion phase. The initial propeller phase, which could be experienced by a fraction of the sources, has not a significant effect on the properties achieved in the accretion and final propeller phases (see the text for details). . . . . 68

- 5.2 The long-term evolutionary model curves of six AXP/SGRs. For all these AXP/SGRs, both  $M_d$  and  $B_0$  are constrained to very narrow ranges with central values given in the middle panel. The names of the sources are shown in the top panel. For these models,  $T_p = 100$  K and  $C = 1 \times 10^{-4}$ .  $B_0$  and  $M_d$  values are given in units of  $10^{12}$  G and  $10^{-6} M_\odot$ . For these sources accretion goes on till  $t \sim 5 \times 10^5$  yr. But, the accretion luminosity remain below the cooling luminosity at  $t \sim$  a few  $10^4$  yr. . . . . 72
- 5.3 The illustrative model curves representing the long-term evolutions of the four AXP/SGRs which have uncertainties in either  $L_x$  or  $\dot{P}$  measurements. The error bars show the uncertainties in measurements. For these sources, unlike the six sources given in Fig. 5.2, our model cannot well constrain the  $M_d$  and  $B_0$  values.  $B_0$  and  $M_d$  values are given in units of  $10^{12}$  G and  $10^{-6} M_\odot$ . The model parameters are given in Table 5.1. The constant  $\dot{P}$  epochs correspond to accretion phases. 1E 1547.0–5408 and XTE J1810–197 enter the accretion phase at times  $\sim 3 \times 10^2$  and  $5 \times 10^3$  yr respectively. . . . . 73
- 5.4 Illustrative model curves that could represent the long-term evolution of 4U 0142+61. Reasonable model fits could be obtained with a large range of disk mass, a narrow  $B_0$  range around  $2.6 \times 10^{12}$  G, and  $T_p \sim 50 - 60$  K. These models are obtained with  $T_p = 54$  K and  $M_d$  values (in units of  $10^{-6} M_\odot$ ) shown in the top panel. The model sources can acquire the source properties at the ages in the range limited by the vertical dashed lines shown in the figure ( $\sim 3 \times 10^4 - 2 \times 10^5$  y). The horizontal dashed lines show the observed properties of the source. For these model curves, accretion remains as the dominant source of luminosity. . . . . 75
- 5.5 The same as Fig. 7, but for 1E 2259+586. For all these model curves,  $B_0 = 1.2 \times 10^{12}$  G,  $T_p = 30$  K and  $C = 1 \times 10^{-4}$ .  $M_d$  values are given in units of  $10^{-6} M_\odot$ . Reasonable model fits for this source could be obtained with  $T_p \sim 30-40$  K at the ages  $t \sim 1-4 \times 10^5$  yr (between the dashed vertical lines). These model sources, like those in Fig 5.4, remain in the accretion phase their births to the present ages. . . . . 76

- 
- 5.6 The  $B_0$  versus  $M_d$  distribution of some AXP/SGRs (present work) and the six XDINs (from Ertan et al. 2014). The error bars represent the  $B_0$  and  $M_d$  ranges for which the model sources acquire the observed source properties  $P$ ,  $\dot{P}$  and  $L_x$  simultaneously. . . . . 81

## List of Tables

3.1	The parameters for the models presented in Fig. 3.4 and 3.5. The basic disc parameters $\alpha_{\text{hot}} = 0.1$ , $\alpha_{\text{cold}} = 0.045$ , $T_{\text{crit}} = 1750$ K are the same for the model curves given in Figs. 3.4 and 3.5. The irradiation efficiency $C = 7 \times 10^{-4}$ for $d = 1.5$ kpc and $C = 3-7 \times 10^{-4}$ for $d = 5$ kpc give good fits to data. See Çalışkan & Ertan (2012) for a detailed explanation of the model parameters. . . . .	42
4.1	The ages and the disk parameters for the six XDINs. The ages are constrained by the theoretical cooling luminosity (Page, 2009) and the estimated bolometric X-ray luminosities. . . . .	55
5.1	The initial disk mass ( $M_{\text{d}}$ ), dipole magnetic field strength at the pole of the star ( $B_0$ ), minimum active disk temperature ( $T_{\text{p}}$ ) and the current age of the sources found from the models with the evolutionary curves given in Fig 4., and the observed properties $L_{\text{x}}$ , $P$ and $\dot{P}$ of the sources. We take the irradiation parameter $C = 10^{-4}$ and the viscosity parameter $\alpha = 0.045$ for all of the sources. . . . .	77
5.2	Observed properties of the six XDINs (see Ertan et al. 2014 and references therein for details). . . . .	77
5.3	The disk parameters and the corresponding ages for the six XDINs. The viscosity parameter $\alpha = 0.045$ for all the model sources. (Taken from Ertan et al. 2014). . . . .	77

## LIST OF ABBREVIATIONS

AXP	Anomalous X-ray Pulsars
SGR	Soft Gamma Repeater
XDIN	Dim Isolated Neutron Star
HBRP	High Magnetic Field Radio Pulsar
CCO	Central Compact Object
RRAT	Rotation Radio Transient
GRB	Gamma-ray Burst
IR	Infrared
LMXB	Low Mass X-ray Binary
HMXB	High Mass X-ray Binary

# Chapter 1

## INTRODUCTION

Soon after the discovery of neutron by James Chadwick in 1932, Sterne (1933) proposed that at the very high densities it is favourable for electrons and protons to combine with each other and form neutrons. This process is called inverse  $\beta$ -decay. Sterne estimated from quantitative statistical calculations that the matter would be extremely neutron-rich above a mass density  $\rho \sim 2.3 \times 10^{10} \text{ g cm}^{-3}$  which is close to the currently accepted critical density obtained from detailed calculations. The relation of neutron physics to the astrophysical objects was noticed by George Gamow in 1936. He suggested that a neutron core could be formed at the center of massive stars after the nuclear fuel is consumed. The calculation of the structure of a neutron star was first performed by Oppenheimer and Volkoff in 1939. In their influential work, they used the EoS for free neutron gas. Their hydrostatic equilibrium included the general relativistic effects (Ghosh, 2007).

Since the first observation of a radio pulsar by Jocelyn Bell and Anthony Hewish in 1967, the nature of such stable and periodic pulses has been argued for more than a decade. Observed period derivative range and very small periods ( $P = 0.033 \text{ s}$  for the Crab pulsar) of radio pulsars showed without doubt that these sources are neutron stars which are the only objects that can have such short and stable rotation periods. The first X-ray pulsar, namely Sco X-1, was clearly detected in 1962 even before the discovery of the first radio pulsar. The importance of this observation had not been understood until the discoveries of binary X-ray pulsars in 1970s. The potential significance of the mass accretion process in binary star system was emphasized by Zel'dovich & Novikov (1965); Zeldovich & Guseynov (1966), stating that it might be possible to observe accreting neutron stars and black holes in these systems. They also remarked that the electromagnetic energy release of particles in accretion process is much more efficient than in nuclear fusion reactions. In those days, the optical counterparts to the X-ray pulsars were

also detected, providing evidence for the binary nature of these systems. In 1967, Iosif Shklovskii proposed that the source of X-ray pulsations observed from Sco X-1 could be due to stream of gas coming from the companion star and flowing continuously onto the neutron star.

How is the energy of matter being accreted onto the surface of the neutron star converted into electromagnetic radiation? Basically, the bulk kinetic energy of the falling material is converted into thermal energy via various dissipative process, and as a first approximation, emitted from the surface as blackbody emission. Magnetic dipole field of a neutron star can channel the accreting plasma towards the magnetic poles, creating two hot-spot regions (Davidson & Ostriker 1973, Lamb, Pethick & Pines 1973). Since, for most sources, magnetic and rotation axes of the star are not aligned, these small and hot regions can produce pulsed thermal X-ray emission due to the spin of the star. For typical accretion rates in neutron star binary systems, the accretion produces blackbody emission from the neutron star surface with effective temperatures in the soft X-rays ( $< 10$  keV). In addition to this soft X-ray emission, there could be other radiative process due to, for instance, the inverse Compton scattering of the seed black body photons by the hot plasma around the neutron star or by the bulk kinetic energy of the matter flowing in the accretion column.

The long-wavelength radio emission of stellar sources can pass through the Earth's atmosphere and can be observed with ground based telescopes. In contrast to radio waves, X-rays cannot penetrate the Earth's atmosphere. For instance, 3 keV photons from the space can only be observed at 80 km altitude. Because of these absorption effects, the observations of X-ray sources become possible only after the use of rockets. The existence of bright cosmic X-ray sources, discovered by rocket flights in 1960, revealed one of the most exciting and challenging problems in astrophysics. What was the physical process that can generate such high X-ray luminosities? The subsequent identification of the X-ray sources Sco X-1 and Cyg X-2, in the optical wavelengths encouraged theoretical astrophysicists to study the physical properties of these newly discovered X-ray sources. A few months after the launch of *UHURU* satellite, two more X-ray sources, Her X-1 and Cen X-3, pulsating regularly with extremely precise periods, were discovered. When these sources were observed during much longer time intervals, it was recognized that both X-ray sources showed eclipses indicating that they are in close binary systems with

orbital periods of  $\sim 1.7$  and  $\sim 2.1$  days, respectively.

Most of the luminous binary X-ray sources host either a black hole or neutron star accreting matter from a normal companion star. If the mass of this companion is higher than  $10 M_{\odot}$ , the system is called high-mass X-ray binary (HMXB). These massive donors can be O or B type young stars. If the mass of the companion is a few solar mass, the system is classified as a low-mass X-ray binary (LMXB). An LMXB contains an old companion star with a spectral type later than B. The mass accretion onto the compact object in LMXBs and HMXBs occur through rather different processes. In LMXBs, a low mass donor star transfers mass through the inner Lagrange point (Lewin, van Paradijs & van den Heuvel, 1995). Due to significant angular momentum of the mass transferred from the inner Lagrangian point, an accretion disk is formed around the compact object. The material in the disk loses its angular momentum due viscous process and flows inward towards the compact object. In HMXBs, the donor star loses its mass mostly through stellar wind (van den Heuvel & Heise, 1972). The compact object continuously captures a fraction of the mass-flow provided by the stellar wind of the companion (Bondi & Hoyle, 1944). For some close HMXB systems, mass-loss from the companion due to Roche lobe overflow, forming a disk could also be possible. In this case, luminous X-rays can be observed from these systems (Bachetti et al., 2014).

Since the first discovery, more than 2500 radio pulsars were discovered. Over the last  $\sim 20$  years, new young and single neutron star populations have been discovered. Many radio pulsars were also observed to emit pulsed radiation from UV to gamma rays (see e.g. Abdo et al. 2013; Pavlov et al. 2001 and references therein). These systems of young isolated neutron stars are anomalous X-ray pulsars (AXPs), soft gamma repeaters (SGRs), dim isolated neutron stars (XDINs, also called “the magnificent seven”), central compact objects (CCOs) in supernova remnants, rotating radio transients (RRATs) and the so-called “high magnetic field” radio pulsars (HBRPs). All these sources are thought to be single star systems due to lack of evidence for companions and different from the standard radio pulsars as well. Each group has different characteristic emission and rotational properties. The evolutionary processes leading to this diversity have not been understood clearly yet. What are the physical conditions causing these systems to emerge as distinct young isolated neutron star populations? All these systems involve a single, young or middle-aged neutron star. Despite their distinguishing properties, like energetic

soft gamma bursts peculiar to AXPs and SGRs, there are also striking similarities, like the periods of AXP/SGRs and XDINs clustering in the same range (2-12 s). Considering the estimated birth rates of these objects together with the galactic supernova rate, it is likely that there are evolutionary connections between some of these populations (Keane & Kramer, 2008). The reason for these single neutron stars to evolve into different classes is likely to be the differences in their initial conditions, while some of these sources could be evolving in different phases of similar evolutionary tracks.

The currently known AXPs and SGRs represent a small fraction of the observed pulsars, however they are the most attractive groups from both theoretical and observational point of view due to their extraordinary properties. The classification of AXPs and SGRs as two different classes has historical reasons. SGRs were first identified with short, energetic soft gamma bursts (Mazets, Golenetskij & Guryan, 1979) and initially considered as a subgroup of  $\gamma$ -ray bursts (GRBs) but with a softer spectra (Norris et al., 1991). Three giant bursts ( $\gtrsim 10^{44}$  erg s $^{-1}$ ) were observed from three different SGRs. Apart from these bursts, other rotational and persistent X-ray properties of SGRs were very similar to those of AXPs which were discovered as X-ray pulsars in the soft X-ray spectrum ( $< 10$  keV) with high luminosities of  $\sim 10^{34} - 10^{36}$  erg s $^{-1}$  similar to SGR luminosities. These X-ray luminosities are much higher than the rotational powers of these sources, which led to the identification of these systems as ‘anomalous X-ray pulsars’ (see Mereghetti & Stella 1995). Later, AXPs were also observed to exhibit soft gamma bursts similar to SGR bursts (Kaspi et al., 2003). At present, considering the similarities in other properties, AXP and SGRs are commonly accepted as member of the same class of objects. Currently, there are 23 confirmed and several candidate AXP/SGR sources (as described in the catalogue <http://www.physics.mcgill.ca/pulsar/magnetar/main.html>). The physical nature of AXP/SGRs has been widely discussed and many theoretical models were proposed to explain their interesting behaviour. Below, we summarize the observed properties of these sources.

All AXP/SGRs show soft X-ray pulsations. Some sources also show pulsed hard X-ray emission (up to a few hundred keV), with luminosities comparable to those in the soft X-ray band (Kuiper, Hermsen & Mendez, 2004; den Hartog et al., 2006; Kuiper et al., 2006). The variations in the pulsed emission are phase-dependent. Their persistent luminosities are  $\sim 10^{33} - 10^{36}$  erg s $^{-1}$  and the rotational powers,  $\dot{E} = -I\Omega\dot{\Omega}$ , are much

lower than the observed X-ray luminosities for most sources. Here  $I$  and  $\Omega$  are moment of inertia and angular velocity of the neutron star,  $\dot{\Omega}$  is the angular velocity derivative. There are also transient AXP/SGRs with quiescent luminosities of  $10^{33} - 10^{34} \text{ erg s}^{-1}$ , or less. The transient sources show X-ray enhancements/outbursts after the soft gamma burst episodes starting with 1–2 orders of magnitude abrupt increase in the X-ray luminosities followed by a slow decay to the quiescent level on time-scales of months to years.

One of the most remarkable general properties of AXP/SGRs is the period clustering. Their periods are between 2 – 12 s range, and period derivatives,  $\dot{P} \sim 10^{-13} - 10^{-10} \text{ s s}^{-1}$  (Olausen & Kaspi, 2014), are relatively high in comparison with those of single pulsar populations. We should note here that the periods of XDINs which are likely to be older than AXP/SGRs, lie in the same narrow period range. The characteristic ages of AXP/SGRs,  $\tau = P/2\dot{P}$ , vary from a few 100 yr to more than  $10^7$  yr. The relatively long periods and high period derivatives of AXP/SGRs, place them on the upper right region of the  $P - \dot{P}$  diagram (see Fig. 1). Most of AXP/SGRs have not been detected in the radio band. Four sources that show pulsed radio emission have quite different radio properties from those of normal radio pulsars (Mereghetti 2013 and references therein).

If a neutron star evolves in vacuum its rotation frequency decreases by magnetic dipole torques. The magnitude of the dipole torque  $\Gamma_B \approx \mu^2 \sin^2(\alpha)\Omega^4/6c^3$  where  $\mu$  is the magnetic moment at the poles of the star,  $\alpha$  is the angle between magnetic and rotation axes and  $c$  is the speed of light. From the equation of motion,  $\Gamma_B = -I\dot{\Omega}$ , the strength of the dipole field at the equator of the neutron star is estimated from the observed period and period derivative of the source using  $B \simeq 3.2 \times 10^{19} \sqrt{P\dot{P}} \text{ G}$  and the field strength on the poles  $B_0 = 2B$ .

It is rather likely that part of the matter from the SN explosion could be re-collected around the neutron star (Colgate, 1971; Chevalier, 1989). Due to the conservation of angular momentum, this fossil matter can flow into as a disk (Michel & Dessler, 1981). Such a fallback disk can provide a continuous mass flow towards the star affecting both rotational and electromagnetic emission properties of the star. When there is a viscously active fallback disk around the neutron star, the disk torques are likely to dominate magnetic dipole torques while the accretion luminosity significantly exceeds the intrinsic cooling and the magnetic dipole radiation luminosity of the star. In the presence of such an active disk, the  $B_0$  values deduced from the dipole torque formula are misleading, the actual field

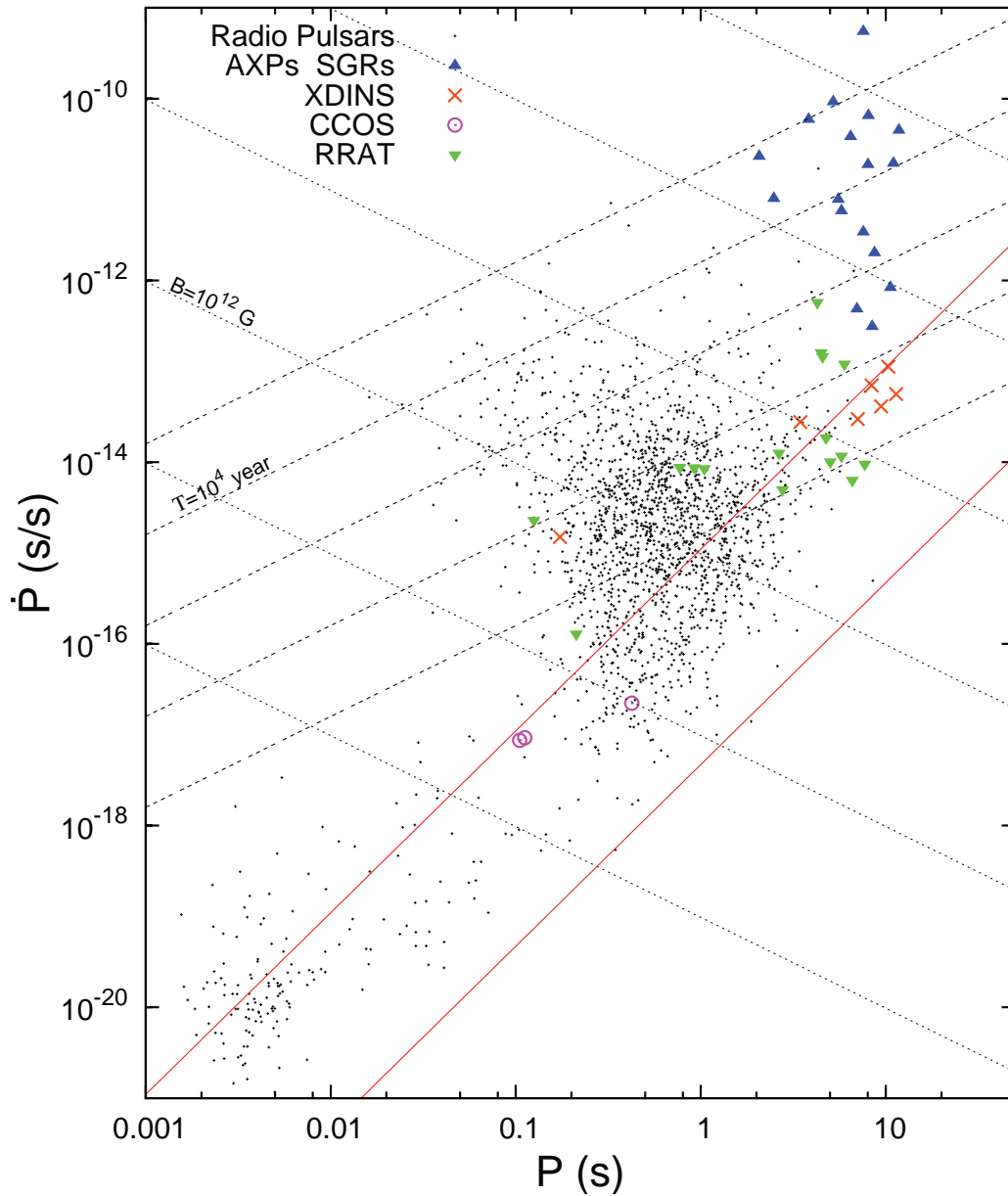


**Figure 1.1:** Period–period derivative diagram ( $P - \dot{P}$  diagram) of isolated neutron stars. Radio pulsars are indicated by dots. The pulsars that are clustered at the bottom-left are millisecond pulsars. Each distinct population is represented by different shaped and coloured points described on the top-left of the figure. The two parallel lines show the upper and lower bounds of the radio pulsar death valley from Chen & Ruderman (1993). The data were taken from ATNF pulsar catalogue (1) and McGill Magnetar catalogue (2).

(1) <http://www.atnf.csiro.au/people/pulsar/psrcat/>

(2) <http://www.physics.mcgill.ca/pulsar/magnetar/main.html>

strength is usually overestimated by one–two orders of magnitude.

The timing characteristics and energetics of the soft gamma bursts of AXP/SGRs are likely to be produced by strong magnetic fields. These bursts together with dipole fields  $B > 10^{14}$  G inferred from measured  $P$  and  $\dot{P}$  assuming purely dipole torques led to the idea that AXP/SGRs have magnetar ( $B > 10^{14}$ ) dipole fields, evolve in vacuum, and slow down by the dipole torques alone. This is the original picture proposed in the magnetar model (Duncan & Thompson, 1992; Thompson & Duncan, 1995). The strong-field-requirement to account for the bursts, does not necessitate presence of magnetar dipole fields. Strong higher multipole fields which are small-scale fields located close to the surface of the star are sufficient to explain the soft gamma bursts. When there is a fallback disk around a neutron star, it interacts with the large-scale dipole field, and apply a torque on the star. In the fallback disk model, the rotational and the electromagnetic emission properties of AXP/SGRs can be explained self-consistently only with conventional ( $10^{12} - 10^{13}$  G) dipole fields of young neutron stars, while a hybrid model involving a super strong dipole field and a fallback disk cannot produce the source properties.

Recently, from the  $P - \dot{P}$  measurement of two AXP/SGR sources the dipole fields were estimated to be significantly weaker than  $10^{14}$  G even with the dipole torque assumption. The first source, SGR 0418+5729, is estimated to have magnetic field  $B \simeq 6 \times 10^{12}$  G on the equator (Rea et al., 2013). Afterwards, another source, Swift J1822.3–1606, was discovered (Cummings et al., 2011; Gogus, Kouveliotou & Strohmayer, 2011) as the second ‘low-B magnetar’ with  $B \sim 2 \times 10^{13}$  G (Livingstone et al., 2011; Rea et al., 2012). Modelling the timing noise effects, Scholz et al. (2012) estimated that  $B \sim 5 \times 10^{13}$  G with the same torque assumption. These values should be taken as an upper limit to the actual strength of the dipole field, since with the disk even weaker fields are sufficient to produce the observed  $P$  and  $\dot{P}$ . The properties of these newly discovered low-B magnetars clearly show that the SGR bursts do not need magnetar dipole fields. This result provided an independent support for the idea that magnetar strength small-scale (multipole) fields are sufficient to produce the bursts.

Dim isolated neutron stars (XDINs) were first discovered with the *ROSAT* satellite in the All Sky Survey, and identified as a new population of isolated neutron. Their periods are in a narrow range, 2 – 12 s, remarkably the same range as observed in AXP/SGRs.

The period derivatives are in the range  $\sim 10^{-14} - 10^{-13} \text{ s s}^{-1}$ . Out of seven XDINs, six sources have measured period and period derivatives. The periods and period derivatives of the seventh source has been measured but not confirmed yet (Pires et al., 2014). The ratio of X-ray flux to optical flux for this class is high (up to  $10^5$ ). The X-ray spectra are very soft with blackbody temperatures  $T_{\text{BB}} \sim 40 - 110 \text{ eV}$  (Haberl, 2007). All known XDINs are nearby sources, located within a distance of  $\sim 400 \text{ pc}$ . Their bolometric X-ray luminosities are systematically low,  $\sim 10^{31} - 10^{32} \text{ erg s}^{-1}$  likely to be produced by the intrinsic cooling of the stars. The ages corresponding to these luminosities on the theoretical cooling curves are a few  $10^5 \text{ yr}$ . The characteristic ages are  $\sim 1 - 4 \times 10^6 \text{ yr}$ . The kinematic ages calculated from estimated space velocities and birth places, and the ages estimated by comparing the X-ray luminosities with theoretical cooling curves (Page, 2009) are much smaller than their characteristic ages.

The seven XDINs lie above the radio pulsar death line (lower border of the death-valley) on  $P - \dot{P}$  diagram (Fig. 1). Nevertheless, no pulsed radio emission has been detected from XDINs. If the actual magnetic field strengths of XDINs are indeed in the  $\sim 10^{13} - 10^{14} \text{ G}$  range, as deduced from the dipole torque formula, it is expected that these sources have radio-pulsar property. While the lack of strong radio pulses from the seven known XDINs might be due to narrow radio beams, this cannot account for the non-detection of radio pulses from the entire XDIN population. From simple statistical calculations, the birthrate of these sources is estimated to be comparable to the normal pulsars (Popov, Turolla & Possenti, 2006).

In recent years, discovery of young radio pulsars with relatively high  $\dot{P}$  values indicated the presence of another single neutron star population, the so-called ‘high magnetic field radio pulsars’ (HBRPs). The dipole field strength of these sources inferred from  $P$  and  $\dot{P}$  values are similar or greater than the quantum critical value  $B_c = 4.4 \times 10^{13} \text{ G}$ , like most of AXP/SGRs. Unlike AXP/SGRs, the spin-down powers of HBRP sources are higher than the X-ray luminosities like normal radio pulsars. The observed periods of these sources are in a range from  $\sim 100 \text{ ms}$  to  $7.7 \text{ s}$ , and the period derivatives are in the  $\sim 10^{-14} - 10^{-12} \text{ s s}^{-1}$  range. An interesting source which belongs to HBRP population, PSR J1846–0258, is an X-ray pulsar, which is a radio pulsar emitting SGR like bursts. Another extreme source in this group is J1734–3333 which has an anomalously low braking index ( $n \simeq 1$ ) which indicates a growing dipole field in purely dipole model. These

properties of HBRPs could be indicating of some evolutionary links between AXP/SGRs and HBRPs, and possibly other young NS populations. Pulsar wind nebule (PWN) are observed from a few HBRPs, i.e. PSR J1846–0258 and PSR 1119–6129, like many other normal young radio pulsars.

Central compact objects (CCOs), another young NS population, were detected close to the center of several supernova remnants. At present, there are nine confirmed CCO sources. None of them show pulsed radio emission. They have no optical counterpart or PWN. Only three CCOs have clear pulsed X-ray detection. The blackbody temperatures corresponding to their spectra are in the soft X-ray band, and the estimated X-ray luminosities are lower than  $10^{33}$  erg s<sup>-1</sup>. The periods of CCOs are between 0.1 – 0.4 s. The timing observations of these sources showed that CCO periods decrease very slowly with the spin periods  $\dot{P} \sim 10^{-17} - 10^{-18}$  s s<sup>-1</sup> and inferred surface dipole fields of a few  $10^{10}$  G, weakest among all young neutron star populations. For a recent review of CCOs see Gotthelf, Halpern & Alford (2013).

Rotating radio transients (RRATs), another population of young neutron stars, were discovered within the last decade (McLaughlin et al., 2006) with their sporadic millisecond-duration radio emissions with recursions in minutes to hours. Until now, there are about eighty sources defined as RRATs (<http://www.atnf.csiro.au/people/pulsar/psrcat/>). Simple population analysis indicates that the birth rate of these sources are comparable to or possibly higher than the normal radio pulsars, like XDINs (e.g. Popov et al. 2010). Detailed recent review of observational properties of RRATs can be found in Keane et al. (2011); Keane (2016).

In the magnetar model, the persistent emissions of AXP/SGRs are believed to be powered by the decay of the strong magnetic fields (see a recent review, Mereghetti 2011, for the details). After the giant flare of SGR 0526–66 in 1979, for the first time, it was suggested independently by Duncan & Thompson (1992) and Paczynski (1992) that the magnetic field energy release of the star possibly cause the flare activities of SGRs. There have been many attempts to explain the persistent rotational and emission properties of AXP/SGRs. The magnetar model, which seems to produce some general properties of the sources, has difficulties in producing the period clustering and X-ray luminosities of AXP/SGRs and XDINs in a self consistent way. To explain the long-term evolution of the low-B magnetars and HBRPs, new assumptions are needed in the magnetar model.

For instance, the rotational properties and the X-ray luminosity of SGR 0418+5729, can be reached only with a very rapid magnetic field decay (Turolla et al., 2011), while for Swift J1822.3–1606, the second low-B magnetar, the required field decay is negligible (Rea et al., 2012). On the other hand, PSR J1734–3333, a HBRP, requires field growth.

The properties and likely evolutionary paths of a neutron star that evolves with a fallback disk are very different from those of the sources evolving in vacuum described above. In the fallback disk model (Chatterjee, Hernquist & Narayan, 2000; Alpar, 2001), the rotational history of a neutron star is determined mainly by the disk torques that are much stronger than the dipole torques in most cases. The X-ray luminosity is produced by mass accretion on to the star from the disk, or by intrinsic cooling of the star when accretion is not possible. It was suggested by Alpar (2001) that the properties of different neutron star populations could be explained if fallback disks are included in the initial conditions in addition to the magnetic field strength and the initial period of the star. The explanation of the optical emission and the long-term evolution of AXP/SGRs in the fallback disk model, requires conventional dipole fields of young neutron stars ( $10^{12} - 10^{13}$  G). The SGR bursts are likely to be powered by strong magnetic fields ( $B > 10^{14}$  G) on the surface of the star as described in the magnetar model. Nevertheless, these magnetar fields could be in the small-scale quadrupole fields rather than the dipole component as indicated by the observations of ‘low-B magnetars’. In the fallback disk model, the dipole component of the magnetic field interacts with the inner disk, while the higher multipoles do not affect the rotational evolution of the neutron star. This means that small-scale magnetar fields close to the surface of the star are compatible with the disk model. However, a hybrid model with a fallback disk around a magnetar dipole field cannot produce the observed rotational properties, in particular the period clustering of AXP/SGRs (Alpar, 2001; Ekşi & Alpar, 2003; Ertan et al., 2007, 2009).

To examine the long-term X-ray luminosity and the rotational evolution of the neutron stars with fallback disk, a numerical code was developed considering the effects of X-ray irradiation of the disk, contribution of the cooling luminosity to irradiation when accretion is not allowed (propeller phase) and inactivation of the disk at low temperatures on the long term evolution (Ertan et al., 2009). Using a simple torque model (Ertan & Erkut, 2008), this code was first employed to show that the general characteristics of AXP/SGRs can be reached by neutron stars evolving with fallback disks and conventional

dipole fields (Ertan et al., 2009). Later, the model was applied to members of different young neutron star populations including the seemingly extreme sources in AXP/SGRs and HBRP systems including the low-B magnetars, SGR 0418+5729 (Alpar, Ertan & Çalışkan, 2011) and Swift J1822.3–1606 (Benli et al., 2013), high-B radio pulsar PSR J1734-3333 (Çalışkan et al., 2013), SGR 0501+4516 (Benli, Çalışkan & Ertan, 2015). To understand the peculiarities in the initial conditions of different groups, it is required that well-known individual source properties should be investigated, and allowed ranges of initial conditions (dipole field strength, initial period and disk mass) should be determined for the members of different neutron star populations. Recently, we performed such a detailed analyses for six XDIN sources (Ertan et al., 2014) and twelve AXP/SGR sources (Benli & Ertan, 2016). Our results imply that these sources from three different populations evolve with fallback disks and conventional dipole fields (the details are given in Chapters 2-5).

A fallback disk can emit radiation from the UV to mid-IR wavelengths depending on the exact position of its inner and outer disk radii, current disk mass-flow rate and irradiation flux from the neutron star. The short-wavelength (UV and optical) radiation is more effectively absorbed by the interstellar medium. A detailed work on observed near IR data of AXP/SGRs, showed that the emission from irradiated and active disks are in agreement with the observed spectrum (Ertan & Çalışkan, 2006). The detection of 4U 0142+61 in the mid-IR band by *Spitzer Space Telescope* was the first significant evidence of a disk around an AXP (Wang, Chakrabarty & Kaplan, 2006). Together with earlier observations, this bright source was detected in a broad-band from the optical to the mid-IR wavelengths. This broad-band spectrum of the source can be fitted with a single active and irradiated disk model (Ertan et al., 2007). This model puts an upper limit on the inner disk radius and thereby also on the dipole field strength. The maximum dipole field strength on the surface of the star that remains consistent with the observed spectrum is a few  $10^{12}$  G. In other models, optical and near-IR emission could be attributed to magnetospheric emission (Wang, Chakrabarty & Kaplan, 2006), nevertheless mid-IR emission seem to be a unique signature of a fallback disk.

The magneto-rotational instability (Balbus & Hawley, 1991) which generates the turbulent viscosity needed for the disk to transport mass and angular momentum will not work at temperatures below a critical temperature,  $T_p$ , because the ionization fraction be-

comes too small. Starting from the outermost disk, the disk gradually becomes passive as the local disk temperatures decrease below  $T_p$ . The general properties of AXP/SGRs previously can be explained with  $T_p \sim 100 - 200$  K (Ertan et al., 2009). This is consistent with the results of the analysis indicating that the disk should be active even at 300 K (Inutsuka & Sano, 2005). The effective temperature profile of the outer disk and, thus, the dynamical outer disk radius are determined mainly by the X-ray irradiation flux from the neutron star. This is because the heating by irradiation dominates over the viscous heating of the disk except inner regions of the disk. The efficiency of the X-ray irradiation depends on the X-ray albedo and geometry of the disk. From the analysis of the X-ray and IR data of AXP/SGRs, irradiation efficiency is restricted to a narrow range for AXP/SGRs (Ertan & Çalışkan, 2006). Together with this range, the long-term evolution model for different populations can be produced self-consistently with  $T_p$  to values less than  $\sim 200$  K. The evolution of the outer radius of the active disk is governed by the X-ray irradiation flux (Shakura & Sunyaev, 1973), The accretion luminosity is related to  $\dot{M}$  through  $L = GM\dot{M}/R$  where  $G$  is the gravitational constant and  $R$  and  $M$  are the radius and mass of the neutron star respectively.

In recent years, observations and the results of theoretical calculations imply that magnetized neutron stars could accrete matter from the disk even in the fast-rotator phase (see, e.g., Rappaport, Fregeau & Spruit 2004). The critical value of the fastness parameter  $\omega_* = \Omega_*/\Omega_K(r_A)$ , above which accretion is completely hindered, is not well known. Here,  $\Omega_K(r_A)$  is the angular velocity of the disk at the Alfvén radius,  $r_A = (GM)^{-1/7} \mu^{4/7} \dot{M}_{\text{in}}^{-2/7}$ ,  $\Omega_*$  is the rotational angular frequency of the neutron star, and  $\mu$  is the magnetic dipole moment of the neutron star. In the fallback disk model, AXP/SGRs are sources accreting in the spin-down phase. For these sources,  $r_A$  is greater than the co-rotation radius,  $r_{\text{co}} = (GM/\Omega_*^2)^{1/3}$ .

We employ the torque model obtained by Ertan & Erkut (2008) through analysis of contemporaneous X-ray luminosity and period evolutions of XTE J1810–197 in the X-ray enhancement phase of the source. In this model, it is assumed that the dipole field interact with the matter in a boundary layer extending from  $r_A$  to  $r_{\text{co}}$ . The magnitude of the torque, nevertheless, is not sensitive to the width of the boundary layer provided that the boundary width is not much smaller than  $r_{\text{co}}$ . Most of the contribution to the total torque comes from the innermost region of the boundary close to  $r_{\text{co}}$ . This is due to sharp

radius dependence of the magnetic torques (see Ertan & Erkut 2008 for details of the torque calculations). To calculate the spin-down torque acting on the star in the accretion phase, we integrate the magnetic torques from  $r_A$  to  $r_{co}$ . In this phase, we assume that the inner disk matter interacts with the dipole field in the boundary region, leaves the boundary close to  $r_{co}$ , and flows along the field lines onto the neutron star.

To follow the evolution of a neutron star with the disk, we make some simplifying assumptions that do not affect the long-term evolutions qualitatively. When  $r_A$  is less than the light cylinder radius,  $r_{LC} = c/\Omega_*$ , we take  $r_{in} = r_A$ . This represents the inner radius of the unperturbed disk, or the outer radius of the boundary layer. Accretion takes place in this regime when  $r_{in} < r_{LC}$ ,  $r_{in} > r_{co}$ . Over the long-term evolution,  $r_{LC}$  increases with decreasing angular frequency of the neutron star,  $\Omega_*$ , while  $r_A$  increases with decreasing  $\dot{M}_{in}$ . When the calculated  $r_A$  is found to be greater than the current value of  $r_{LC}$ , we set  $r_{in} = r_{LC}$ . In this propeller phase, we assume that the boundary can not extend to  $r_{co}$ ,  $r_{in}$  remains close to  $r_{LC}$ , and there is no accretion onto the neutron star while the source continues slowing down with the disk torques. With the ‘‘propeller phase’’ we mean the phase over which the inner disk matter flowing to the boundary is ejected from the system. (A detailed description of the disk field interaction is given in Chapter 4.)

Depending on the initial parameters, the model sources could follow rather different evolutionary paths. The X-ray luminosity and the rotational evolution of a source could pass through three basic evolutionary phases, namely the initial propeller phase, the accretion phase and the final propeller phase. We illustrate these evolutionary phases in Fig. 2. The top panel shows the X-ray luminosity,  $L_x$ , evolution of the source. The abrupt rise in  $L_x$  at  $t \simeq 5 \times 10^2$  yr is due to penetration of the inner disk into the light cylinder and the onset of the accretion phase. This might happen at different times of evolution for different sources. Some sources may never enter the initial propeller phase, while some others remain always in this phase as radio pulsars depending on the initial conditions. The dashed line in the top panel represents the cooling history of a neutron star with a dipole field strength of  $10^{12}$  G on the surface of the star. It is seen that the cooling luminosity of the neutron star (dashed line),  $L_{cool}$ , defines the luminosity, when accretion is not allowed or in the late phases of the accretion episode. The evolution is easier to follow from the period derivative,  $\dot{P}$ , curve. The torque acting on the star is most efficient in the accretion phase. When the positive term is negligible, that is, when  $r_A$  is not very

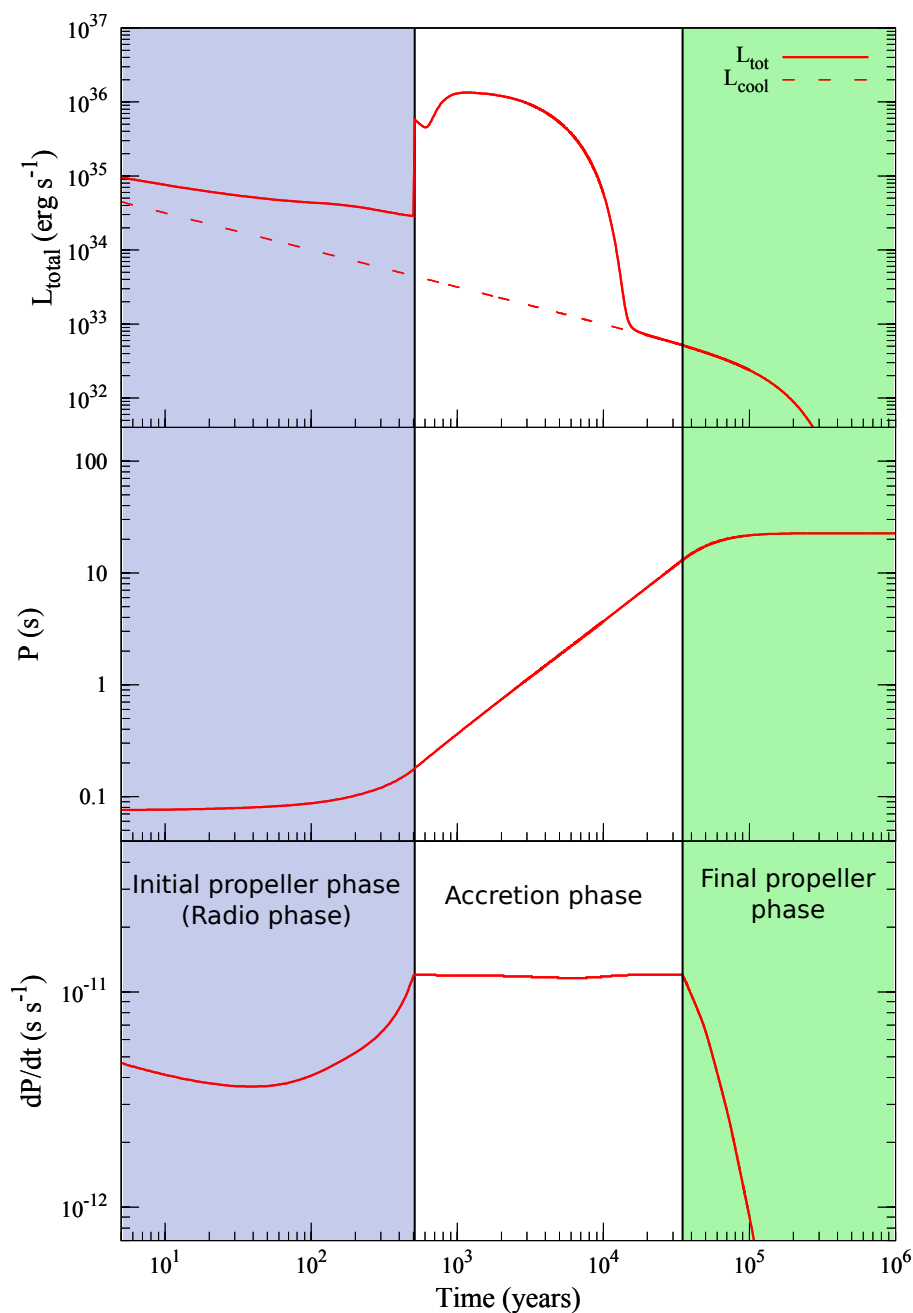


**Figure 1.2:** A sample model curve that shows three basic evolutionary episodes of a neutron star-fallback disk system. For this illustrative model,  $B_0 = 2 \times 10^{12}$  G,  $M_d = 5.7 \times 10^{-4} M_\odot$ ,  $P_0 = 75$  ms and  $T_p = 150$  K. Durations of initial propeller phase (blue region), accretion phase (white region) and final propeller phases (green region) depend on the initial conditions. To reach the long periods of several seconds, a source should pass through the accretion phase. The initial propeller phase, which could be experienced by a fraction of the sources, has not a significant effect on the properties achieved in the accretion and final propeller phases (see the text for details).

close to  $r_{\text{co}}$ ,  $\dot{P}$  is found to be independent of both  $\dot{M}$  and  $P$ . This constant  $\dot{P}$  behaviour in the accretion phase is seen in the bottom panel of Fig. 1.2.

With decreasing  $\dot{M}_{\text{in}}$ ,  $r_{\text{A}}$  moves outward faster than the light cylinder radius,  $r_{\text{LC}}$ . In the model, accretion is switched off when  $r_{\text{A}}$  is found to be greater than  $r_{\text{LC}}$ . For the illustrative model in Fig. 1.2, this corresponds to  $t \simeq 3 \times 10^4$  yr. From this point on,  $\dot{P}$  decreases with decreasing  $\dot{M}_{\text{in}}$ . The sources in this final propeller phase do not accrete but still spin-down by the disk torques. It is seen in the middle panel of Fig. 1.2. that  $P$  remains almost constant in this phase because of decreasing torque efficiency after termination of the accretion episode.

In the initial and final propeller phases, there is no accretion on to the star, and the pulsed radio emission is allowed. We expect that sources could show pulsed radio emission only in the initial propeller phase, since in the final propeller stage, the sources with conventional dipole fields and long periods are usually not capable of producing pulsed radio emission. When the accretion phase terminates, the sources are already below the so-called pulsar death–line, that is, they cannot produce pulsed radio emission.

The X-ray outbursts/enhancements seen in AXP/SGRs can be explained in both the magnetar model and the fallback disk model. In the magnetar model, part of the energy powering the soft gamma burst is injected into the crust; the resultant heating and subsequent cooling of the crust produce the observed outburst light curve (see, e.g., Camero et al. 2014). In the fallback disk model, the disk in the quiescent state mimics a steady-state geometrically thin disk. Part of the burst energy is absorbed by the inner disk. The inner disk matter is pushed back by the burst, and piles up at a larger radius forming a density gradient. Subsequent evolution of the inner disk can produce the X-ray and IR enhancement light curve of AXP/SGRs (Ertan & Alpar 2003; Ertan, Göğüş & Alpar 2006, see Çalışkan & Ertan 2012 for a detailed explanation of this model). Results of earlier work on the enhancement light curves of transient and persistent AXP/SGRs imply that fallback disks of all these sources make a transition between hot and cold viscosity states at a critical temperature  $T_{\text{crit}} \sim 1500 - 2000$  K. This model gives reasonable fits to observed X-ray enhancement light curves of different AXP/SGRs with the same basic disk parameters (Çalışkan & Ertan, 2012; Benli et al., 2013; Benli, Çalışkan & Ertan, 2015).

In this thesis. we have studied : (1) that the long-term evolution of “low–B magnetar” Swift J1822.3–1606 together with its recently observed X-ray enhancement light curve

, (2) the long-term evolution and the short-term X-ray enhancement and the optical/IR emission from the fallback disk of SGR 0501+4516, (3) the long-term evolution and the radio emission properties of individual sources in the XDIN population, (4) and finally, the long-term evolution of individual AXP/SGRs with relatively well known properties. These are summarized below.

## 1.1 X-ray Enhancement and Long-term Evolution of SWIFT J1822.3–1606

The soft gamma repeater Swift J1822.3–1606 is an extreme SGR source defined as a "low-B magnetar" (Livingstone et al., 2011; Rea et al., 2012; Scholz et al., 2012). The period of the source is 8.4 s and the period derivative is estimated in the  $\sim 4 \times 10^{-13} - 10^{-12} \text{ s s}^{-1}$  range. For a distance of  $d = 1.6 \text{ kpc}$  (Nielbock et al., 2001), the quiescent bolometric luminosity is estimated between  $2.5 \times 10^{31} \text{ erg s}^{-1}$  and  $2.6 \times 10^{33} \text{ erg s}^{-1}$ . We have used this source properties to test our model. We have employed the code developed by (Ertan et al., 2009).

The earlier accomplishment of this model in the explanation of the properties of the extreme sources, SGR 0418+5729 (Alpar, Ertan & Çalışkan, 2011) and PSR J1734–3333 (Çalışkan et al., 2013), motivated us to study the properties of the recently discovered, second similar source. This source was discovered in the X-ray outburst/enhancement phase. If the outburst is produced by the enhancement in the mass flow rate following a burst episode as described by Ertan & Alpar (2003), the source should be in the accretion phase at present. This does not guarantee that the source had been evolving in the accretion phase prior to the onset of the X-ray outburst. We have tried to obtain reasonable evolutionary scenarios of this source consistent with its X-ray enhancement properties. The details of our calculations and results are presented in Chapter 2.

## 1.2 Long-term Evolution, X-ray Outburst and Optical/IR emission of SGR 0501+4516

SGR 0501+4516 is a typical AXP/SGR source with  $P \simeq 5.76 \text{ s}$  (Göğüş, Woods & Kouveliotou, 2008) and  $\dot{P} \simeq 5.8 \times 10^{-12} \text{ s s}^{-1}$  (Göğüş et al., 2010). The source also showed

optical pulsations with the same period (Dhillon et al., 2011). The bolometric luminosities obtained for the possible distance range (1.5–5 kpc) are between  $4.7 \times 10^{33} - 5.2 \times 10^{34} \text{ erg s}^{-1}$ .

The source is attractive in that it has clear rotational and X-ray luminosity properties, an X-ray enhancement light curve, and optical/IR observations at a known luminosity level. That is, the source provides three different, independent tests of the model. Using the results of these calculations we also try to constrain the magnetic field, disk mass and the age of the source. In Chapter 3, the properties of SGR 0501+4516 indicated by our results are discussed and compared to those of the “low-B magnetars” and “high-B radio pulsar” PSR J1734–3333. In addition, application of our X-ray enhancement model to SGR 0501+4516 and the comparison of the estimated optical/IR flux of the disk with the observed data are also given in Chapter 3.

### 1.3 Long-term Evolution of Dim Isolated Neutron Stars

Currently, seven isolated neutron stars are identified as XDIN sources, six of them have well measured rotational properties. They all lie within a distance of  $\sim 400 \text{ pc}$ . From their statistical analysis, a galactic birthrate of  $\sim 1 \text{ Myr}^{-1}$  was estimated (Popov, Turolla & Possenti, 2006). The periods are observed to be in the narrow interval,  $2 - 12 \text{ s}$  similar to AXP/SGRs. The kinematic ages of four XDIN sources were measured in the range  $\sim 10^5 - 10^6 \text{ yr}$  (Mignani et al., 2013). The X-ray luminosities are between  $10^{31} - 10^{32} \text{ erg s}^{-1}$ . These relatively older, thermally emitting pulsars do not have a pulsed radio emission which could not be explained up to now, with dipole slow-down models.

In Chapter 4, we examine the period, the period derivative and the total X-ray luminosity evolution of the individual XDIN sources. Tracing the initial conditions, namely the initial period,  $P_0$ , strength of the magnetic dipole field on the pole of the star,  $B_0$ , and the initial disc mass,  $M_d$ , we try to constrain  $M_d$  and  $B_0$ .

The detailed observed properties of individual sources are give in Section 4.3. We show that the fallback disc model can account for the observed individual properties of all these sources with  $B_0$  values in the  $10^{11} - 10^{12} \text{ G}$  range which are much smaller than those inferred from the purely dipole spin-down torques. Our model results imply

that these sources completed the accretion phase and now they are in the final propeller phase. We also discuss the radio properties of these sources indicated by our results, with a comparison to the magnetic dipole torque model.

## **1.4 Long-term Evolution of Anomalous X-ray Pulsars and Soft Gamma Repeaters**

In Chapter 5, we present our work on the long-term evolutions of twelve individual AXP/SGR sources with relatively small uncertainties in distances and period derivatives in the quiescent states. After our work on the XDIN population (Chapter 4) this is the second comprehensive work on the individual source properties of an other neutron star population, AXP/SGRs. Using the same model applied to XDINs, we try to determine the allowed ranges of the initial conditions for each source. We also check whether there is a correlation between the initial disk masses and the magnetic field strengths of AXP/SGR and XDIN sources indicated by our results.

Estimated current evolutionary phases of the sources and a comparison of the general source properties between AXP/SGR and XDIN groups are also described in Chapter 5.

Our results well constrain the dipole field strengths of both XDINs and AXP/SGRs, and imply that the dipole fields of XDINs are systematically weaker than those of AXP/SGRs (see Chapter 5 for details).

# Chapter 2

## X-RAY ENHANCEMENT AND LONG-TERM EVOLUTION OF SWIFT J1822.3–1606

This chapter was published in *The Astrophysical Journal*, 2013,  
Volume 778, Issue 2, pp. 119–126.

**Onur Benli, Şirin Çalışkan, Ünal Ertan, Mehmet Ali Alpar, Joachim E. Trümper &  
Nikos D. Kylafis**

Some parts of the introduction were removed or modified.

## 2.1 Introduction

The soft gamma repeater (SGR) Swift J1822.3–1606 was recently discovered (Cummings et al., 2011; Gogus, Kouveliotou & Strohmayer, 2011) as the second “low-B magnetar” with  $B \sim 2 \times 10^{13}$  G inferred from the dipole torque formula (Livingstone et al., 2011; Rea et al., 2012). Modelling the timing noise effects, Scholz et al. (2012) estimated that  $B \sim 5 \times 10^{13}$  G with the same torque assumption. The first such source, the SGR 0418+5729, indicates a magnetic dipole field of  $6 \times 10^{12}$  G on the surface (equator) of the neutron star assuming that the source is spinning down by the dipole torques (Rea et al., 2013). This can actually be taken as an upper limit to the strength of the dipole field. If the neutron star is evolving with an active fallback disk, the dipole field strength that can produce the properties of this source could be in the  $1 - 2 \times 10^{12}$  G range on the surface of the neutron star (Alpar, Ertan & Çalışkan, 2011). These results clearly show that soft gamma bursts of anomalous X-ray pulsars (AXPs) and SGRs do not require magnetar ( $B > 10^{14}$  G) dipole fields. The properties of these two SGRs, which are likely to be older than the other known AXP/SGRs (see Mereghetti 2008 for a recent review of AXP/SGRs), provide tight constraints for models in explaining the long-term luminosity and the rotational evolution of AXP/SGRs in accordance with their statistical properties, like luminosity, period and period derivative distribution at different ages, and with possible evolutionary connections to the other young neutron star populations.

In the magnetar model, the X-ray luminosity and the rotational properties of SGR 0418+5729 and Swift J1822.3–1606 require rapid decay of the dipole component of the magnetic field. Models for field decay require a strong crustal toroidal field decaying together with the dipole field (Turolla et al., 2011; Rea et al., 2013). For SGR 0418+5729, the initial toroidal field should be extremely strong ( $4 \times 10^{16}$  G), while the initial dipole field should be  $\sim 2 - 3 \times 10^{14}$  G to produce the current properties of the source (Turolla et al., 2011). For Swift J1822.3–1606, the model sources have initial toroidal and dipole fields of  $4 \times 10^{14}$  G and  $1.5 \times 10^{14}$  G, respectively (Rea et al., 2012). On the other hand, PSR J1734–3333 seems to follow a completely different evolutionary path with an increasing period derivative. In the frame of the same model, this source could be in a short-term field growth phase. How this is related to the radio pulsar property and low X-ray luminosity of the source at a young age of  $\sim 10^4$  yr remains unclear.

Here, we investigate the long-term evolution of the second “low-B magnetar,” Swift J1822.3–1606. We try to determine the evolutionary epoch of the source and constrain the strength of the dipole field that gives consistent solutions for the long-term evolution. We also try to explain the X-ray enhancement of Swift J1822.3–1606 and discuss its possible effects on the current rotational properties of the source. We summarize the basic evolutionary stages of a neutron star evolving with a fallback disk and investigate the evolution of Swift J1822.3–1606 in Section 2.2. A summary of our X-ray enhancement model and its application to the X-ray outburst light curve of Swift J1822.3–1606 are given in Section 2.3. We discuss the results and summarize our conclusions in Section 2.4.

## 2.2 Long-term Evolution of Swift J1822.3-1606

For comparison with the model, we use the rotational properties and X-ray luminosity of Swift J1822.3–1606 obtained from the most recent observational analysis of the source performed by (Scholz et al., 2012). For an estimated distance of  $\sim 1.6$  kpc, the quiescent bolometric luminosity of Swift J1822.3–1606 is estimated between  $2.5 \times 10^{31} - 2.6 \times 10^{33}$  erg s $^{-1}$ . The period  $P$  is 8.4 s (Gogus, Kouveliotou & Strohmayer, 2011). X-ray timing analysis, taking the noise effects into account, cannot constrain  $\dot{P}$  and gives  $\dot{P} \gtrsim 3 \times 10^{-13}$  s s $^{-1}$ . Timing solutions with greater  $\dot{P}$  and marginally lower  $\chi^2$  values could be obtained adding higher order derivatives of the frequency in the solutions to eliminate the noise effects (Scholz et al., 2012). In the accretion phase of the source, we adopt  $\dot{P} \sim 4 \times 10^{-13} - 4 \times 10^{-12}$  s s $^{-1}$ . Details and applications of our long-term evolution model are given in (Ertan et al., 2009; Alpar, Ertan & Çalışkan, 2011; Çalışkan et al., 2013). Here, we briefly describe the basic long-term evolutionary phases of a neutron star evolving with a fallback disk.

We follow the viscous evolution of an extended thin disk with an initial surface density profile  $\Sigma = \Sigma_0 (r_{\text{in}}/r)^{3/4}$ , where  $r_{\text{in}}$  is the inner radius of the disk. Interaction of the inner disk with the magnetic dipole field governs the rotational evolution ( $P, \dot{P}, \ddot{P}$ ) of the neutron star. In the disk diffusion equation, we use the  $\alpha$ -prescription of the kinematic viscosity (Shakura & Sunyaev, 1973). Results of our earlier work on the enhancement light curves of transient and persistent AXP/SGRs imply that fallback disks of all these

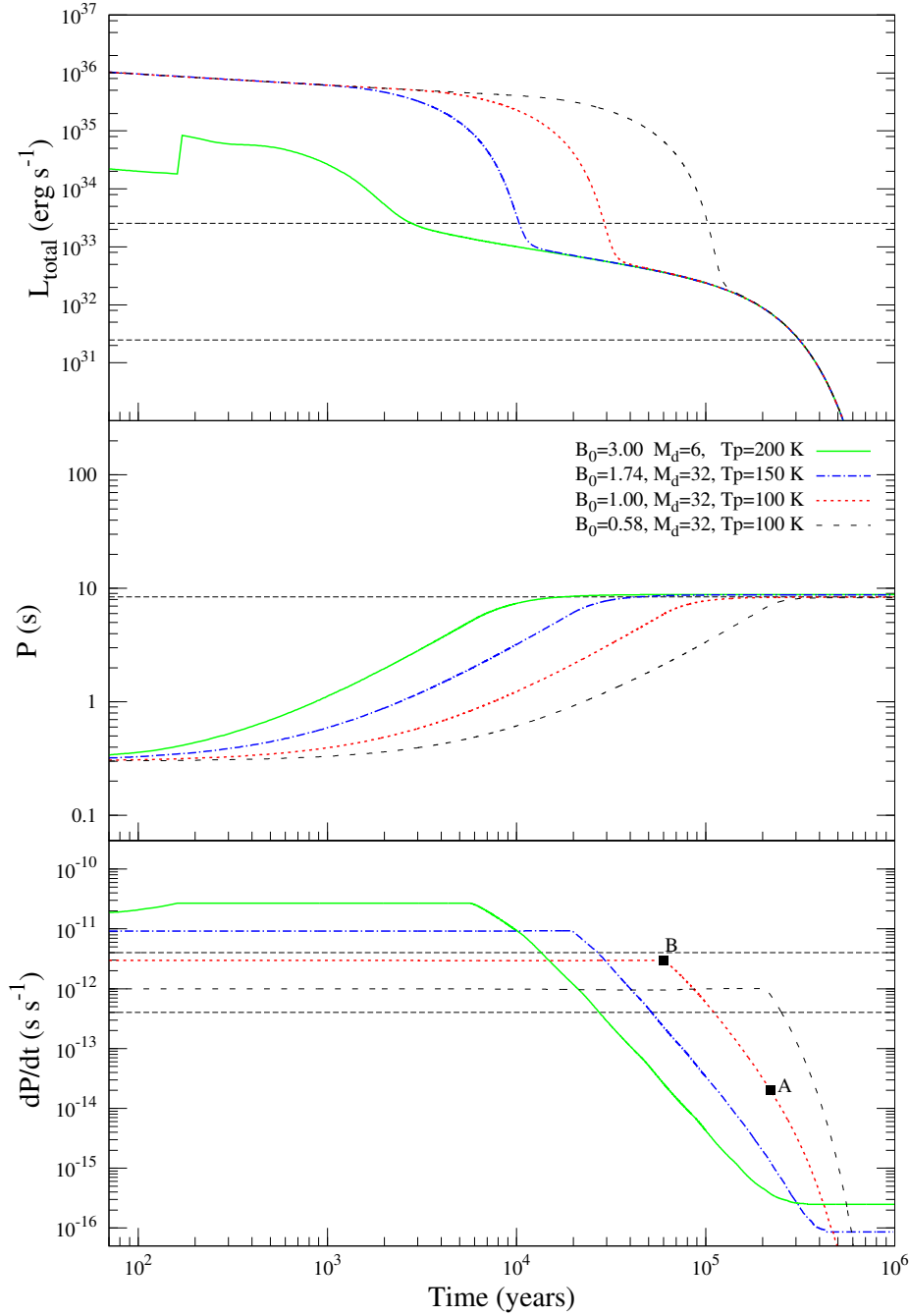


**Figure 2.1:** Long-term luminosity, period and period derivative evolution of the model sources. The values of  $M_d$  and  $B_0$  employed in the models are given in the middle panel in units  $10^{-6} M_\odot$  and  $10^{12}$  G respectively. Horizontal lines in the top panel show the observational error bars of  $L$  (Scholz et al., 2012). For these models,  $C = 1 \times 10^{-4}$  except for the dashed (black) line which has  $C = 7 \times 10^{-4}$  and represents the evolution with minimum  $B_0$ . In the bottom panel, horizontal lines show the range of  $\dot{P}$  for Swift J1822.3–1606 adopted in the present work. The model sources with  $B_0$  values 0.58 and  $1.00 \times 10^{12}$  G could represent the evolution of Swift J1822.3–1606 if the source is not in the accretion phase in quiescence. The points A and B seen in the bottom panel are for a discussion of possibilities for the source properties in quiescence (see the text for explanation).

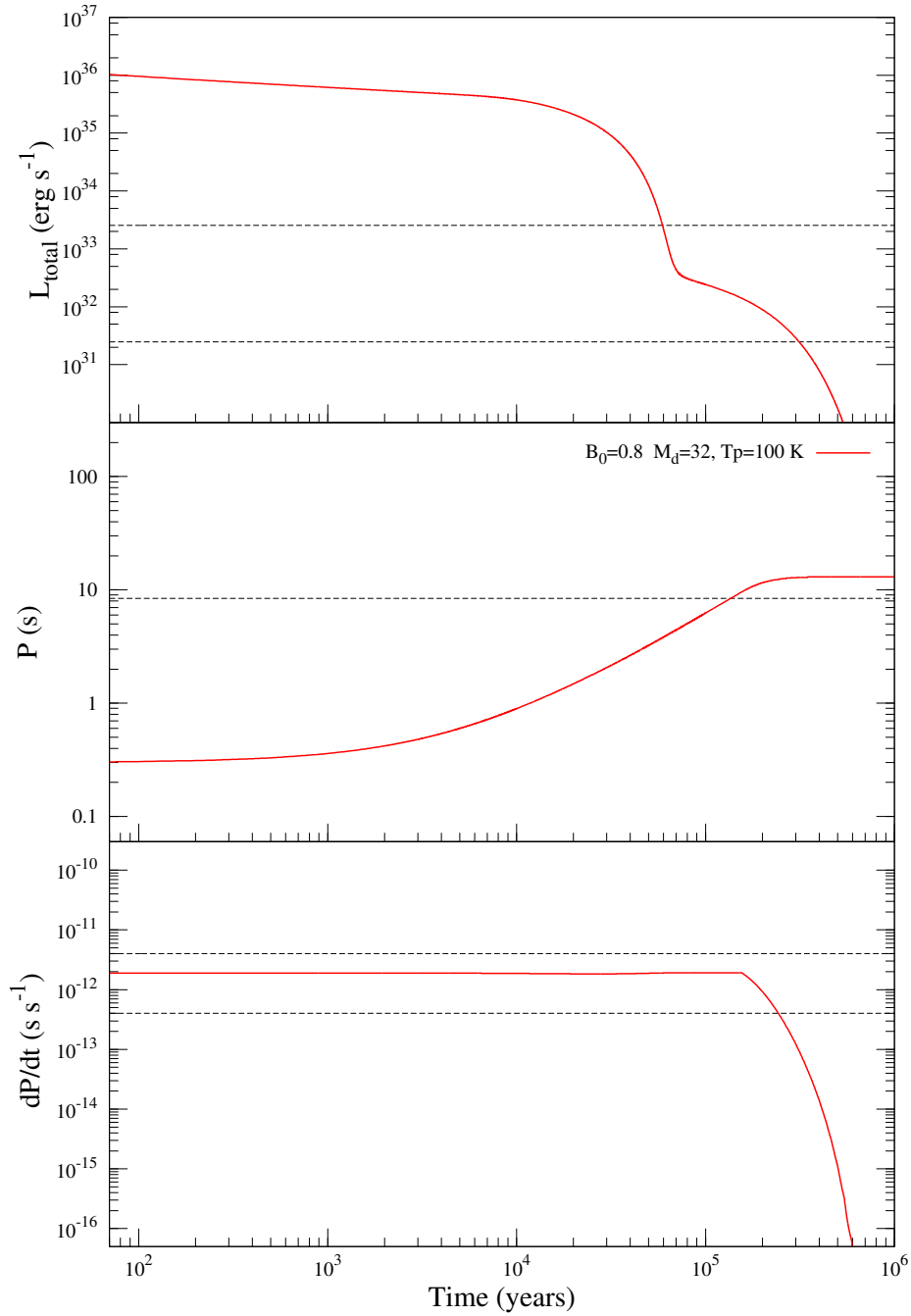


**Figure 2.2:** Evolution of an illustrative model source which could acquire the properties of Swift J1822.3–1606 simultaneously if the source is in the long-term accretion phase at present in the quiescent state. The values of  $M_d$  and  $B_0$  are given in the figure in units of  $10^{-6} M_\odot$  and  $10^{12}$  G respectively. For these models we take  $C = 3 \times 10^{-4}$ .

sources make a transition between hot and cold viscosity states at a critical temperature  $T_{\text{crit}} \sim 1500 - 2000$  K. This model with  $\alpha$  parameters  $\alpha_{\text{hot}} \simeq 0.1$  and  $\alpha_{\text{cold}} \simeq 0.045$  for the hot and cold viscosity states gives reasonable fits to observed X-ray enhancement light curves of different AXP/SGRs (Çalışkan & Ertan, 2012). We use the same  $\alpha$  parameters in the long-term evolution of the disk. Note that (1) both  $\alpha_{\text{hot}}$  and  $\alpha_{\text{cold}}$  represent turbulent viscosities of an active disk, (2) the hot inner disk does not affect the long-term evolution of the disk, that is, the long-term history of the mass inflow rate of the disk is determined by the outer disk, and (3) the disk becomes passive at a temperature  $T_p \sim 100 - 200$  K (Ertan et al., 2009), which is much lower than  $T_{\text{crit}}$ . The transition temperature  $T_{\text{crit}}$  between the viscosity states is important only for short-term events like X-ray enhancements (see Section 2.3), and should not be confused with  $T_p$  below, at which turbulent activity stops.

All our simulations start with an outer disk radius  $r_{\text{out}} = 5 \times 10^{14}$  cm. Subsequent evolution of the outer radius of the active disk is governed by the X-ray irradiation flux  $F_{\text{irr}} = C\dot{M}c^2/4\pi r^2$  (Shakura & Sunyaev, 1973), where  $c$  is the speed of light,  $\dot{M}$  is the mass accretion rate onto the surface of the star, and the parameter  $C$  represents the efficiency of X-ray irradiation. The X-ray luminosity is related to  $\dot{M}$  through  $L = GM\dot{M}/R$  where  $G$  is the gravitational constant and  $R$  and  $M$  are the radius and mass of the neutron star respectively. The mass-flow rate at the inner disk  $\dot{M}_{\text{in}} = \dot{M}/f$ , where  $f$  represents the fraction of  $\dot{M}_{\text{in}}$  that is accreted onto the surface of the star. We take  $f = 1$ ; this simplification does not significantly affect our quantitative results. The analysis of the X-ray and infrared data of AXP/SGRs indicates that for all sources the irradiation efficiency  $C$  is in the  $1 - 7 \times 10^{-4}$  range for an inclination angle  $i = 0^\circ$  between the normal of the disk and the line of sight of the observer (Ertan & Çalışkan, 2006).

Starting from the outermost disk, the disk gradually becomes passive as the local disk temperatures decrease below  $T_p$ . The general properties of AXP/SGRs can be explained with  $T_p \sim 100 - 200$  K (Ertan et al., 2009). This is consistent with the results of the analysis indicating that the disk should be active even at 300 K (Inutsuka & Sano, 2005). In our long-term evolution model  $T_p$  and  $C$  are degenerate parameters. In the model, if  $C$  is increased from  $1 \times 10^{-4}$  to  $7 \times 10^{-4}$ , a similar model curve can be obtained by increasing  $T_p$  only by a factor of  $\sim 1.6$ . That is, the lower and upper bounds on the range of  $C$  obtained from earlier results (Ertan & Çalışkan, 2006) remove the degeneracy and

constrain  $T_p$  to values less than  $\sim 200$  K.

In recent years, observations and the results of theoretical calculations imply that magnetized neutron stars could accrete matter from the disk even in the fast-rotator phase (see, e.g., Rappaport, Fregeau & Spruit 2004). The critical value of the fastness parameter  $\omega_* = \Omega_*/\Omega_K(r_A)$ , above which accretion is completely hindered, is not well known. Here,  $\Omega_K(r_A)$  is the angular velocity of the disk at the Alfvén radius,  $r_A = (GM)^{-1/7} \mu^{4/7} \dot{M}_{\text{in}}^{-2/7}$ ,  $\Omega_*$  is the rotational angular frequency of the neutron star, and  $\mu$  is the magnetic dipole moment of the neutron star. In the fallback disk model, AXP/SGRs are sources accreting in the spin-down phase. For these sources,  $r_A$  is greater than the co-rotation radius,  $r_{\text{co}} = (GM/\Omega_*^2)^{1/3}$ . We employ the torque model obtained by Ertan & Erkut (2008) through analysis of contemporaneous X-ray luminosity and period evolutions of XTE J1810–197 in the X-ray enhancement phase of the source. This spin-down torque acting on the star can be written as

$$N = I \dot{\Omega}_* = \dot{M}_{\text{in}} (GM r_{\text{in}})^{1/2} (1 - \omega_*^2), \quad (2.1)$$

where  $r_{\text{in}}$  is the inner radius of the disk and  $M$  is the mass of the neutron star which we take to be  $1.4M_\odot$ . In the accretion phase, this torque is equivalent to the integration of the magnetic torques from  $r_A$  to  $r_{\text{co}}$  taking the ratio of the poloidal and azimuthal components of the magnetic dipole field to be constant. When  $r_A < r_{\text{LC}} = c/\Omega_*$ , the light cylinder radius, we assume that the source is in the accretion phase and take  $r_{\text{in}} = r_A$ . It is assumed that the boundary layer of the disk could extend down to the co-rotation radius, while  $r_{\text{in}}$  represents the inner radius of the thin disk or the outer radius of the boundary layer. For the accretion phase, from Equation (2.1) it is found that the period derivative,  $\dot{P}$ , of the neutron star is independent of both  $\dot{M}$  and  $P$  if the source is not close to rotational equilibrium, that is, when  $\omega_*^2$  is not close to unity. The neutron star reaches maximum  $\dot{P}$  in the accretion phase. The maximum value of  $\dot{P}$  is proportional to  $B_0^2$ , where  $B_0$  is the dipole field strength on the pole of the star. Depending on  $B_0$ , the initial period,  $P_0$ , and the disk mass,  $M_d$ , some of the model sources begin their evolution in the accretion phase, some of them enter the accretion phase at a later epoch, or others possibly never accrete over their entire lifetimes. The sources that cannot accrete are likely to be active radio pulsars as long as they remain above the pulsar deathline with their dipole field and current period.

A fallback disk evolves to lower mass and  $\dot{M}_{\text{in}}$ . In the long-term accretion phase,  $r_{\text{in}}$  increases while the outer radius of the active disk  $r_{\text{out}}$  decreases with gradually decreasing accretion rate, which brings about a decrease in the irradiation flux illuminating the disk. As more regions of the outer disk become passive, the outer radius of the active disk,  $r_{\text{out}}$  moves inward. Propagation of  $r_{\text{out}}$  inward also decreases the mass-flow rate from the outer to the inner disk regions. While  $r_{\text{out}}$  approaches  $r_{\text{in}}$ , with rapidly decreasing  $\dot{M}_{\text{in}}$ , accretion luminosity enters the cut-off phase. The accretion luminosity first decreases below the cooling luminosity of the neutron star, and later accretion stops when the inner disk radius recedes to the light cylinder,  $r_{\text{A}} = r_{\text{LC}}$ . For the subsequent evolution, we take  $r_{\text{in}} = r_{\text{LC}}$ . In this phase, from Equation (2.1), it is found that  $\dot{P} \propto B^2 \dot{M}_{\text{in}}$ . Even after the accretion phase, the disk torque prevails and continues to dominate the dipole torque, in most cases, over the visible lifetime of the sources. In this late phase of evolution, the disk torque and  $\dot{P}$  decrease with decreasing  $\dot{M}_{\text{in}}$  converging to the level of the dipole torque, while  $P$  remains almost constant. After the accretion has stopped, the X-ray luminosity is produced by the intrinsic cooling of the neutron star. In the total luminosity calculation, we include the cooling luminosity calculated by Page (2009) and the contribution of intrinsic dissipative heating due to the external (disk and dipole) torques acting on the star (Alpar, 2007).

The important parameters of our model are  $B_0$ ,  $M_{\text{d}}$ ,  $P_0$ , and  $T_{\text{p}}$ . Consistently with our earlier results, we keep  $T_{\text{p}} < 200$  K. Tracing  $B_0$ ,  $M_{\text{d}}$  and  $T_{\text{p}}$ , we obtain allowed ranges of these parameters that can produce the properties of Swift J1822.3–1606. Monte Carlo simulation of the radio pulsar population indicates that the initial periods could be represented by a Gaussian distribution centered around 300 ms with a width  $\sim 150$  ms (Faucher-Giguère & Kaspi, 2006). In our simulations, we take  $P_0 = 300$  ms. When we obtain a reasonable solution, we repeat the calculations with lower  $P_0$  values to find the minimum  $P_0$  value that allows the model source to enter the accretion phase and acquire the observed properties.

Illustrative model curves that can represent the long-term evolution of Swift J1822.3–1606 are given in Figs. 2.1 and 2.2. We investigate the evolutionary tracks considering the possibilities in quiescence: (1) the source is still in the accretion phase, and (2) the accretion phase terminated at an earlier time of evolution. For both cases, disturbances of the inner disk by soft gamma bursts could start a transient enhanced accretion epoch

that can last for as long as decades. Considering this possibility, in Section 2.3, we also investigate whether the currently observed X-ray enhancement of the source could be produced by enhanced mass-flow rate of the disk caused by the soft gamma burst epoch that was observed just before the onset of the X-ray outburst (Rea et al., 2012). We discuss the possibilities for the quiescent-state properties of Swift J1822.3–1606 considering the results of both the long-term evolution and the X-ray enhancement models in Section 2.4.

### 2.3 X-ray Enhancement of Swift J1822.3-1606

Starting in 2011 July, Swift J1822.3–1606 underwent an X-ray outburst (Rea et al., 2012). The X-ray flux of the source in 1-10 keV range reached its maximum at  $t \sim 0.76$  days after the burst epoch. The subsequent smooth decay phase of the light curve was closely monitored by *Swift*, *RXTE*, *Chandra*, *Suzaku* and *XMM-Newton* for  $\sim 400$  days (Rea et al., 2012; Scholz et al., 2012).

The model we use in the present work is the same as that applied to the other AXPs and SGRs showing X-ray enhancements (see Çalışkan & Ertan 2012 and Chapter 1 for a detailed description of the model). The simple idea in this model can be summarized as follows: The fallback disk around the star has a thin disk profile in the quiescent state. A soft gamma-ray burst will push back part of the inner disk matter, which piles up at a larger radius, forming a density gradient at the innermost region of the disk. After the burst, starting with this new initial condition, relaxation of the disk to the pre-burst conditions with an enhanced mass-flow and accretion rate determines the X-ray luminosity evolution of the neutron star.

The pile-up at the inner disk is described by a Gaussian mass distribution,  $\Sigma = \Sigma_{\max} \exp[-(r - r_0)^2/\Delta r^2]$ , centered at a radius  $r_0$ . We represent the extended thin disk by a power-law surface density profile,  $\Sigma = \Sigma_0 (r_{\text{in}}/r)^{3/4}$ . For the viscosity parameters ( $\alpha_{\text{hot}}$ ,  $\alpha_{\text{cold}}$ ), the irradiation efficiency ( $C$ ), and the critical temperature ( $T_{\text{crit}}$ ) that determines the transition between the viscosity states, we use similar values to those obtained for other AXP and SGRs (Çalışkan & Ertan, 2012).

For Swift J1822.3–1606,  $r_{\text{LC}} = 4 \times 10^{10}$  cm, and the results of the long-term evolution model imply that  $r_{\text{in}}$  is close to  $r_{\text{LC}}$  in quiescence. We take the position  $r_0$  of the pile-up to be outside the light cylinder,  $r_0 > r_{\text{LC}}$ . X-ray enhancement light curves of the

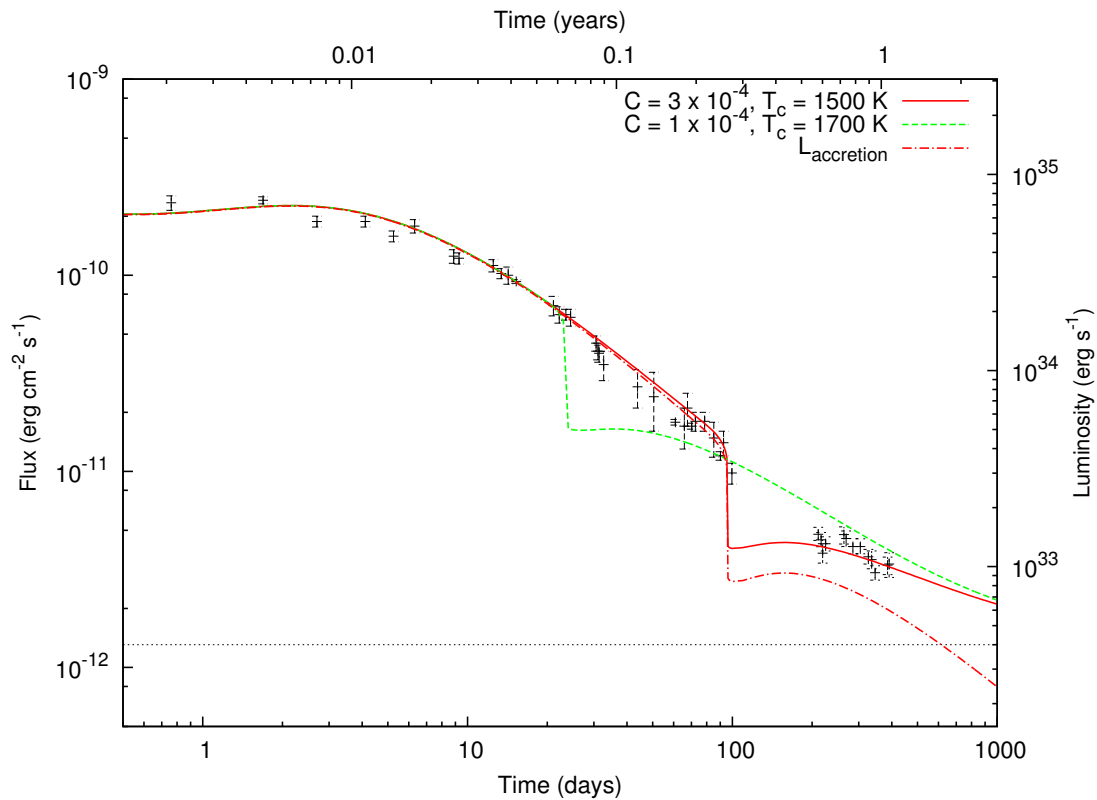


**Figure 2.3:** X-ray enhancement data of Swift J1822.3–1606. The data is taken from Rea et al. (2012) and . The luminosity is given on the right axis, assuming a distance of 1.6 kpc. Values of the parameters  $T_{\text{crit}}$  and  $C$  are given in the figure. For both models  $\alpha_{\text{hot}} = 0.1$ ,  $\alpha_{\text{cold}} = 0.045$  and  $B_0 = 1 \times 10^{12} \text{ G}$ . The abrupt decrease seen in the model curves are produced when the innermost disk enters the cold viscosity state (see the text for explanation). The accretion luminosity (dot-dashed line) and the level of cooling luminosity taken in the models (horizontal line) are also given separately in the figure.

model sources are not sensitive to the exact positions of  $r_0$ ,  $r_{\text{in}}$ , and the details of the Gaussian distribution, but sensitive to initial relative positions of these radii and the total mass included in the Gaussian distribution (Ertan, Göğüş & Alpar 2006, Çalışkan & Ertan 2012). In the simulations, we set  $r_0 = 4.1 \times 10^{10}$  cm, leaving  $\Sigma_{\text{max}}$  and  $\Delta r$ , which define the pile-up mass under the Gaussian, and  $r_{\text{in}}$  as free parameters. The enhancement light curve is given in Fig. 2.3.

The abrupt decrease in the decay phases of the model light curves seen in Fig. 2.3 occurs when the radial position of the hot - cold viscosity border of the disk with radius  $r_{\text{h}}$  approaches the inner disk radius. The innermost disk, which is rapidly depleted by the hot state viscosities, cannot be refilled by the matter in the cold viscosity state at the same rate, causing a sharp decrease in the luminosity. Subsequent refilling of the evacuated innermost disk leads to a small increase in the luminosity, followed by a smooth decay to the level of the cooling luminosity. This effect does not modify the X-ray light curve in the early decay phase, when  $r_{\text{h}}$  is not very close to  $r_{\text{in}}$ , since the surface density gradients and local variations in the mass-flow rate occurring at larger radii are smoothed out on the way to the inner disk radius. A detailed investigation of this feature on the model light curves for different quiescent luminosities can be found in Çalışkan & Ertan (2012).

For comparison with data, we adopt a distance of 1.6 kpc for Swift J1822.3–1606 (Scholz et al., 2012). In the luminosity calculation, we also add the contribution of the cooling luminosity. With  $L_{\text{cool}} = 4 \times 10^{32}$  erg s<sup>-1</sup>, we obtain a better fit to the last data points (Fig. 2.3). This is consistent with the estimated range of the quiescent luminosity of the source. For the  $\alpha$  parameters of the viscosity, we use the same values ( $\alpha_{\text{hot}} = 0.1$  and  $\alpha_{\text{cold}} = 0.045$ ) employed in the long-term evolution model (Section 2.2) and in the X-ray enhancement models of other AXP/SGRs (Çalışkan & Ertan, 2012). In Fig. 2.3, it is seen that the solid model curve is in good agreement with the X-ray data of Swift J1822.3–1606. For this model,  $C = 3 \times 10^{-4}$  and  $T_{\text{crit}} = 1500$  K. The cooling luminosity (horizontal line) and the accretion luminosity,  $L_{\text{acc}}$ , curves are also presented separately in Fig. 2.3. The accretion continues even after  $L_{\text{acc}}$  decreases below  $L_{\text{cool}}$  and converges to its quiescent level, or it could stop at a critical  $L_{\text{acc}}$  depending on the dipole field strength and the current period of the source. For the allowed  $B_0$  range obtained from the long-term evolution model, and with the condition  $r_{\text{A}} = r_{\text{LC}}$  for termination of accretion, this critical accretion luminosity could be  $\sim 10^{30}$  erg s<sup>-1</sup>.

## 2.4 Discussion and Conclusion

Comparing the results of the X-ray enhancement and the long-term evolution models, we try to understand the properties of Swift J1822.3–1606 in the quiescent state. In our long-term evolution model, the magnitude and  $\dot{M}_{\text{in}}$  dependence of the disk torque are quite different during and after the accretion phase. In the accretion phase, the disk torque given in Equation (2.1) has a weak dependence on  $\dot{M}_{\text{in}}$ , and  $\dot{P}$  remains constant close to its maximum value provided that the source does not come close to rotational equilibrium. For the model sources given in Figs 2.1 and 2.2, the time intervals with constant  $\dot{P}$  correspond to this phase. In the model, the accretion phase terminates when  $r_{\text{A}} = r_{\text{LC}}$ , afterward  $r_{\text{in}}$  remains attached to  $r_{\text{LC}}$ . For this phase, from Equation (2.1), we obtain  $\dot{P} \propto \dot{M}_{\text{in}}$ .

Our results show that the X-ray enhancement light curve of Swift J1822.3–1606 could be explained by additional enhanced mass flow from the inner disk onto the surface of the star. This does not guarantee that the source is in the accretion phase in the quiescent phase. It is possible that the source could currently be in a transient accretion phase that could come to an end when the accretion luminosity decreases below a critical level depending on the dipole field strength of the source. To sum up, from the observed properties of the source in the current enhancement phase, we do not know whether the star accretes matter in quiescence.

At present, in the enhancement phase, the evolution of  $\dot{P}$  depends on the state of the source in quiescence: (1) if the star is accreting matter in the quiescent state, the currently observed  $\dot{P}$  remains roughly constant while the accretion luminosity is gradually decreasing to the quiescent level, (2) if the source does not accrete in quiescence, it is now in a transient accretion phase; accretion stops at a critical  $\dot{M}_{\text{in}}$ , and subsequently  $\dot{P}$  starts to decrease with decreasing  $\dot{M}_{\text{in}}$ . Note that, for case (2),  $\dot{P}$  of the source in quiescence could be much lower than in the enhancement phase.

First, we consider the case that the source was not in the accretion phase before the onset of the X-ray enhancement. In Fig. 2.1, the illustrative model curves with  $B_0$  values  $1.74$  and  $3.0 \times 10^{12}$  G give very high  $\dot{P}$  values in the accretion phase and could be eliminated. Let us consider the long-term evolution represented by the dotted (red) curve with  $B_0 = 1 \times 10^{12}$  G in Fig. 2.1. The long-term accretion phase of this model source

ends at point B shown on the  $\dot{P}$  curve (bottom panel). Note that the period is less than the observed period (8.4 s) of Swift J1822.3–1606 at point B. In the quiescent phase, the source could be at a point on the decay phase of  $\dot{P}$ , say at point A seen on the  $\dot{P}$  curve with  $P \simeq 8.4$  s. After the burst epoch, with enhanced mass-flow rate, the inner disk penetrates the light cylinder, which begins accretion, thus causing the onset of the X-ray enhancement phase.  $\dot{P}$  increases to a level close to its maximum value reached earlier during the long-term accretion phase. As long as the inner disk remains inside the light cylinder ( $r_{\text{in}} = r_{\text{A}}$ ),  $\dot{P}$  remains constant. After  $\dot{M}_{\text{in}}$  decreases below the level corresponding to the critical condition  $r_{\text{A}} = r_{\text{LC}}$ , accretion stops, while  $\dot{P}$  decreases gradually with decreasing  $\dot{M}_{\text{in}}$  converging to its quiescent level indicated by point A on this illustrative model curve (Fig. 2.1).

Here, we assume that in the transient accretion event, the disk can build up the boundary layer conditions prevailing in the steady-state long-term accretion phase. A transient accretion may take place with a less efficient disk torque acting on the star than in the long-term accretion epoch. In this case, observed rotational properties do not give information about the maximum  $\dot{P}$  of the long-term evolution, and none of the model curves given in Fig. 2.1 can be excluded, since they all reproduce the period and the X-ray luminosity of Swift J1822.3–1606 simultaneously.

Alternatively, in quiescence, the source could already be in the accretion phase. If that is the case, then we expect that the source will continue to remain in the accretion state until the long-term accretion phase terminates without a significant change in  $\dot{P}$ . The model curve given in Fig. 2.2 illustrates a long-term evolution of this type. This model source continues to accrete matter when  $P$  reaches the observed value. Now, it is close to the end of the long-term accretion phase with an accretion luminosity that remained below the cooling luminosity a few  $10^4$  yr ago. For this alternative scenario, our model cannot produce the source properties if the actual  $\dot{P}$  is less than  $\sim 6 \times 10^{-13} \text{ s s}^{-1}$ .

The condition  $r_{\text{A}} = r_{\text{LC}}$  to terminate the accretion phase is a simplification of our model. The accretion could stop earlier when  $r_{\text{A}}$  increases gradually to some fraction of  $r_{\text{LC}}$ , and the phase with  $\dot{P} \propto \dot{M}_{\text{in}}$  could start at an earlier epoch. This does not affect the qualitative features of the long-term model curves, but increases the critical mass-flow rate of the disk below which we expect significant torque variations with decreasing  $\dot{M}_{\text{in}}$ . In the late decay phase of the enhancement, the accretion luminosity,  $L_{\text{acc}}$ , decreases

and the viscous timescale of the inner disk increases. It is not possible to observe the decrease in  $L_{\text{acc}}$  once it falls below  $L_{\text{cool}}$ . The expected decrease in  $\dot{P}$  would be observed without a significant accompanying change in the X-ray luminosity. If  $r_{\text{A}} = r_{\text{LC}}$  is a close representation of the condition for the onset of accretion, it may take decades for  $r_{\text{A}}$  to reach  $r_{\text{LC}}$  and terminate accretion in view of the long period of the source (8.4 s), which gives  $r_{\text{LC}} = cP/2\pi \simeq 4 \times 10^{10}$  cm. If accretion stops for a smaller  $r_{\text{A}}$ , the effect could be observable within years.

In alternative models (see, e.g., Pons & Rea 2012), the X-ray enhancement light curve of Swift J1822.3–1606 is produced by cooling of the neutron star’s crust that is heated by the mechanism producing soft gamma bursts.

We have shown that both the X-ray enhancement light curve and the long-term evolution of Swift J1822.3–1606 can be explained in the frame of the fallback disk model. Main disk parameters used in the present work are very similar to those employed in earlier work to explain the X-ray enhancements and the evolution of AXP and SGRs (Alpar, Ankay & Yazgan 2001, Ertan et al. 2009, Çalışkan & Ertan 2012, Çalışkan et al. 2013). The model sources with the dipole field strength in the  $0.5 - 1.0 \times 10^{12}$  G range on the pole of the star and with the initial periods greater than  $\sim 55$  ms can reach the X-ray luminosity and the rotational properties of Swift J1822.3–1606 simultaneously.

We conclude that the source is accreting matter from the disk at present in the X-ray enhancement phase. Accretion could persist after the enhancement phase with the accretion luminosity decaying to quiescent level that could remain below the cooling luminosity. A more interesting possibility is that the mass transfer onto the star could stop at a critical accretion rate, and subsequently the disk torque and the  $\dot{P}$  of the source could start to decrease in proportion to decreasing mass-flow rate arriving at the inner disk. In this phase, since the accretion luminosity remains below the cooling luminosity, variation in  $\dot{P}$  could be observed without a significant change in the observed luminosity of the source.

# Chapter 3

## LONG-TERM EVOLUTION, X-RAY OUTBURST AND OPTICAL/IR EMISSION OF SGR 0501+4516

This chapter was published in *Monthly Notices of the Royal Astronomical Society*, 2015, Volume 447, Issue 3, pp. 2282-2286.

**Onur Benli, Şirin Çalışkan & Ünal Ertan**

Some parts of the Sections 3.1 and 3.2 were removed or modified.

### 3.1 Introduction

SGR 0501+4516 was discovered by *Swift*–*BAT* during a burst episode starting from 2008 August 22 (Barthelmy et al., 2008; Holland et al., 2008). The source was observed by *RXTE* following the *Swift* detection and a period of 5.762067(2) s was found from the coherent X-ray pulsations (Göğüş, Woods & Kouveliotou, 2008). The source also showed optical pulsations with a period of  $5.7622 \pm 0.0003$  s which is in good agreement with the X-ray spin period (Dhillon et al., 2011). The subsequent observations with combined *RXTE/PCA*, *Swift/XRT*, *CXO/ACIS-S* and *XMM-Newton/EPIC-PN* observations revealed a period derivative of  $\dot{P} \simeq 5.8 \times 10^{-12} \text{ s s}^{-1}$  (Göğüş et al., 2010).

The minimum distance to SGR 0501+4516 is estimated to be  $\sim 1.5$  kpc based on a likely association of the source with the supernova remnant HB9 (Aptekar et al., 2009). We have converted the observed X-ray flux into the X-ray luminosity assuming that the source lies at a distance in the 1.5–5 kpc range. A blackbody plus a power-law model fitted well to the quiescent soft X-ray spectrum of SGR 0501+4516 (Camero et al., 2014). The best-fitting parameters are  $kT = 0.52 \pm 0.02$  keV with a blackbody radius of  $0.39 \pm 0.05$  km,  $N_{\text{H}} = 0.85(3) \times 10^{22} \text{ cm}^{-2}$  and the power law index  $\Gamma = 3.84 \pm 0.06$ . The bolometric luminosities obtained from these models are  $4.7 \times 10^{33} \text{ erg s}^{-1}$  and  $5.2 \times 10^{34} \text{ erg s}^{-1}$  for distances 1.5 and 5 kpc.

In the present work, we analyze both the enhancement light curve and the long-term evolution of SGR 0501+4516 with the fallback disc model. We also compare the estimated optical/infrared (IR) flux of the disc with the observed data. We describe the model parameters briefly, and give the results for the short-term and the long-term evolution models in Sections 3.2 and 3.3 respectively. Properties of SGR 0501+4516 indicated by our results are discussed and compared to those of the low-B magnetars and ‘high-B radio pulsar’ PSR J1734–3333. There is a summary of our conclusions in Section 3.4.

### 3.2 Long-Term Evolution of SGR 0501+4516

In this section, we investigate the long-term X-ray luminosity and rotational evolution of SGR 0501+4516 with a fallback disc (for details and applications of this model see Ertan et al. (2009); Alpar, Ertan & Çalışkan (2011); Benli et al. (2013); Çalışkan et al.

(2013). We solve the diffusion equation for a geometrically thin disc. The disc evolves interacting with the dipole field of the neutron star. When the inner disc can penetrate the light cylinder, we take the inner disc radius,  $r_{\text{in}}$ , to be equal to the Alfvén radius,  $r_{\text{A}} \cong (GM)^{-1/7} \mu^{4/7} \dot{M}_{\text{in}}^{-2/7}$  where  $\dot{M}_{\text{in}}$  is the rate of mass-flow to the inner disc,  $\mu$  is the magnetic dipole moment and  $M$  is the mass of the neutron star. When  $r_{\text{A}}$  is found to be greater than the light-cylinder radius,  $r_{\text{LC}}$ , we set  $r_{\text{in}} = r_{\text{LC}}$ . The disc evolves under the effect of the X-ray irradiation. At a given time during the evolution, the disc is viscously active from  $r_{\text{in}}$  to the radius  $r_{\text{out}}$  at which the effective temperature is currently equal to the minimum critical temperature  $T_{\text{p}}$ . During the long-term evolution,  $r_{\text{out}}$  propagates inward with decreasing X-ray irradiation flux that is defined through  $F_{\text{irr}} = C\dot{M}c^2/(4\pi r^2)$  (Shakura & Sunyaev, 1973) where  $c$  is the speed of light,  $\dot{M}$  is the accretion rate on to the neutron star and  $C$  is the X-ray irradiation efficiency parameter. The X-ray and IR analysis of AXP/SGRs in quiescence constrains  $C$  into the  $1-7 \times 10^{-4}$  range (Ertan & Çalışkan, 2006). In our earlier work, we obtain reasonable model curves with the minimum temperature of the active disc  $T_{\text{p}} \sim 100$  K.

We use the torque model described in Ertan & Erkut (2008). See also Chapter 1 for the model description. The initial parameters of the model are the dipole field strength on the pole of the star,  $B_0$ , the disc mass,  $M_{\text{d}}$ , and the initial period  $P_0$ .

The model curves given in Fig. 3.1 are obtained for distances 1.5 and 5 kpc with the disc masses  $1.8 \times 10^{-6}$  and  $1.8 \times 10^{-5} M_{\odot}$  respectively. Independent of the disc mass, the dipole field strength on the pole of the star is well constrained to a narrow range with  $B_0 \simeq 1.4 \times 10^{12}$  G which is more than two orders of magnitude weaker than that inferred from the dipole torque formula. Since the source does not come close to the rotational equilibrium,  $\dot{P} \propto B_0^2$  and remains almost constant in the accretion phase (see e.g. Çalışkan et al. 2013 for the  $\dot{P}$  behaviour in different phases of evolution). It is seen in Fig. 3.1 that the X-ray luminosity (upper panel), the period (middle panel) and the period derivative (bottom panel) are reached simultaneously by the model sources in the accretion phase at an age  $\sim 3 \times 10^4$  yr which is about 2 times greater than the characteristic age ( $P/2\dot{P}$ ) of SGR 0501+4516. The source could remain in the accretion phase (constant  $\dot{P}$  phase) until an age  $\sim 2-5 \times 10^5$  yr depending on its actual initial disc mass. The accretion epoch terminates when the inner disc cannot penetrate the light cylinder, and the system enters the tracking phase with  $r_{\text{in}} = r_{\text{LC}}$ . During the tracking phase,  $\dot{P}$  decreases

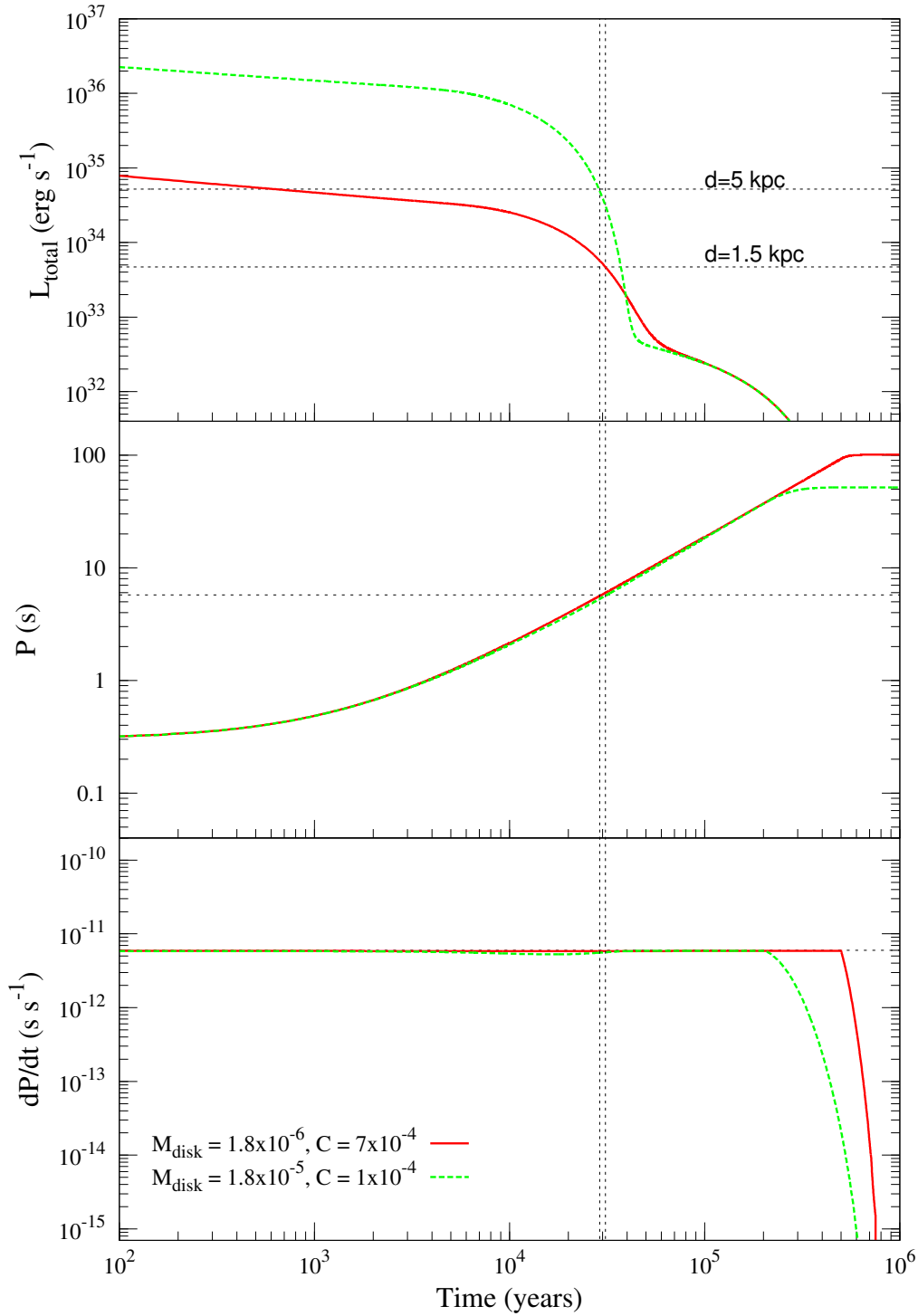


**Figure 3.1:** Illustrative model curves that can represent the long-term evolution of SGR 0501+4516. The model sources are still accreting at present. The dipole field strength  $B_0 \simeq 1.4 \times 10^{12}$  G for both models. The disc masses in solar mass and the values of the irradiation parameter  $C$  are given in the bottom panel. Horizontal dotted lines show the properties of SGR 0501+4516. The lower and upper limits in the luminosity correspond to distances of  $\sim 1.5$  and  $5$  kpc.

with decreasing  $\dot{M}_{\text{in}}$ , that is, the maximum  $\dot{P}$  is obtained in the accretion phase.

It is also possible that some of the sources could start their evolution in the tracking phase with an inefficient torque. Whether these sources can enter the accretion phase at a later time of evolution depends on the initial period,  $P_0$ , for a given dipole field and disk mass. If  $P_0$  is below a minimum critical value the disk torque cannot sufficiently slow-down the neutron star such that the inner disk can never penetrate the light cylinder in the active lifetime of the disk. In this case,  $\dot{P}$  decreases continuously converging to the  $\dot{P}$  level of the dipole torque. These sources are likely to become radio pulsars following an evolutionary track rather different from those of accreting sources (see Fig. 3.2).

In the simulations, we take the initial period  $P_0 = 300$  ms. The long-term evolution of a model source is not sensitive to  $P_0$  provided that the star enters the long-term accretion phase. The model light curves shown in Fig. 3.2 illustrate evolutions with different  $P_0$  values. We repeat the simulations tracing the  $P_0$  values to find the minimum  $P_0$  that allows the onset of the accretion. We find that the minimum  $P_0$  for SGR 0501+4516 is  $\sim 60$  ms (see Fig. 3.2).

For SGR 0501+4516 assuming that the inner disc extends down to the co-rotation radius, we estimate  $i'$ ,  $u'$ ,  $g'$  and  $K$  band fluxes for a distance of 1.5 kpc using the model described in Ertan & Çalışkan (2006). For  $N_{\text{H}} = 10^{22} \text{ cm}^{-2}$  (Rea et al., 2009) we have converted the observed magnitudes when the X-ray luminosity is close to the quiescent level [ $i' = 24.4 \pm 0.4$ ,  $u' > 24.7$ ,  $g' > 26.9$ ,  $K = 19.7 \pm 0.1$  (Dhillon et al., 2011)] into the unabsorbed flux values. It is seen in Fig. 3.3 that the irradiated fallback disc model is in good agreement with optical/IR data. We obtain the model fluxes given in Fig. 3.3 with  $C = 1 \times 10^{-4}$  and  $\dot{M} = 1.4 \times 10^{14} \text{ g s}^{-1}$  which are consistent with long-term evolution and the short-term X-ray enhancement models within the distance uncertainties (see Fig. 3.1).

### 3.3 X-ray Outburst of SGR 0501+4516

The details and applications of our X-ray enhancement model (see also 2.3) can be found in Çalışkan & Ertan (2012). The model can be summarized as follows: The disc in the quiescent state mimics a steady state geometrically thin disc and evolves with  $r_{\text{in}} = r_{\text{A}}$ . Part of the energy emitted during a burst episode moves the inner disc matter to a larger

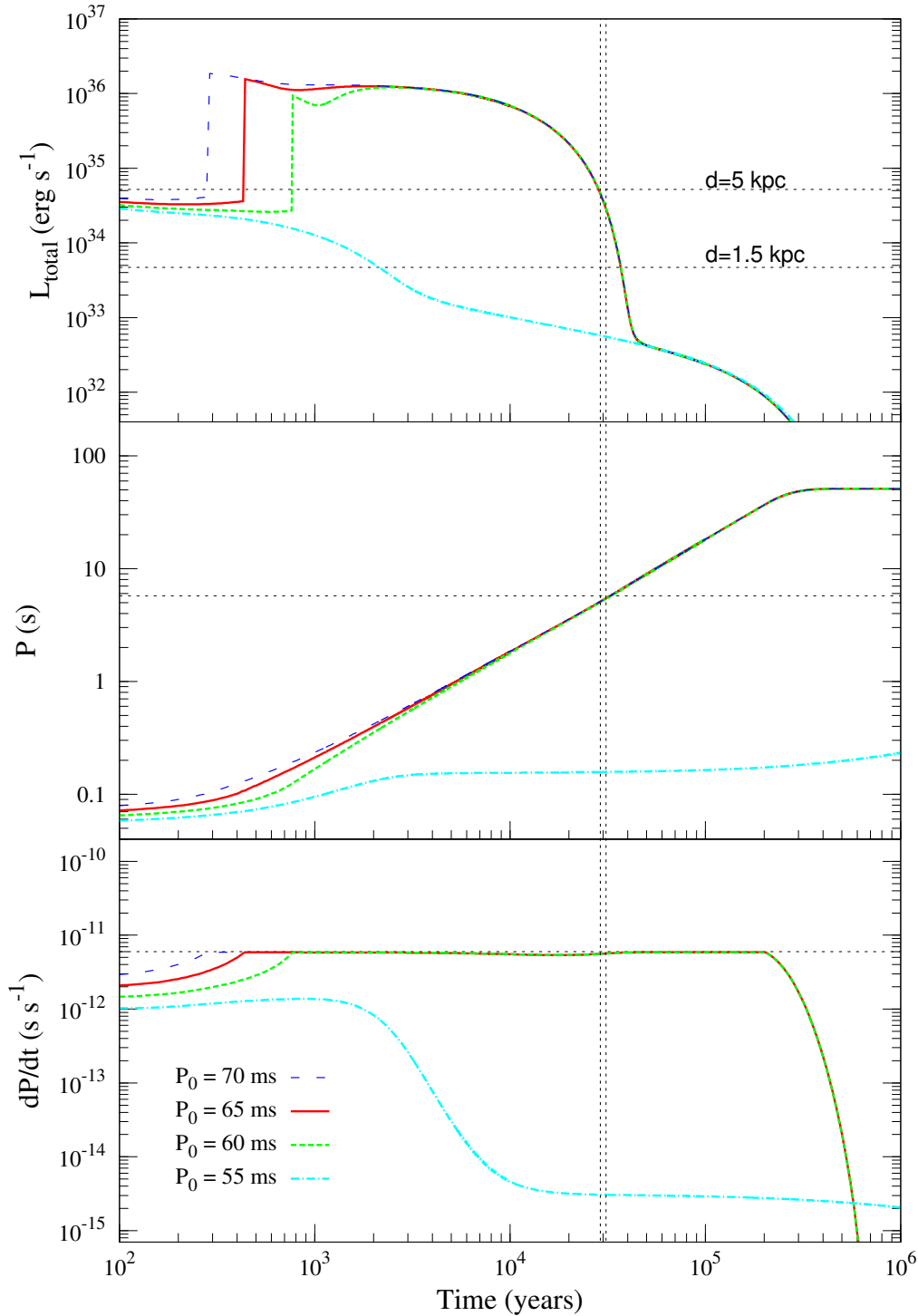


**Figure 3.2:** Model curves with the same parameters as those of the dashed curve in Fig. 3.1, but with different initial periods ( $P_0$ ) given in the bottom panel. It is seen that the model results are not sensitive to  $P_0$  if  $P_0 \gtrsim 60$  ms. For lower values of  $P_0$ , the sources cannot enter the light cylinder and are likely to evolve as radio pulsars that cannot reach the properties of SGR 0501+4516.

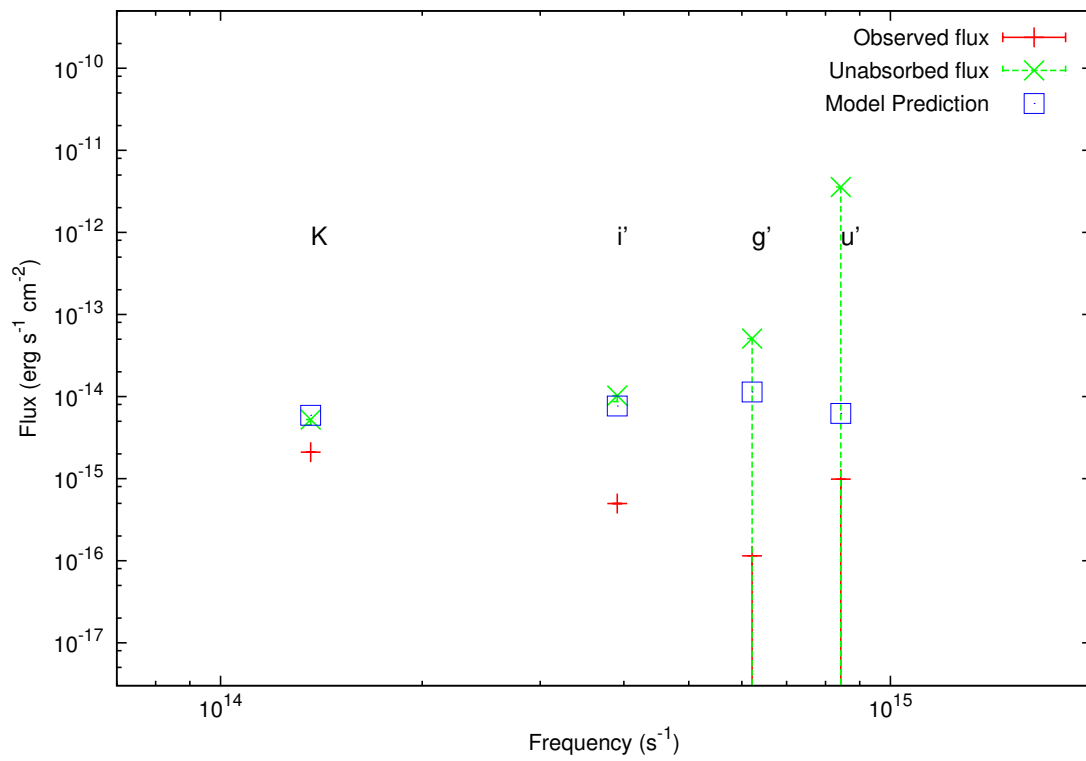


**Figure 3.3:** Optical/IR emission of SGR 0501+4516. The blue boxes show the model predictions of an irradiated fallback disc in four different energy bands.  $\dot{M}_{\text{in}} = 1.4 \times 10^{14} \text{ g s}^{-1}$ , disc inclination angle is  $\sim 70^\circ$  and irradiation efficiency  $C = 10^{-4}$ . For the bands  $g'$  and  $u'$  the data show  $3\sigma$  upper limits.

radius. This causes the inner disc mater to pile-up at the inner disc which we represent by a Gaussian mass distribution as the initial condition in our model. The evolution of this density gradient first leads to an abrupt increase in the mass-flow rate of the inner disc, the accretion rate on to the star and thus the X-ray luminosity. Subsequently, the X-ray luminosity decreases with a rate governed by the viscous relaxation of the disc yielding the decay phase of the X-ray luminosity.

Early decay phase ( $\sim 150$  d) of the X-ray outburst of SGR 0501+4516 was investigated earlier by Çalışkan & Ertan (2012). With the addition of the new data, covering the time period from  $\sim 150$ –600 d after the burst (Camero et al., 2014), we revisited the model fits, to test the model predictions from the maximum to the end of the decay phase. The available absorbed data for the first  $\sim 150$  d of the decay phase were obtained from different satellites, and with fits to different spectral models. Due to difficulties in obtaining the unabsorbed X-ray data of this source in a systematic way, Çalışkan & Ertan (2012) used the absorbed X-ray data considering also that the absorption does not significantly affect the light curve close to the peak of the outburst when the X-ray luminosity and the temperatures are sufficiently high.

From 150 to 600 d of the decay phase, the X-ray light curve gradually decreased to the quiescent X-ray flux level of the source (Camero et al., 2014). In this late decay phase, increasing absorption with decreasing luminosity probably alters the light curve morphology significantly. In the present work, we use only the six XMM-Newton unabsorbed X-ray data points of SGR 0501+4516 covering the whole decay phase. A similar study was also done by Camero et al (2014, Fig. 11) applied to the outburst model of Pons & Rea (2012). The first five data points are taken from Rea et al. (2009) and the sixth data point is taken from Camero et al. (2014).

Figs. 3.4 and 3.5 show the 0.5–10 keV unabsorbed flux of SGR 0501+4516 obtained from the six XMM-Newton observations of the source together with our model fits for the distances 1.5 and 5 kpc respectively. For a given distance, we give model curves for two different irradiation efficiencies (red solid and green dashed). It is seen in Figs. 3.4 and 3.5 that the model light curves are in very good agreement with the X-ray data.

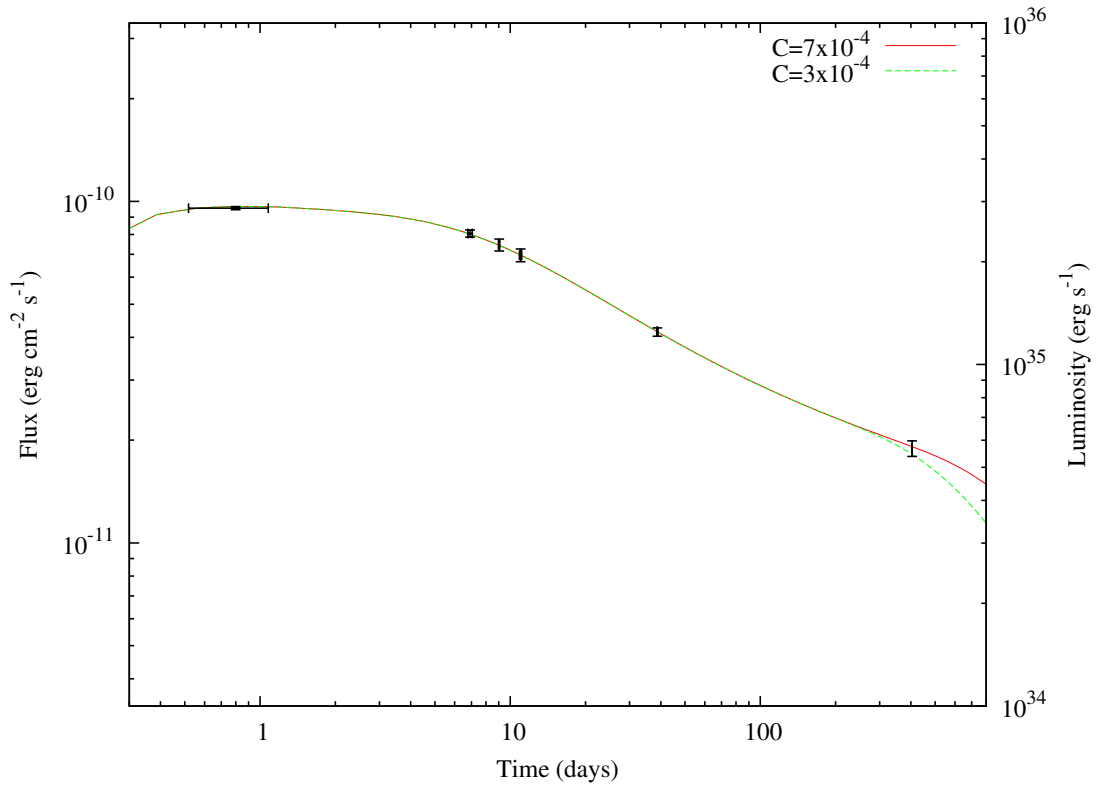


**Figure 3.4:** X-ray outburst decay lightcurve of SGR 0501+4516. The unabsorbed 0.5–10 keV flux data points are from XMM-Newton observations. The first five data points are taken from Rea et al. (2009) and the sixth data point is taken from Camero et al. (2014). The X-ray luminosity is calculated assuming a distance of 5 kpc. The horizontal error bar of the first data point denotes the time interval of observation.

**Table 3.1:** The parameters for the models presented in Fig. 3.4 and 3.5. The basic disc parameters  $\alpha_{\text{hot}} = 0.1$ ,  $\alpha_{\text{cold}} = 0.045$ ,  $T_{\text{crit}} = 1750$  K are the same for the model curves given in Figs. 3.4 and 3.5. The irradiation efficiency  $C = 7 \times 10^{-4}$  for  $d = 1.5$  kpc and  $C = 3\text{--}7 \times 10^{-4}$  for  $d = 5$  kpc give good fits to data. See Çalışkan & Ertan (2012) for a detailed explanation of the model parameters.

Parameter	$d = 1.5$ kpc	$d = 5$ kpc
$r_{\text{in}}$ (cm)	$3.1 \times 10^9$	$3 \times 10^9$
$r_0$ (cm)	$6 \times 10^9$	$6 \times 10^9$
$\Delta r$ (cm)	$7 \times 10^8$	$3 \times 10^9$
$\Sigma_{\text{max}}$ ( $\text{g cm}^{-2}$ )	4.1	14.4
$\Sigma_0$ ( $\text{g cm}^{-2}$ )	2.7	13.1
$C$	$7 \times 10^{-4}$	$3\text{--}7 \times 10^{-4}$

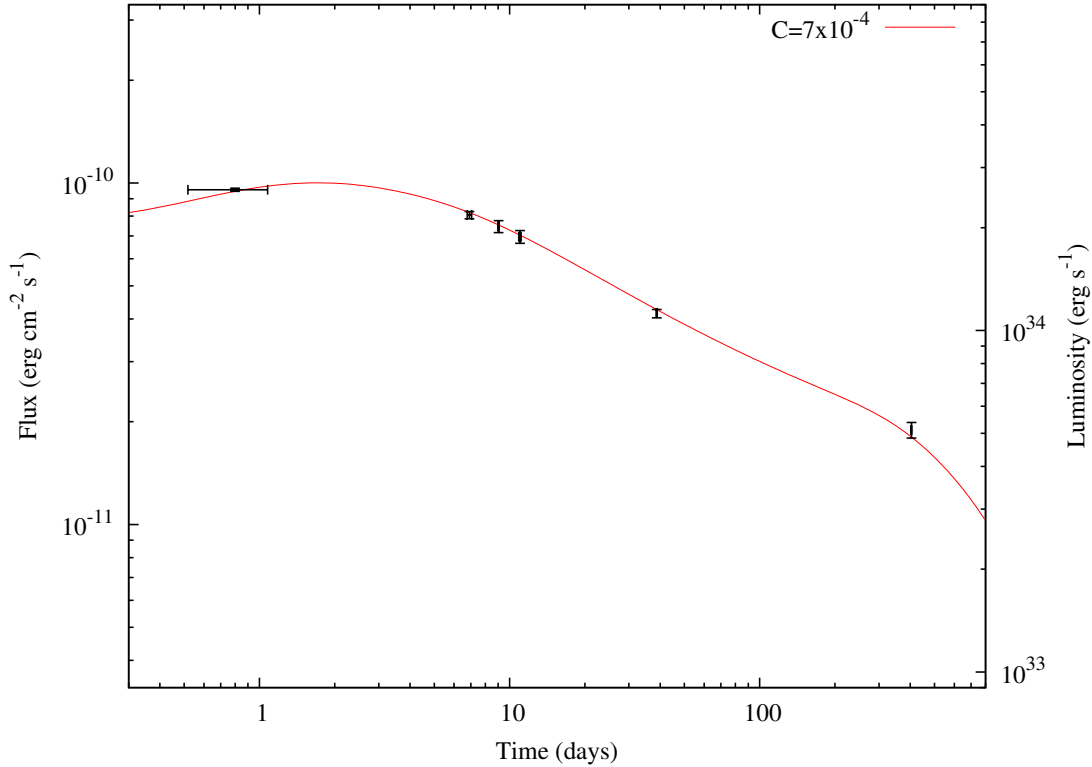


**Figure 3.5:** The same as Fig. 3.4, but for a source distance of 1.5 kpc. This model curve is obtained with the irradiation efficiency  $C = 7 \times 10^{-4}$ . Smaller irradiation efficiencies do not give reasonable fits for this particular distance.

We note that the viscosity parameters  $\alpha_{\text{cold}}$  and  $\alpha_{\text{hot}}$ , irradiation strength  $C$  and the critical temperature  $T_{\text{crit}}$  are the basic disc parameters that are expected to be the same for different AXP/SGRs in the same accretion regime within the distance uncertainties. For comparison with the results obtained by Çalışkan & Ertan (2012), we present our model parameters in Table 3.1.

### 3.4 CONCLUSIONS

We have investigated the possible long-term evolutionary scenarios and the short-term X-ray outburst light curve of SGR 0501+4516 in the fallback disc model. Our results show that a neutron star with a fallback disc and with a dipole field strength of  $\sim 1.4 \times 10^{12}$  G on the pole of the star acquires the X-ray and rotational properties of SGR 0501+4516 in  $\sim 3 \times 10^4$  yr. We have also shown that the X-ray enhancement light curve of the source can be reproduced by the evolution of the inner disc after the soft gamma burst episode.

For both the long-term evolution and the X-ray enhancement models, the source properties are achieved with the same basic parameters used earlier to explain the enhancement curves of other AXP/SGRs (Çalışkan & Ertan, 2012) and the long-term evolution of ‘high-B radio pulsar’ PSR J1734–3333, the low-B magnetars and the dim isolated neutron stars (Ertan et al., 2014). This indicates that in the fallback disc model, all these apparently rather different sources are actually neutron stars with fallback discs and conventional dipole fields in different phases of their long-term evolution. The model is also consistent with the radio properties of these sources. For PSR J1734–3333, our results imply that the source is evolving in the early phase before the onset of accretion with a rotation rate sufficiently high for radio emission. The low-B magnetars, like dim isolated neutron stars (Ertan et al., 2014), are evolving in the tracking phase after the accretion epoch, and located below the pulsar death line on the  $P$ – $B$  plane.

For SGR 0501+4516, we do not expect pulsed radio emission, since the source is currently accreting matter from the fallback disc. Our results indicate that this source will find itself below the pulsar death line at the end of its accretion phase. Even at present, if accretion is hindered by any reason, the rotational rate of the source with  $B_0 \sim 1.4 \times 10^{12}$  G is not sufficient to produce pulsed radio emission.

Furthermore, we have shown that the observed optical/IR properties of SGR 0501+4516 are in agreement with the spectrum expected from a fallback disc with current properties indicated by our long-term evolutionary model.

# Chapter 4

## LONG-TERM EVOLUTION OF DIM ISOLATED NEUTRON STARS

This chapter was published in *Monthly Notices of the Royal Astronomical Society*, 2014, Volume 444, Issue 2, pp. 1559-1565.

**Ünal Ertan, Şirin Çalışkan, Onur Benli & Mehmet Ali Alpar**

Some parts of the introduction were removed or modified.

## 4.1 Introduction

Considering the estimated birth rates of young neutron star populations together with the galactic supernova rate, it is likely that there are evolutionary connections between some of these populations (Keane & Kramer, 2008). Recent efforts concentrate on the unification of the long-term X-ray luminosity and the rotational evolution of these neutron star systems in a single picture. With the assumption that these sources are evolving in vacuum with dipole torques, their surface dipole fields,  $B$ , inferred from the dipole torque formula range from  $\sim 10^{10}$  G for CCOs to more than  $10^{15}$  G for AXP/SGRs. In this picture, the diversity of evolutionary paths is attributed to the differences in the initial dipole and the crustal toroidal fields of the sources (Kaspi, 2010). In the magnetar model, the apparently missing link between CCOs and other classes was suggested to be due to field burial to the crust by the accretion of the supernova matter in the early phase of evolution (Viganò & Pons, 2012). The timescale for the subsequent re-emergence and the growth of the field to its original strength is estimated to be  $10^3 - 10^5$  yr depending on the initial conditions by the same authors. The dipole field's decay is supposed to proceed after the initial burial and re-emergence. If there are fallback disks around these systems the picture is rather different. It was proposed by Alpar (2001) that the source properties, in particular the period clustering, could be explained by the presence (or absence) and the properties of fallback disks around these systems. Fallback disk models do not involve burial, re-emergence or decay of the dipole field, which is taken to be constant at its initial value.

Our earlier results obtained from the application of the same model with similar basic parameters to sources with rather different observational properties, encourages us to investigate the evolution and possible evolutionary links between AXP/SGRs (see Mereghetti 2008, 2011 for recent reviews) and other young neutron star populations. This will help us understand the differences in the initial conditions that lead to emergence of different classes of neutron stars. In particular, understanding whether there is a relation between the disk masses and the dipole field strengths requires detailed investigations of AXP/SGRs and other young neutron star populations. In the present work, we concentrate on the dim isolated neutron stars (XDINs).

At present, there are seven known dim isolated neutron stars (Haberl, 2007; Turolla,

2009). All these sources lie within a distance of  $\sim 400$  pc. Since the solar neighborhood is part of the Gould Belt, a ring of young stellar systems, the relatively high rate of supernova events in the Gould Belt should be taken into account in estimating the birth rate of XDINs. In the vicinity of the Sun, about two thirds of the neutron stars are born in the Gould Belt, while the remaining fraction belongs to the Galactic disk (Grenier, 2000). Assuming the ages of XDINs are  $\sim 1$  Myr, simple statistical calculations give a galactic birth rate of  $\sim 1 \text{ century}^{-1}$  (Popov, Turolla & Possenti, 2006). The thermal X-ray luminosities of XDINs are in the  $10^{31} - 10^{32} \text{ erg s}^{-1}$  range. The ages corresponding to these luminosities on the theoretical cooling curves are a few  $10^5$  yr. Kinematic ages of four XDINs estimated from the space velocities and likely birth places are, with large uncertainties, in the range of  $\sim 0.1 - 1$  Myr (Motch et al., 2009; Tetzlaff et al., 2010; Mignani et al., 2013). These kinematic ages and the cooling ages estimated from the X-ray luminosities of XDINs, imply that the characteristic ages, estimated assuming isolated pulsar spin-down,  $P/2\dot{P} \sim 1 - 4$  Myr, could be significantly greater than the true ages of these sources.

XDINs do not show pulsed radio emission. Weak radio emission from two sources were reported (Malofeev, Malov & Teplykh, 2007), but not confirmed yet (Haberl, 2007; Turolla, 2009). Strength of the surface dipole fields of XDINs inferred from the dipole torque formula are  $\sim 10^{13} - 10^{14}$  G. If these sources are indeed evolving in vacuum with dipole torques, many of them should be active as radio pulsars. Nondetection of radio pulses from these sources might be due to narrow beaming angles of long-period systems. It is not clear why a large population of galactic XDINs with rotational properties of the known sources do not show up as radio pulsars. Alternatively, these sources may not have sufficiently strong dipole fields for radio emission. Our results support the latter possibility.

In the present work, we try to explain the long-term evolution of XDINs in the frame of the fallback disk model. We also discuss the radio properties of XDINs based on the predictions of our evolutionary model. We briefly describe the model in Section 4.2. The results of the simulations are given in Section 4.3. We summarize our conclusions in Section 4.4.

## 4.2 Model

We use the code developed to investigate the long-term evolution of AXPs and SGRs (see Ertan & Erkut 2008; Ertan et al. 2009; Alpar, Ertan & Çalışkan 2011; Çalışkan et al. 2013 for details and applications). We examine the period, the period derivative and the total X-ray luminosity evolution of the model sources, tracing the initial conditions, namely the initial period,  $P_0$ , strength of the magnetic dipole field on the pole of the star,  $B_0$ , and the initial disk mass,  $M_d$ . In addition to these initial parameters, the evolution is also affected by the irradiation efficiency  $C$  and the minimum critical temperature,  $T_p$ , for the disk to be viscously active. The magneto-rotational instability (Balbus & Hawley, 1991) which generates the turbulent viscosity needed for the disk to transport mass and angular momentum will not work at temperatures below  $T_p$ , because the ionization fraction becomes too small.

The Alfvén radius of the disk could be written as

$$r_A \simeq (GM)^{-1/7} \mu^{4/7} \dot{M}_{\text{in}}^{-2/7} \quad (4.1)$$

(Lamb, Pethick & Pines, 1973; Davidson & Ostriker, 1973) where  $G$  is the gravitational constant,  $M$  and  $\mu$  are the mass and magnetic dipole moment of the neutron star, and  $\dot{M}_{\text{in}}$  is the mass-flow rate arriving at the inner disk radius,  $r_{\text{in}}$ . When  $r_A$  is less than the light cylinder radius,  $r_{\text{LC}} = c/\Omega_*$ , we take  $r_{\text{in}} = r_A$ . Accretion will take place in this regime. Typically for the sources we consider, in the accretion phase  $r_{\text{in}} < r_{\text{LC}}$  and the inner disk radius is greater than the co-rotation radius,  $r_{\text{in}} > r_{\text{co}} = (GM/\Omega^2)^{1/3}$ . The star is in the propeller phase, spinning down under the disk torques while accreting. Over the long-term evolution,  $r_{\text{LC}}$  increases with decreasing angular frequency of the neutron star,  $\Omega_*$ , while  $r_A$  increases with decreasing  $\dot{M}_{\text{in}}$ . When  $r_A$  calculated by equation (4.1) is found to be greater than the current value of  $r_{\text{LC}}$ , we set  $r_{\text{in}} = r_{\text{LC}}$ . In this “propeller phase”, we assume that there is no accretion onto the neutron star.

We solve the diffusion equation for an extended disk with an initial surface-density distribution in the power-law form,  $\Sigma(r) \propto r^{-3/4}$ , which is the characteristic surface-density profile for steady thin accretion disks (see e.g. Frank, King & Raine 2002). At a given time, the temperature in the disk decreases with increasing radial distance  $r$  from the center. At a given  $r$ , the temperature decreases with time because of fallback disk

evolution and decreasing irradiation strength. In the calculations, for numerical reasons, we start with  $r_{\text{out}} = 5 \times 10^{14}$  cm. After the first time step, the radius at which the disk temperature is as low as the minimum temperature  $T_p$  for the disk to be active is identified as the dynamical outer radius,  $r_{\text{out}}$ , of the viscously active disk. As the temperatures, starting from the outermost disk, decrease below  $T_p$ ,  $r_{\text{out}}$  propagates inward. The X-ray irradiation of the disk is important in the evolution of the neutron star, since it prolongs the lifetime of the disk by delaying the inward propagation of  $r_{\text{out}}$ . X-ray irradiation flux can be written as  $F_{\text{irr}} = C \dot{M} c^2 / (4\pi r^2)$  (Shakura & Sunyaev, 1973) where  $c$  is the speed of light. From the results of our earlier work on the IR and X-ray emission of persistent AXP/SGRs (Ertan & Çalışkan, 2006), we found the value of the irradiation efficiency  $C$  to be in the range of  $\sim 1 - 7 \times 10^{-4}$  which is similar to the range of  $C$  estimated for low-mass X-ray binaries (Dubus et al., 1999). There is a degeneracy between the parameters  $C$  and  $T_p$ . With two extreme values of  $C$ , similar evolutionary curves can be obtained by changing  $T_p$  only by a factor of  $\sim 1.6$ . The range of  $C$  obtained in our earlier work constrains  $T_p$  to below  $\sim 200$  K (Ertan et al., 2009), consistent with the results of Inutsuka & Sano (2005).

Accretion onto the surface of the neutron star is the dominant source of the X-ray luminosity. The accretion rate,  $\dot{M}$ , is related to the X-ray luminosity through  $L_x = GM\dot{M}/R$  where  $R$  is the radius of the neutron star. In the fallback disk model of AXP/SGRs, the sources are in the propeller regime and a fraction of the matter arriving at the inner disk radius is accreted onto the star (Chatterjee, Hernquist & Narayan, 2000; Alpar, 2001). This can be written as  $\dot{M} = \eta \dot{M}_{\text{in}}$  where  $\eta \leq 1$ . For simplicity, we take  $\eta = 1$  in all our calculations. Similar results can be obtained with  $\eta < 1$ . Depending on the initial conditions, the sources can enter the accretion phase at different epochs of the evolution. Some sources may never enter the accretion phase and probably continue their evolution as radio pulsars until their rotational power is no longer sufficient to produce pulsed radio emission. Other sources, with different initial conditions, may evolve through an initial pulsar phase into a subsequent accretion epoch. When accretion is not possible, that is, when the inner disk cannot penetrate the light cylinder, the X-ray emission is mainly due to intrinsic cooling of the star. For the cooling luminosity,  $L_{\text{cool}}$ , we use the theoretical cooling curves calculated for the neutron stars with conventional magnetic dipole fields (Page, 2009). In the luminosity calculation, in addition to  $L_{\text{cool}}$  we also include the intrinsic

sic dissipative heating of the neutron star under the dipole and disk torques acting on the star (Alpar, 2007).

We use the  $\alpha$  prescription for the kinematic viscosity  $\nu = \alpha c_s h$  where  $c_s$  and  $h$  are the local sound speed and the pressure scale-height of the disk respectively (Shakura & Sunyaev, 1973). In the long-term evolution of the disk, the mass-flow rate from the outer to the inner disk is determined by the viscosities in the cold outer disk. Following the results of the detailed work on the X-ray enhancement light curves of AXP/SGRs (Çalışkan & Ertan, 2012) we take  $\alpha = 0.045$ .

The disk could remain stable (i.e., not blown away by radiation pressure) when  $r_{\text{LC}} < r_{\text{in}}$  for a certain range of  $r_{\text{in}}$  values depending on the angle  $\theta$  between the magnetic dipole and the rotation axes of the neutron star (Ekşi & Alpar, 2005). The maximum  $r_{\text{in}}$  for the disk to remain stable is a few  $r_{\text{LC}}$  for large  $\theta$ , while the disk is stable for all  $r_{\text{in}}$  values if the axes are aligned (Ekşi & Alpar, 2005). Even if the disk remains stable, it cannot apply an efficient torque on the star if the inner disk loses contact with the closed field lines. An alternative and stronger possibility in this regime is that the inner disk matter cannot be propelled efficiently from the system and piles up at the inner disk. In this case, because of the increasing surface-density gradient at the inner disk,  $r_{\text{in}}$  approaches to  $r_{\text{LC}}$  and a steady state is reached with an inner disk that remains in contact with the closed dipole field lines. The system then follows a propeller phase with  $r_{\text{in}} \sim r_{\text{LC}}$  (Ertan et al., 2009; Alpar, Ertan & Çalışkan, 2011; Çalışkan et al., 2013). As in our earlier work, we adopt that the inner disk follows this propeller phase when it cannot penetrate the light cylinder.

In the accretion regime, the disk spin-down torque acting on the star can be written as  $N = \dot{M} (GM r_A)^{1/2} F(\omega_*)$  where the dimensionless torque  $F(\omega_*)$  is a function of the fastness parameter  $\omega_* = \Omega_*/\Omega_K(r_A)$  where  $\Omega_K(r_A)$  is the angular frequency of the disk at  $r = r_A$ . From our earlier analysis, we found that the dimensionless torque in the form  $F(\omega_*) = \beta(1 - \omega_*^p)$  can produce the period evolution of AXP/SGRs with  $\beta = 0.5$  and  $p = 2$  (Ertan & Erkut, 2008; Ertan et al., 2009). Substituting  $F(\omega_*)$  in the torque equation, we have

$$N = \frac{1}{2} \dot{M}_{\text{in}} (GM r_{\text{in}})^{1/2} (1 - \omega_*^2) = I \dot{\Omega}_* \quad (4.2)$$

where  $I$  is the moment of inertia of the neutron star. When  $r_A < r_{\text{LC}}$ , we calculate  $N$  with  $r_{\text{in}} = r_A$  using equation (4.1). When  $r_A$  is found to be greater than  $r_{\text{LC}}$ , we take

$$r_{\text{in}} = r_{\text{LC}}.$$

In the spin-down with accretion phase ( $r_{\text{co}} < r_{\text{in}} < r_{\text{LC}}$ ), substituting equation (4.1) in equation (4.2), the period derivative,  $\dot{P}$ , of the neutron star is found to be independent of both  $\dot{M}$  and  $P$  when  $\omega_*$  is sufficiently beyond unity. This is probably the case for most of the persistent AXPs and SGRs currently in the accretion phase except for a few sources which are likely to be close to rotational equilibrium.

The “low-B magnetars” SGR 0418+5729 and Swift J1822.3–1606, which seem to have completed the accretion epoch, are evolving in the final propeller phase with  $r_{\text{in}} \simeq r_{\text{LC}}$  (Alpar, Ertan & Çalışkan, 2011; Benli et al., 2013). In this phase, the disk torque is proportional to  $\dot{M}_{\text{in}}$ . The ratio of the ram pressure to magnetic pressure at  $r_{\text{LC}}$ , and the disk torque, decrease with time. By the time the magnetic dipole torque dominates the disk torque, the X-ray cooling luminosity of the source is already below the detection limits in most cases. In the final propeller phase following the accretion phase, the possibility of pulsed radio emission depends on the dipole field strength and the period of the source (see Sections 4.3 and 4.4). We assume that magnetic field decay is negligible within the observable timescale of the AXP/SGRs and XDINs ( $\tau \sim 10^6$  yr). Sources with appropriate initial conditions could start their evolution in propeller phase. These are likely to be observed as radio pulsars until they cross the radio pulsar “death line”.

### 4.3 Results

Out of seven XDINs, six sources have measured periods and period derivatives<sup>1</sup>. For comparison with our model results, we have converted the reported X-ray fluxes of the six XDINs with known  $P$  and  $\dot{P}$  into the unabsorbed fluxes and luminosities using the distances,  $N_{\text{H}}$  values and blackbody temperatures given in the corresponding papers. There are large uncertainties in the distances of some XDINs which are reflected in the uncertainties of the X-ray luminosities. Corrections to luminosities could require modification of our model parameters reported here.

For RX J0420.0-5022,  $P = 3.453$  s (Haberl, 2004) and  $\dot{P} = 2.8 \pm 0.3 \times 10^{-14}$  s s<sup>-1</sup> (Kaplan & van Kerkwijk, 2011). The distance of this source was estimated as  $\sim 345$  pc

<sup>1</sup>When we were submitting this paper the detection of the period ( $\simeq 3.39$  s) and a tentative ( $2\sigma$ ) period derivative ( $\sim 1.6 \times 10^{-12}$  s s<sup>-1</sup>) was reported for the seventh source RX J1605.3+3249 (Pires et al., 2014). We intend to investigate the evolutionary possibilities of this source when the period derivative is confirmed.

by Posselt et al. (2007). The 0.1 – 2.4 keV observed flux was reported as  $\sim 5 \times 10^{-13}$  erg  $s^{-1}$   $cm^{-2}$  (Haberl et al., 2004). Using the properties of their spectral fit, we calculate the bolometric luminosity as  $L_x \simeq 2.6 \times 10^{31}$  erg  $s^{-1}$ .

The period of RX J1308.6+2127 (RBS 1223) is  $P = 10.31$  s (Haberl, 2004). The most recent timing analysis gives  $\dot{P} = 1.120(3) \times 10^{-13}$  s  $s^{-1}$  (Kaplan & van Kerkwijk, 2005). The distance is estimated to be 76 – 380 pc by Schwöpe et al. (2005) and  $380_{-30}^{+15}$  pc by Hambaryan et al. (2011). Using  $d = 380$  pc and the observed flux reported by Schwöpe, Schwarz & Greiner (1999), we obtained  $L_x = 7.9 \times 10^{31}$  erg  $s^{-1}$ .

For RX J0806.4-4123,  $P = 11.37$  s and  $\dot{P} = 5.5(30) \times 10^{-14}$  s  $s^{-1}$  (Kaplan & van Kerkwijk, 2009b). The distance of this source was estimated as 235 - 250 pc by Posselt et al. (2007). Using  $d = 240$  pc and with the observed X-ray flux reported by Haberl et al. (2004), we find  $L_x = 2.5 \times 10^{31}$  erg  $s^{-1}$ .

The period of RX J1856.5-3754 is 7.055 s (Tiengo & Mereghetti, 2007) and  $\dot{P} = 2.97(7) \times 10^{-14}$  s  $s^{-1}$  (van Kerkwijk & Kaplan, 2008). The distance is highly uncertain. Estimates range from  $123_{-15}^{+11}$  pc (Walter et al., 2010) to  $167_{-15}^{+18}$  pc (Kaplan, van Kerkwijk & Anderson, 2007). Posselt et al. (2007) estimate the distance as  $135 \pm 25$  pc. With  $d = 135$  pc,  $L_x$  is found between  $\sim 5 \times 10^{31}$  erg  $s^{-1}$  and  $\sim 1 \times 10^{32}$  erg  $s^{-1}$  (Walter & Lattimer, 2002; Pons et al., 2002; Drake et al., 2002; Burwitz et al., 2003). We take  $L_x = 9.5 \times 10^{31}$  erg  $s^{-1}$  obtained by Burwitz et al. (2003) with the lowest  $\chi^2$ .

For RX J2143.0+0654 (RBS 1774), the timing analysis by Kaplan & van Kerkwijk (2009a) gives  $P = 9.428$  s and  $\dot{P} = 4.1(18) \times 10^{-14}$  s  $s^{-1}$ . The upper limit to the distance was given as 300 pc by Posselt, Neuhäuser & Haberl (2009) and as 390–430 pc Posselt et al. (2007). The unabsorbed X-ray fluxes reported by Kaplan & van Kerkwijk (2009a); Zane et al. (2005) and Rea et al. (2007b) are  $4.8$ ,  $6.1$  and  $5.6 \times 10^{-12}$  erg  $s^{-1}$   $cm^{-2}$  respectively. Using the flux reported by Rea et al. (2007b), we find  $L_x \simeq 1.1 \times 10^{32}$  erg  $s^{-1}$  with  $d = 400$  pc.

The period of RX J0720.4-3125 is  $P = 8.39$  s (Haberl et al., 1997). The most recent analyses give  $\dot{P} \sim 7 \times 10^{-14}$  s  $s^{-1}$  (van Kerkwijk et al., 2007; Hohle et al., 2010). The distance was estimated as 235 – 270 pc by Posselt et al. (2007) and as  $360_{-90}^{+170}$  pc by Kaplan, van Kerkwijk & Anderson (2007). We use  $d = 270$  pc in our calculations, since it agrees with both estimates. The X-ray flux was reported as  $(9 \pm 2) \times 10^{-12}$  erg  $s^{-1}$   $cm^{-2}$  by Kaplan et al. (2003), which corresponds to a bolometric luminosity of

$\sim 1.6 \times 10^{32} \text{ erg s}^{-1}$ .

In the present work, we have investigated the long-term evolution of these six XDINs (Table 4.1). The present day X-ray luminosities, periods and period derivatives of these sources can be produced simultaneously by the neutron star's evolution with a fallback disk. For a neutron star with a magnetic dipole field  $\sim 10^{12}$  G to evolve into the observed period range of XDINs (3 – 12 s) the system should pass through an accretion phase. Our results indicate that these sources slowed down to long periods during accretion epochs lasting from a few  $10^4$  yr to a few  $10^5$  yr. They completed their accretion phases in the past, and now they are in the final phase, still spinning down by disk torques, which are weaker than in the accretion epoch. At present, the X-ray luminosities of these sources are likely to be powered by the intrinsic cooling of the neutron star. If the inner disk had never penetrated into the light cylinder the disk torque could not have spun down a neutron star with a conventional  $\sim 10^{12}$  G dipole field to XDIN periods within the cooling timescale,  $\tau_{\text{cool}} \sim 10^6$  yr (e.g. Page 2009).

We present illustrative model curves in Figures 4.1 and 4.2 to show the dependence of evolutionary paths on the disk mass,  $M_d$ , and the dipole field strength on the pole of the star,  $B_0$ , respectively. Different phases of evolution can be followed from the  $\dot{P}$  curves given in the bottom panels of Figures 4.1 and 4.2. In the accretion phase ( $r_{\text{co}} < r_{\text{in}} < r_{\text{LC}}$ ), from equation (4.1), it is found that  $\dot{P}$  is proportional to  $B_0^2$ , and independent of  $\dot{M}_{\text{in}}$  and  $P$ . That is, the evolutionary phases with constant  $\dot{P}$  correspond to accretion epochs. In this phase, for a given  $M_d$ , the sources with higher  $B_0$  reach longer periods. After the accretion phase, the system enters the final propeller phase in which  $r_{\text{in}} \simeq r_{\text{LC}}$ . The disk torque decreases with decreasing  $\dot{M}_{\text{in}}$  (the mass inflow rate arriving at  $r_{\text{in}} \simeq r_{\text{LC}}$ ). Accretion onto the neutron star has stopped,  $\dot{M} = 0$ , and the X-ray luminosity is supplied by the intrinsic cooling of the neutron star. In Figure 4.1, we also give illustrative model curves that could represent the evolution of AXP/SGRs (the two upper curves). These model sources with relatively high  $B_0$  values cannot acquire the properties of XDINs. Our results indicate that XDINs could be distinguished from AXP/SGRs by having weaker  $B_0$  fields.

In Figure 4.2, we give the evolutionary curves for different disk masses keeping the initial dipole magnetic field constant at  $B_0 \simeq 1.2 \times 10^{12}$  G. It is seen that systems with greater  $M_d$  have longer accretion phases. We obtain these illustrative model curves with

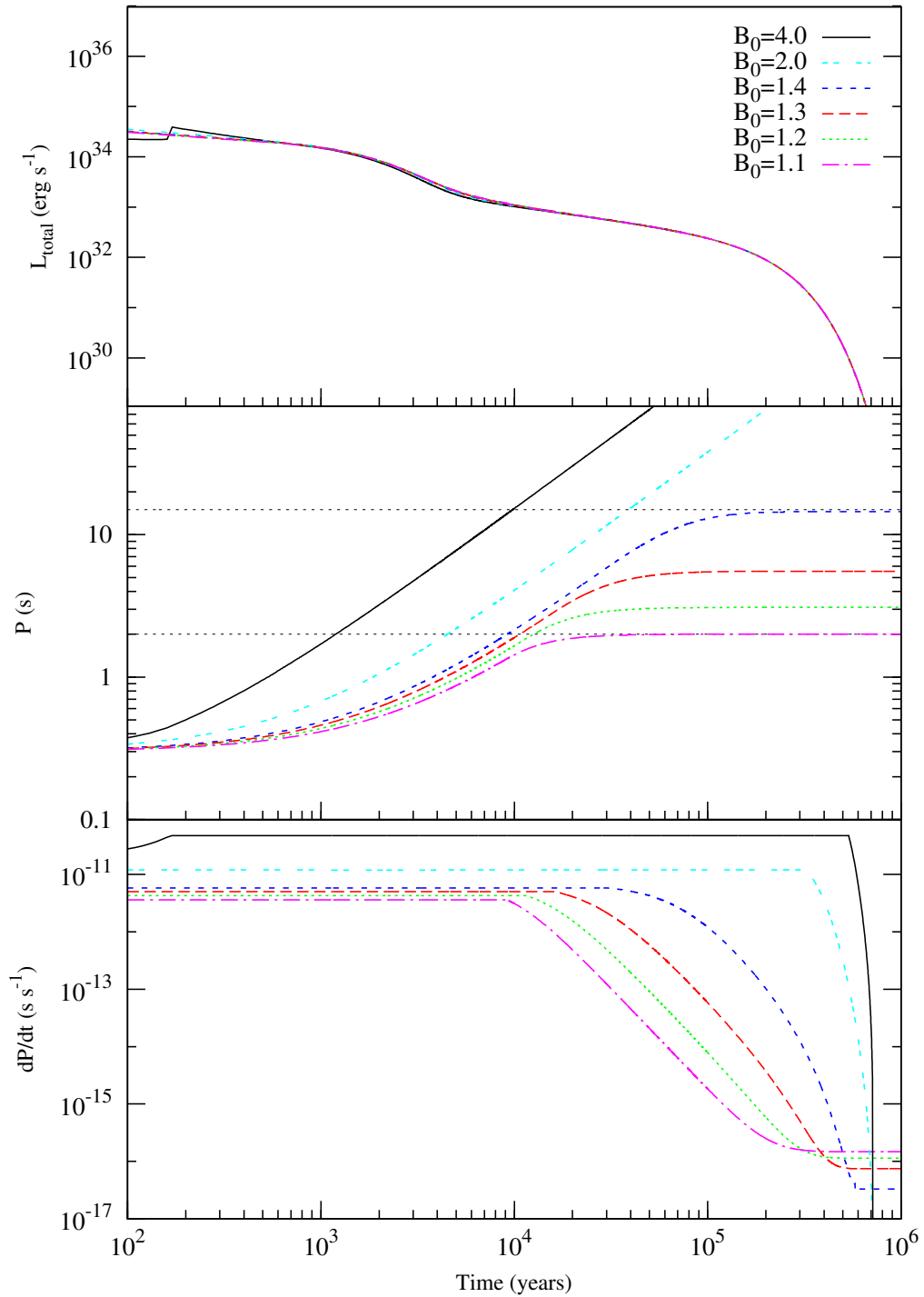


**Figure 4.1:** Total luminosity, period and period derivative evolution of the model sources with different magnetic dipole fields. For all model sources  $M_d = 3 \times 10^{-6} M_\odot$ . The magnitudes of the magnetic dipole field on the pole of the star,  $B_0$ , are given in units of  $10^{12}$  G in the top panel (see the text for a discussion).

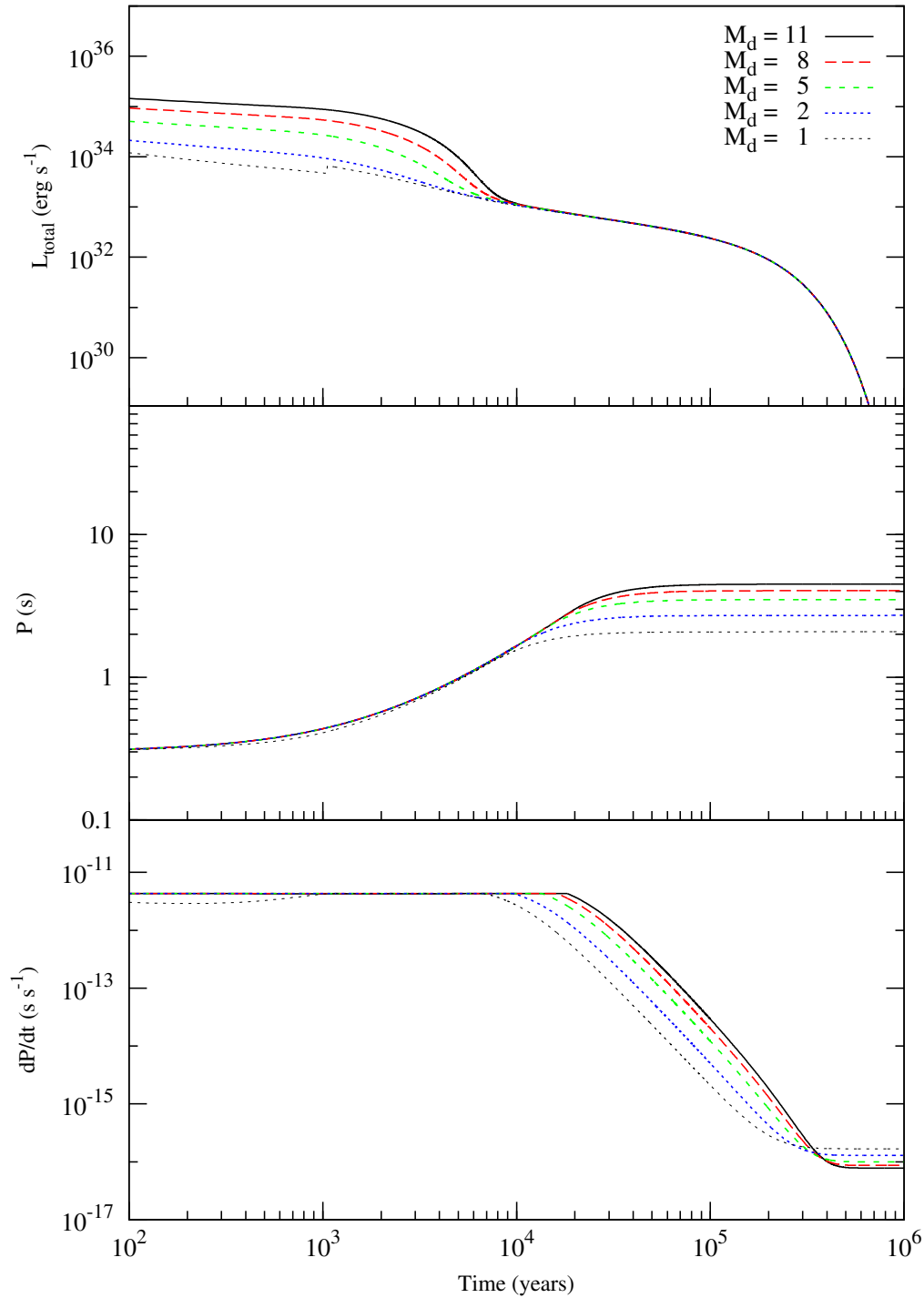


**Figure 4.2:** The luminosity, period and period derivative evolution of the model sources with different initial disk masses. The magnetic dipole field is the same ( $B_0 = 1.2 \times 10^{12}$  G) for all sources. The disk masses are given in units of  $10^{-6} M_{\odot}$  in the top panel.

**Table 4.1:** The ages and the disk parameters for the six XDINs. The ages are constrained by the theoretical cooling luminosity (Page, 2009) and the estimated bolometric X-ray luminosities.

	$B_0$ ( $10^{12}$ G)	$M_{disk}$ ( $10^{-6} M_{\odot}$ )	$T_p$ (K)	$C$ ( $10^{-4}$ )	age ( $10^5$ y)
RX J0720.4-3125	1.1 - 1.3	0.8 - 12	106	1	1.45
RX J1856.5-3754	0.9 - 1.1	0.8 - 18	100	1	1.85
RX J2143.0+0654	1.0 - 1.2	1.0 - 12	100	1	1.9
RX J1308.6+2127	0.9 - 1.0	0.6 - 18	100	1.5	2.1
RX J0806.4-4123	0.8 - 0.9	0.5 - 18	100	2.3	3.1
RX J0420.0-5022	0.35 - 0.38	4.8 - 18	82	7	3.2

$T_p \sim 200$  K and  $C = 7 \times 10^{-4}$ . Using  $C = 1 \times 10^{-4}$ , evolutionary curves similar to those in Figure 4.2 can be obtained with  $T_p \simeq 125$  K. Even with the highest reasonable value of  $C$ , the model curves obtained with  $T_p > 300$  K do not lead to XDIN or AXP/SGR properties for any disk mass.

Comparing Figures 4.1 and 4.2, it is seen that the dipole magnetic field strength  $B_0$ , rather than the disk mass, is the more effective initial condition for determining the long-term rotational evolution of the sources. In Figure 4.1,  $M_d$  is the same for all model sources, and the  $B_0$  values vary only by a factor of 4. We see that the model curves trace rotational properties of AXP/SGR and XDINs from the smallest to the largest observed  $P$  and  $\dot{P}$  values. For a given  $B_0$ , different  $M_d$  values do not yield significantly different evolutionary paths. In Figure 4.2, disk masses change by an order of magnitude, while the final periods at  $t = 1$  Myr remain in the 2 – 5 s range. The  $\dot{P}$  curves of the sources with the same  $B_0$  but different  $M_d$  are also very similar. In the accretion phase, the accretion power is the dominant source of the X-ray luminosity, and depends on the initial disk mass  $M_d$ .

With more detailed analysis, we also tried to reproduce the individual properties of XDINs with known  $P$  and  $\dot{P}$  values. The evolutionary tracks of these sources are seen in Figure 4.3. Since all these XDINs are currently powered by the intrinsic cooling luminosity of their neutron stars, observed luminosities and the theoretical cooling curves constrain the ages of the model sources. In all these calculations, we first take  $C = 1 \times 10^{-4}$  and  $T_p = 100$  K. In some cases, we obtained better fits with slightly different  $C$  and  $T_p$  values. The model curves given in Figure 4.3 are obtained with  $T_p$  values that remain in a narrow range between 80 and 110 K. Assuming that AXP/SGRs and XDINs have similar

disk compositions, we expect that they have similar critical temperatures. The irradiation efficiency might change with the accretion rate; it is expected to be similar for sources in the same accretion regime. We perform simulations tracing all possible values of  $M_d$  and  $B_0$  with  $P_0 = 300$  ms. For the model sources that can enter the accretion phase, the source properties at the end of this phase are not sensitive to  $P_0$  (Ertan et al., 2009). For all XDINs, the  $B_0$  values that can produce the reasonable evolutionary curves remain in the  $\sim 0.3 - 1.3 \times 10^{12}$  G range. The ranges of model parameters that can produce the individual properties of the six XDINs are listed in Table 4.1.

Our results imply that all six XDINs completed the long-term accretion phase. They are not accreting matter from the disk at present, while they are still being slowed down by the disk torques. Without accretion, these sources are free to emit pulsed radio emission. However, the dipole fields  $B_0$  inferred in the fallback disk model are significantly weaker than those inferred from the dipole torque formula, so that at present the XDINs do not have sufficient voltages to sustain pulsed radio emission. Allowed ranges of  $B_0$  values for each XDIN are given in Table 4.1 and plotted in Figure 4.4. All these sources are indeed well below the lower border of the radio pulsar death valley in the extended galactic population, and are not expected to show radio pulses. Younger XDINs with shorter periods should be able to emit radio pulses, however they would still be evolving in the long-term accretion phase during which mass-flow onto the neutron star hinders the radio emission. Once the accretion epoch is over, XDINs have weak rotational power and are not likely to produce radio emission.

The inner disk conditions of XDINs in the efficient propeller phase could be rather different from those of persistent AXPs in the accretion phase, for which the boundary layer extends down to the co-rotation radius in a steady state with magnetic heating in the boundary layer negligible compared to viscous dissipation (Rappaport, Fregeau & Spruit, 2004). By contrast, in the propeller phase, magnetic heating in the boundary layer could be a significant extra heating source in addition to viscous dissipation and irradiation. This additional heating in the propeller phase can supply the difference ( $\sim 2 - 3$  orders of magnitude) between the observed R band flux (Kaplan et al., 2011) and the model calculation, for an irradiated face on thin disk. A calculation of the magnetic heating is beyond the scope of the present work; a detailed study is in progress.

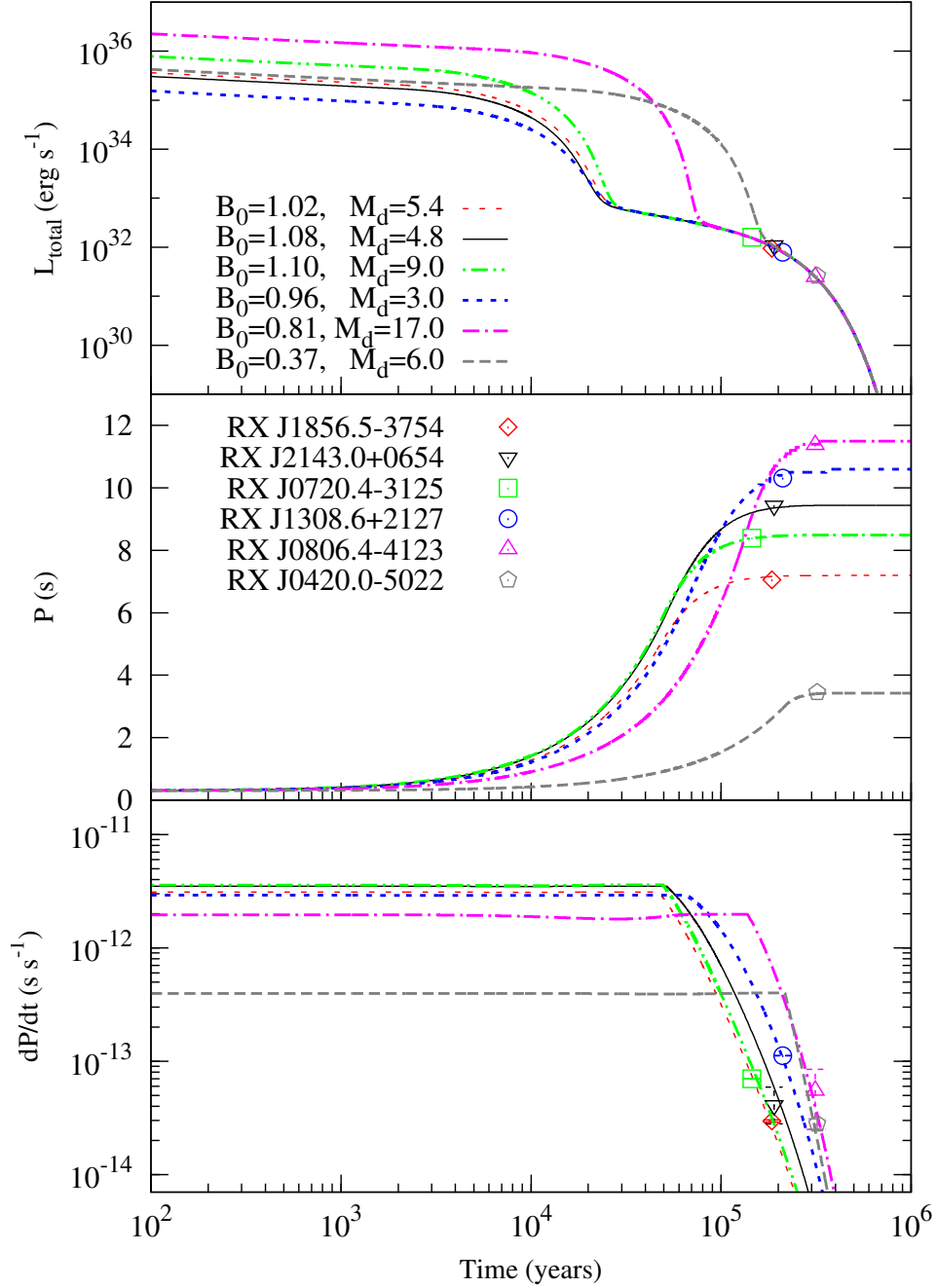


**Figure 4.3:** The model curves that can simultaneously produce the luminosity, period and period derivative of the six XDINs. For each source, we determined the ranges of  $M_d$  and  $B_0$  that can produce the source properties (see Table 4.1). Here, we show illustrative model curves that can represent the long-term evolution of these XDINs. The values of  $B_0$  and  $M_d$  used in the models are given in the top panel in units of  $10^{12}$  G and  $10^{-6} M_\odot$  respectively.

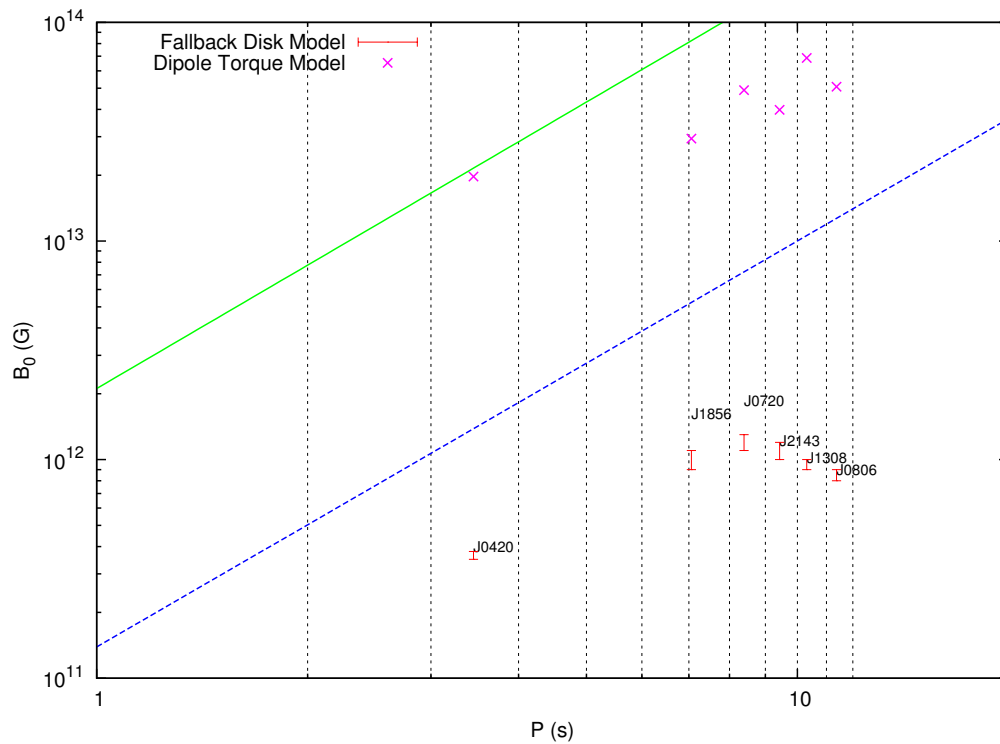


**Figure 4.4:** Magnetic dipole field strength on the pole of the neutron star versus period distribution for six XDINs. The two parallel lines (green and blue) show the upper and lower bounds of the radio pulsar death valley from Chen & Ruderman (1993). Crosses are the  $B_0$  values inferred from the dipole torque formula. Vertical bars show the ranges of  $B_0$  that can produce the properties of the sources in the fallback disk model (see Figure 4.3). It is seen that all these sources remain below the lower boundary of the death valley (death line) indicating that these XDINs cannot be normal radio pulsars, if they are evolving with fallback disks.

## 4.4 Discussion and Conclusion

We have examined the long-term evolution of the six XDIN sources, with measured  $\dot{P}$  out of the current total 7 XDINs. First, we find that the fallback disk model is successful in producing the observed individual properties of all these sources. XDIN properties are obtained after the source has gone through a past accretion phase with spin-down, with the fallback disk protruding into the neutron star's magnetosphere. At present, the fallback disk is tracking the light cylinder, with continuing spin-down under the disk torques, but no accretion onto the neutron star. The X-ray luminosities of XDINs are provided by cooling. Next, tracing the initial parameters, we have determined the allowed ranges of the dipole field strength on the pole of the star,  $B_0$ , and the disk mass,  $M_d$ , for each source (Table 4.1). Our results constrain the  $B_0$  values of the six XDINs into the  $\sim 0.3 - 1.3 \times 10^{12}$  G range. Comparing this range of dipole field strength with earlier results obtained by Ertan et al. (2009) for AXP/SGRs, we surmise that XDINs tend to have dipole fields weaker than those of most known AXP/SGRs. This result should be confirmed through further detailed work on the persistent and transient AXP/SGRs.

Reasonable evolutionary model curves for XDINs can be obtained with a wide range of initial fallback disk masses,  $M_d$ , for all sources (Table 4.1). We could not test whether there is a correlation between  $M_d$  and  $B_0$ , since our results do not constrain the disk masses. For the sources that do not accrete at present, like XDINs, it is not possible to constrain the initial mass of the disk in most cases. A possible  $M_d - B_0$  correlation could be tested through further investigation of persistent AXP/SGRs which are powered by accretion onto the star. This analysis will help us understand the differences in the initial conditions of different young neutron star populations.

All known XDINs are close-by objects within  $\sim 400$  pc of the Sun. Statistical analysis considering the properties of the Gould Belt gives a galactic birth rate of  $\gtrsim 1$  century $^{-1}$  (Popov, Turolla & Possenti 2006; see also Chapter 1). This raises a critical question for the models: Only the XDINs in the solar neighborhood are observable in X-rays. The inferred large galactic population should be detectable in the radio band if they are active radio pulsars. If these sources evolve in vacuum without fallback disks, their dipole field on the pole of the star can be estimated as  $B_0 \simeq 6.4 \times 10^{19} \sqrt{P\dot{P}}$  G. Observed  $P$  and  $\dot{P}$  values give  $B_0 \sim 10^{13} - 10^{14}$  G. It is expected to see these sources as radio pulsars, if

XDINs indeed slow down by magnetic dipole torques with these strong fields. Five out of seven XDIN sources, located within 0.4 kpc, have periods greater than 7 s. Among the currently known radio pulsars in the ATNF pulsar catalog (Manchester et al., 2005), there is only a single radio pulsar with  $P > 7\text{s}$  ( $P = 7.7\text{ s}$ ) and  $B > 10^{13}\text{ G}$  which is located at a distance of 3.3 kpc. We are not sure whether this can be accounted for with the selection effects and even the most conservative beaming fraction formulas for the long-period systems, if XDINs and radio pulsars with large dipole magnetic fields are taken to be members of the same population. A detailed population synthesis or statistical analysis will not be attempted here.

This problem encountered in the dipole torque model is naturally resolved in the fallback disk model. During the initial long-term accretion phase radio emission is suppressed due to mass-flow onto the star. Is it possible to observe pulsed radio emission from these sources after the mass accretion terminates? The neutron stars that evolve like the six XDINs we studied here are not likely to produce beamed radio emission when accretion stops, because: (1) their dipole fields are much weaker than inferred from the dipole torque formula (Table 4.1), and (2) at the end of the accretion phase, they have already attained long periods. In Figure 4.3, accretion phases correspond to the epochs with constant  $\dot{P}$  given in the lower panel. The period at the end of the accretion phase corresponds to a location in the  $B_0 - P$  plane which is already below the lower border of the death valley. Subsequent evolution moves the source even further away from the death valley, to the present locations shown in Figure 4.4.

To sum up: (1) The rotational properties and the X-ray luminosities of XDINs can be explained by the fallback disk model that was employed earlier to explain the general properties of AXP/SGRs (Figure 4.1). The main disk parameters used in the present work for different XDIN sources are similar to each other and also to those used in the long-term evolution models of AXP/SGRs (Table 4.1). (2) The distinction between XDINs and AXP/SGRs seems to be that the former have weaker dipole magnetic fields. Finally, (3) the model can also account for non-detection of many radio pulsars evolving to the properties of known XDINs. A neutron star with a conventional dipole field must have passed through the long-term accretion phase to acquire the periods of known XDINs within the cooling timescale. In the accretion phase, the radio emission is quenched by the mass flow onto the neutron star. After termination of the accretion phase, the sources

no longer have sufficient rotational power for radio emission.

# Chapter 5

## LONG-TERM EVOLUTION OF ANOMALOUS X-RAY PULSARS AND SOFT GAMMA REPEATERS

This chapter was published in *Monthly Notices of the Royal Astronomical Society*, 2016,  
Volume 457, Issue 4, pp. 4114-4122

**Onur Benli & Ünal Ertan**

Some parts of the introduction were removed or modified.

## 5.1 Introduction

The general behaviours of AXP/SGR population is presented in Chapter 1 and individual source properties are given in 5.3. In this part, we employ the fallback disk model developed by Ertan et al. (2009) to 12 AXP/SGR sources. The evolutionary curves obtained from our model are significantly different from those given by the analytical fallback disk solutions which cannot take dynamical outer disk radius and irradiation effects into account.

The limitations of our models could be understood through source-by-source analyses of each population. This systematic approach could also help to determine the differences in the initial conditions of different populations together with their likely evolutionary connections. In the previous Chapter, we performed a detailed study for XDINs in the fallback disk model, and showed that the X-ray luminosity, period and period derivative of each XDIN source could be acquired simultaneously by neutron stars with fallback disks for certain ranges of the disk-mass and the dipole field strength. In the present Chapter, we perform the same analysis for AXP/SGR sources with relatively well-known quiescent state properties, and compare our results with those obtained for XDINs by Ertan et al. (2014) (Chapter 4).

We briefly describe the model in Section 5.2. In Section 5.3, we summarize the observational properties of AXP/SGRs studied in the present work. Our results for twelve AXP/SGRs with a comparison to XDIN properties obtained by the same model are given in Section 5.4. We discuss and summarize our conclusions in Section 5.5.

## 5.2 Description of the model

We employ the fallback disk model developed by Ertan et al. (2009). We solve the disk diffusion equation with an initial surface density profile of a steady thin disk using the  $\alpha$ -prescription of the kinematic viscosity (Shakura & Sunyaev, 1973). At a given radial distance  $r$  from the star, the effective temperature of the disk is  $T_{\text{eff}} \cong \sigma^{1/4}(D + F_{\text{irr}})^{1/4}$  where  $D$  is the viscous dissipation rate and  $F_{\text{irr}} = (C\dot{M}c^2)/(4\pi r^2)$  is the irradiation flux, where  $c$  is the speed of light,  $C$  is the irradiation parameter which depends on the albedo and geometry of the disk. The dynamical outer radius,  $r_{\text{out}}$ , of the viscously active

disk corresponds to the current radial position of a critical minimum temperature,  $T_p$ , for the disk to generate viscosity and be able to transport mass and angular momentum that is,  $r_{\text{out}} = r(T = T_p)$ . In the long-term evolution,  $r_{\text{out}}$  propagates inward with decreasing X-ray luminosity,  $L_x$ , leaving inactive matter beyond  $r_{\text{out}}$ . Results of earlier work on the long-term evolution of AXP/SGRs and XDINs indicate that  $T_p \sim 100$  K, for a plausible range of irradiation efficiencies. In the simulations, we start with an initial  $r_{\text{out}} \sim 10^{14}$  cm at which the effective temperature of the disk is  $\sim T_p$  with the initial X-ray luminosity. The results obtained by Inutsuka & Sano (2005) imply that the turbulent viscosity mechanism in the disk remains active for temperatures as low as  $\sim 300$  K, which is in agreement with the critical temperatures we obtained from the model fits.

In the fallback disk model, the main X-ray source of accreting AXP/SGRs is the accretion on to the poles of the star, which can be written as  $L_{\text{acc}} = GM\dot{M}/R$  where  $G$  is gravitational constant,  $M$  and  $R$  is the mass and radius of the star,  $\dot{M}$  is the mass flow rate on to the star. Intrinsic cooling luminosity,  $L_{\text{cool}}$ , powers the star in the propeller phase or when the accretion luminosity decreases below  $L_{\text{cool}}$  in the late phases of evolution. We use the theoretical cooling luminosity curve calculated by Page, Geppert & Weber (2006) for neutron stars with conventional dipole fields. When the accretion is not allowed, we calculate the total cooling luminosity considering also the energy dissipation due to magnetic and disk torques as suggested by Alpar (2007). In the fallback disk model, starting from the earlier works (e.g. Chatterjee, Hernquist & Narayan 2000; Alpar 2001), it is assumed that part of the inflowing disk matter is accreted onto the surface of the star in the spin-down phase. There are theoretical works (e.g. Rappaport, Fregeau & Spruit 2004 and D'Angelo & Spruit 2012), and strong observational evidences supporting this assumption. For instance, for the recently discovered transitional millisecond pulsars, it is estimated that the accretion – propeller transition takes place at accretion rates that are orders of magnitude lower than the rate corresponding to the spin up-down transition (Archibald et al. 2014, Papitto et al. 2015). The critical condition for the accretion–propeller transition is not well known. In our model, we assume that the mass-flow onto the star is allowed when the light cylinder radius,  $r_{\text{LC}}$ , is greater than the Alfvén radius  $r_A = (GM)^{-1/7} \mu^{4/7} \dot{M}_{\text{in}}^{-2/7}$ , where  $\mu$  is the magnetic dipole moment of the neutron star and  $\dot{M}_{\text{in}}$  is the rate of mass-flow arriving the inner disk radius,  $r_{\text{in}}$ .

The torque acting on the neutron star can be found by integrating the magnetic torque

from  $r_A$  to the corotation radius,  $r_{\text{co}} = (GM/\Omega_*^2)^{1/3}$  (see Ertan & Erkut 2008 and Ertan et al. 2009 for details of the torque model). This assumes a wide boundary layer between  $r_A$  and  $r_{\text{co}}$ . Most of the contribution to the spin-down torque comes from the radii close to  $r_{\text{co}}$ . Therefore, the magnetic torques integrated from  $r_A$  to  $r_{\text{co}}$ , or across a narrow boundary layer, say from  $2r_{\text{co}}$  to  $r_{\text{co}}$ , give similar results. This is due to the very sharp radial dependence of the magnetic pressure ( $\propto r^{-6}$ ). The total spin-down torque integrated from  $r_A$  to  $r_{\text{co}}$  can be written as,

$$N_{\text{sd}} = I \dot{\Omega}_* = \frac{1}{2} \dot{M}_{\text{in}} (GM r_A)^{1/2} (1 - \omega_*^2) \quad (5.1)$$

where  $I$  is the moment of inertia,  $\dot{\Omega}_*$  is the rate of change of the angular velocity of the star,  $\omega_* = \Omega_*/\Omega_K(r_A)$  is the fastness parameter,  $\Omega_*$  is the rotational angular frequency of the neutron star and  $\Omega_K(r_A)$  is the Keplerian angular velocity of the disk at the Alfvén radius. Accretion from the inner disk on to the neutron star is allowed when  $r_{\text{co}} < r_A < r_{\text{LC}}$ . In this phase, we assume that  $\dot{M}_{\text{in}} = \dot{M}$ , that is, we neglect losses through the propeller effect. This assumption does not affect our results qualitatively.

In the accretion phase, there is also a spin-up torque associated with the mass accretion on to the star from the co-rotation radius,  $\sim \dot{M} (GM r_{\text{co}})^{1/2}$ . When  $\omega_*^2 \gg 1$ , this torque is negligible in comparison with the spin-down torque given in equation 5.1. Nevertheless, some of the sources, especially those with relatively large disk masses, could approach the rotational equilibrium for a certain epoch of the evolution, with decreasing efficiency of the net spin-down torque (Section 5.4). In general, we can write down the total torque acting on the star as the sum of the spin-down and spin-up torques,  $N_{\text{tot}} = N_{\text{sd}} + N_{\text{su}}$  where  $N_{\text{su}} \cong \dot{M} (GM r_{\text{co}})^{1/2}$ . The magnetic dipole radiation also contributes to the spin-down torque, while the disk torque is usually the dominant spin-down mechanism. When  $N_{\text{su}}$  is negligible, the total torque becomes equal to the spin-down torque given by equation 5.1. In Section 5.4, we will show that most AXP/SGRs are in the accretion phase with  $\omega_*^2 \gg 1$ . We estimate that only two AXPs, namely 1E 2259+586 4U 0142+61, are evolving close to rotational equilibrium at present.

In our calculations, we neglect the magnetic field decay which could affect the evolution of AXP/SGRs in the accretion phase. From the magnetic field decay models (e.g. Geppert, Urpin & Kononkov 1996, Konar & Bhattacharya 1999), we estimate that this effect is not significant for most of these sources which have ages between  $10^3$  and a few

$10^4$  yr and dipole fields strengths  $\sim 1 - 4 \times 10^{12}$  G (on the pole). Initial magnetic dipole fields of these sources could be a few times stronger than their field at present. The field could have decayed by a relatively large factor for the two AXPs, namely 1E 2259+586 and 4U 0142+61, which seem to evolve with relatively high disk masses. Our simplification about the transition between the accretion and the propeller phases puts an uncertainty on the ages of the model sources. The ages indicated by our model calculations could be taken as an upper limit to the actual ages of the sources. Nevertheless, incorporating a detailed field decay model in our calculations would not change the current field strengths of the sources estimated in the present work. After we complete our study on different neutron star systems with our current simple model, a detailed population analysis of the young neutron star systems in the fallback disk model, considering also the effects of the field decay on the model curves, will be presented in an independent work.

For AXP/SGRs and XDINs, our results are not sensitive to the initial period  $P_0$  (see e.g. Ertan et al. 2009). With different  $P_0$  values, model curves converge to the same source properties in the long-term, provided that the sources enter the accretion phase in the early phases of their evolution. The minimum temperature of the viscously active disk,  $T_p$ , is a basic disk property that is expected to be the same for all the fallback disks around young neutron star systems, even if the disk composition is not well-known. Following Ertan et al. (2009), we keep  $T_p$  in the  $\sim 50 - 150$  K range in the models of all different sources like low-B magnetars, ‘high-B radio pulsars’, and XDINs to remain self consistent. Similarly, we fixed the other main disk parameters, namely the irradiation strength  $C = 1 \times 10^{-4}$  and the viscosity parameter  $\alpha = 0.045$  following the results of Ertan & Çalışkan (2006) and Çalışkan & Ertan (2012). The actual disk mass,  $M_d$ , and the magnetic field strength,  $B_0$ , at the pole of the star could differ from source to source. We repeat the simulations many times, tracing the values of  $M_d$  and  $B_0$ , to find the ranges of these quantities that can reproduce the source properties. The disk mass,  $M_d$ , is estimated by integrating the initial surface density profile from the inner to the initial outer disk radius ( $\sim 5 \times 10^{14}$  cm).

### 5.2.1 Long-term Evolutionary Phases of a Neutron Star with a Fall-back disc

In our model, there are four basic parameters that determine the evolutionary curves of the model sources: magnetic dipole field strength on the pole of the star,  $B_0$ , the initial disk mass,  $M_d$ , the initial period of the star,  $P_0$ , and the minimum critical temperature,  $T_p$ , below which the disk becomes passive. The critical temperature  $T_p$  is degenerate with the irradiation parameter  $C$ , which is constrained to  $\sim 1-7 \times 10^{-4}$  range with the results obtained by Ertan & Çalışkan (2006).

Depending on the initial parameters, the model sources could follow rather different evolutionary paths. The X-ray luminosity and rotational evolution of a source could pass through three basic evolutionary phases, namely the initial propeller phase, accretion phase and final propeller phase as seen in Fig. 5.1. The top panel shows the X-ray luminosity,  $L_x$ , evolution of the source. The abrupt rise in  $L_x$  at  $t \simeq 5 \times 10^2$  yr is due to penetration of the inner disk into the light cylinder and the onset of the accretion phase. This might happen at different times of evolution for different sources. Some sources may never enter the initial propeller phase, while some others remain always in this phase as radio pulsars, depending on the initial conditions. The dashed line in the top panel represents the cooling history of a neutron star with a dipole field strength of  $10^{12}$  G on the surface of the star. It is seen that  $L_{\text{cool}}$  dominates  $L_{\text{acc}}$  when accretion is not allowed or in the late phase of the accretion episode. The evolution is easier to follow from the period derivative,  $\dot{P}$ , curve. The torque acting on the star is most efficient in the accretion phase. When the positive term is negligible, that is, when  $r_A$  is not very close to  $r_{\text{co}}$ ,  $\dot{P}$  is found to be independent of both  $\dot{M}$  and  $P$ . This constant  $\dot{P}$  behaviour of the illustrative model source in the accretion phase is seen in the bottom panel of Fig. 5.1.

With decreasing  $\dot{M}_{\text{in}}$ ,  $r_A$  moves outward faster than the light cylinder radius,  $r_{\text{LC}}$ . In the model, accretion is switched off when  $r_A$  is found to be greater than  $r_{\text{LC}}$ . For the illustrative model in Fig. 5.1 this correspond to  $t \simeq 3 \times 10^4$  yr. From this point on,  $\dot{P}$  decreases with decreasing  $\dot{M}_{\text{in}}$ . In this final propeller phase, the sources do not accrete but still spin-down by the disk torques. It is seen in the middle panel of Fig. 5.1 that  $P$  remains almost constant in this phase because of decreasing torque efficiency after termination of the accretion episode.

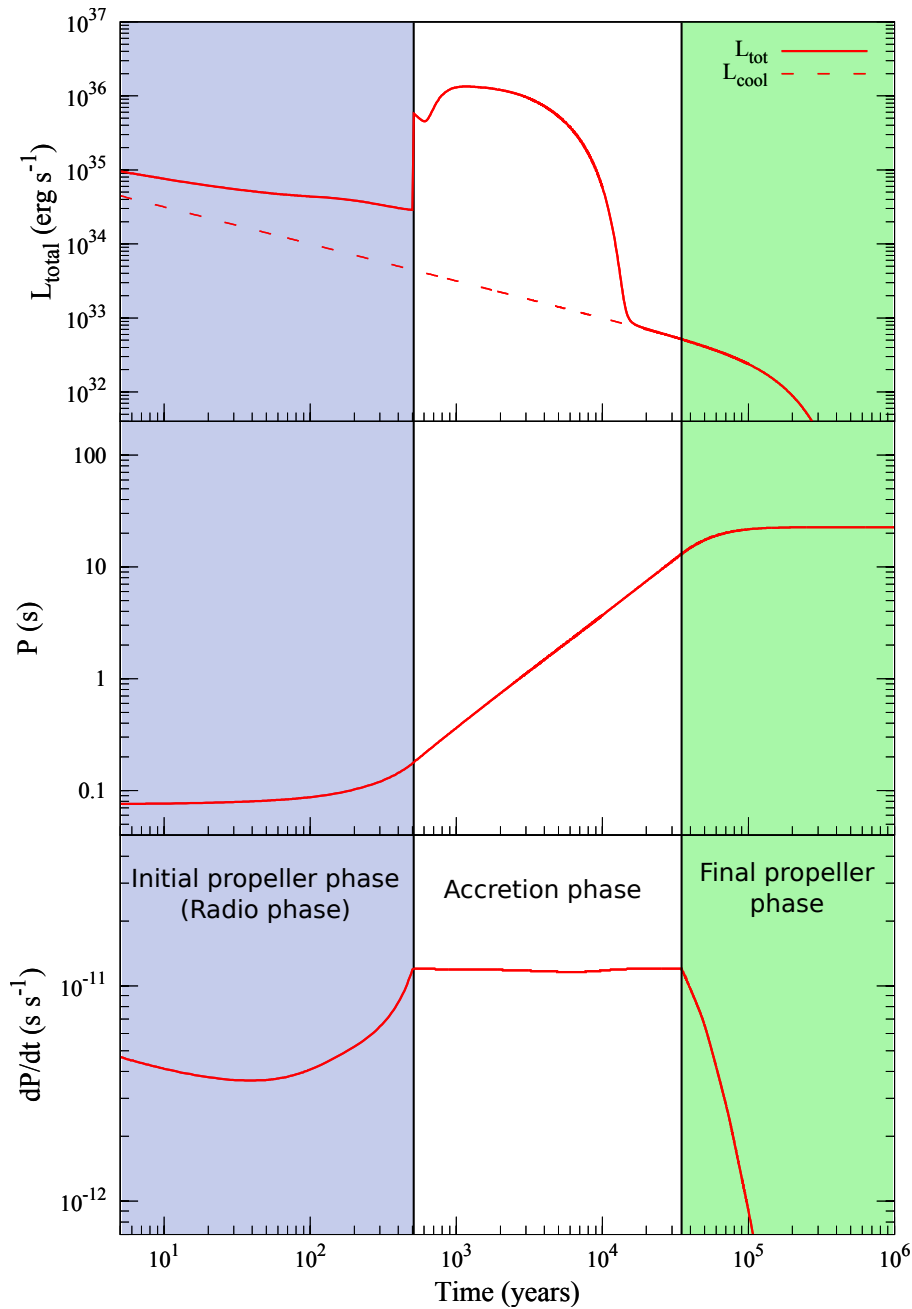


**Figure 5.1:** A sample model curve that shows three basic evolutionary episodes of a neutron star-fallback disk system. For this illustrative model,  $B_0 = 2 \times 10^{12}$  G,  $M_d = 5.7 \times 10^{-4} M_\odot$ ,  $P_0 = 75$  ms and  $T_p = 150$  K. Durations of initial propeller phase (blue region), accretion phase (white region) and final propeller phases (green region) depend on the initial conditions. To reach the long periods of several seconds, a source should pass through the accretion phase. The initial propeller phase, which could be experienced by a fraction of the sources, has not a significant effect on the properties achieved in the accretion and final propeller phases (see the text for details).

In the initial and final propeller phases, there is no accretion on to the star, and the pulsed radio emission is allowed. Nevertheless, we expect that sources could show pulsed radio emission only in the initial propeller phase, since in the final propeller stage, the sources with conventional dipole fields and long periods are usually not capable of producing pulsed radio emission; they are already below the pulsar death–line. Note that known and non-detected XDINs, and their progenitors would be expected to be radio pulsars as well if they had indeed strong dipole fields ( $B = 10^{13} - 10^{14}$  G) inferred from their observed  $P$  and  $\dot{P}$ . In the fallback disk model, XDIN properties could be achieved with  $B \simeq 10^{12}$  G (Ertan et al., 2014) which together with long periods, place these sources under the pulsar death–line in the  $B - P$  diagram.

### 5.3 Source Properties

#### **SGR 0526–66:**

For SGR 0526–66,  $P \simeq 8.1$  s and  $\dot{P} \simeq 3.8 \times 10^{-11}$  s s<sup>-1</sup> (Tiengo et al., 2009). The 0.5–10 keV unabsorbed flux was reported as  $\sim 10^{-12}$  erg s<sup>-1</sup> cm<sup>-2</sup> and for a distance of 50 kpc, which corresponds to LMC region, the bolometric X-ray luminosity of the source is  $\sim 5 \times 10^{35}$  erg s<sup>-1</sup> (Park et al., 2012).

#### **SGR 0501+4516:**

For SGR 0501+4516,  $P = 5.76$  s (Göğüş, Woods & Kouveliotou, 2008),  $\dot{P} \simeq 5.8 \times 10^{-12}$  s s<sup>-1</sup> (Göğüş et al., 2010). Based on a likely association of the source with the supernova remnant HB9, Aptekar et al. (2009) estimated the minimum distance to the source as 1.5 kpc. We have converted the observed X-ray flux into a bolometric X-ray luminosity range assuming that the source lies at a distance in the 1.5–5 kpc range. A black body + power-law model fit well to the quiescent soft X-ray spectrum of SGR 0501+4516 (Camero et al., 2014). The best-fitting parameters are  $kT = 0.52 \pm 0.02$  keV with a blackbody radius of  $0.39 \pm 0.05$  km,  $N_{\text{H}} = 0.85(3) \times 10^{22}$  cm<sup>2</sup> and the power law index  $\Gamma = 3.84 \pm 0.06$ . This corresponds to an  $L_{\text{x}}$  range from  $4.7 \times 10^{33}$  to  $5.2 \times 10^{34}$  erg s<sup>-1</sup> for distances from 1.5 to 5 kpc.

**XTE J1810–197:**

XTE J1810–197 has  $P = 5.5$  s and  $\dot{P} \sim 4 - 10 \times 10^{-12}$  s s $^{-1}$  (Camilo et al., 2007a). The source showed transient pulsed radio emission during an X-ray outburst phase (Halpern et al., 2005). It was the first pulsed radio detection from an AXP/SGR source. For a distance  $d = 3.5$  kpc (Bernardini et al., 2009; Minter et al., 2008), converting the absorbed 0.6–10 keV data of Bernardini et al. (2009) into 0.1–10 keV unabsorbed X-ray flux using the same spectral fit parameters, we estimate  $L_x \sim 1.6 \times 10^{34}$  erg s $^{-1}$ .

**1E 1841–045:**

1E 1841–045 was discovered by *Einstein HRI* (Kriss et al., 1985) and is the first source identified as an AXP with an X-ray pulse period of 11.8 s by Vasisht & Gotthelf (1997). This source is located in the supernova remnant Kes 73 with a distance of 8.5 kpc (Tian & Leahy, 2008). This source has the longest period in the currently known AXP/SGR population. A recent temporal analysis of the source gives  $\dot{P} \simeq 4.1 \times 10^{-11}$  s s $^{-1}$  (Dib & Kaspi, 2014). From the parameters of 0.5–10 keV spectrum in the quiescent state that is well described by black body + power-law with  $\Gamma = 1.9 \pm 0.2$  and  $kT = 0.43 \pm 0.003$  keV (Kumar & Safi-Harb, 2010), we estimate  $L_x \sim 5 \times 10^{35}$  erg s $^{-1}$  with  $d = 8.5$  kpc.

**1E 1048.1–5937:**

A detailed temporal analysis of 1E 1048.1–5937 data, that were taken by *RXTE* between 1996 July 3 and 2008 January 9 gives  $P \simeq 6.5$  s and  $\dot{P} \sim 2.25 \times 10^{-11}$  s s $^{-1}$  (Dib, Kaspi & Gavriil, 2009). The source showed fluctuations and anomalies during its temporal evolution for more than decades. We adopt  $P$  and  $\dot{P}$  values measured by Dib, Kaspi & Gavriil (2009) in our analysis. Based on the X-ray spectral parameters obtained by Tam et al. (2008), we estimate  $L_x$  as  $10^{35}$  erg s $^{-1}$  for a distance of  $d \sim 9$  kpc (Durant & van Kerkwijk, 2006).

**PSR J1622–4950:**

The PSR J1622–4950 was discovered in the radio band with a spin period of 4.3 s (Levin et al., 2010). From the timing analysis of the radio pulses, Levin et al. (2012) measured a factor of 2 decrease in the period derivative of the source since the discovery of the source

in radio. In the present work, we assume a  $\dot{P}$  range from 1 to  $2 \times 10^{-11} \text{ s s}^{-1}$ . Single BB fits to the X-ray spectra of PSR J1622–4950, extracted from *Chandra* and *XMM-Newton* observations, at four different dates (Anderson et al., 2012), give an unabsorbed flux  $\sim 1.1 \times 10^{-13} \text{ erg s}^{-1} \text{ cm}^{-2}$  in 0.3–10 keV. From the dispersion measure, Levin et al. (2010) gives a distance  $\sim 9 \text{ kpc}$ . We estimate the bolometric X-ray luminosity  $\sim 9.2 \times 10^{32} \text{ erg s}^{-1}$  for  $d = 9 \text{ kpc}$ .

### **SGR 1900+14:**

SGR 1900+14 has a period  $P = 5.2 \text{ s}$  (Hurley et al., 1999; Kouveliotou et al., 1999). The most recent timing analysis indicated a spin-down rate,  $\dot{P} = 9.2(4) \times 10^{-11} \text{ s s}^{-1}$  (Mereghetti et al., 2006). The distance of the source is 12–15 kpc (Vrba et al., 1996). We use the spectral fit parameters obtained by Mereghetti et al. (2006). For a hydrogen column density,  $N_{\text{H}} = 2.12 \times 10^{22} \text{ cm}^{-2}$ , converting the 2–10 keV unabsorbed flux into 0.1–10 keV unabsorbed flux by using WebPIMMS, we estimate the bolometric luminosity of the source  $L_{\text{x}} \sim 3 \times 10^{35} \text{ erg s}^{-1}$  for  $d = 12.5 \text{ kpc}$  (Davies et al., 2009).

### **CXOU J010043.1–721134:**

The period and period derivative of CXOU J010043.1–721134 are  $P = 8 \text{ s}$  and  $\dot{P} = 1.9 \times 10^{-11} \text{ s s}^{-1}$  (McGarry et al., 2005). The source is located in Small Magellanic Cloud (SMC), dwarf satellite of our galaxy, with  $d \sim 60 \text{ kpc}$ . The X-ray spectra of this source can be fit by a 2BB model with the parameters,  $R_{\text{BB1}} \sim 12.1 \text{ km}$ ,  $R_{\text{BB2}} \sim 1.7 \text{ km}$ ,  $kT_1 \sim 0.3 \text{ keV}$ ,  $kT_2 \sim 0.7 \text{ keV}$  (Tiengo, Esposito & Mereghetti, 2008). With  $N_{\text{H}} = 5.9 \times 10^{20} \text{ cm}^{-2}$  (Dickey & Lockman, 1990) we obtain  $L_{\text{x}} \sim 6.5 \times 10^{34} \text{ erg s}^{-1}$ .

### **1RXS J170849.0–400910:**

This source has  $P = 11 \text{ s}$ , and  $\dot{P} = 1.9 \times 10^{-11} \text{ s s}^{-1}$  (Dib & Kaspi, 2014), and a distance of 3.8 kpc (Durant & van Kerkwijk, 2006). From the unabsorbed 0.5–10 keV flux reported by Rea et al. (2007a) we estimate  $L_{\text{x}} = 1.5 \times 10^{35} \text{ erg s}^{-1}$ .

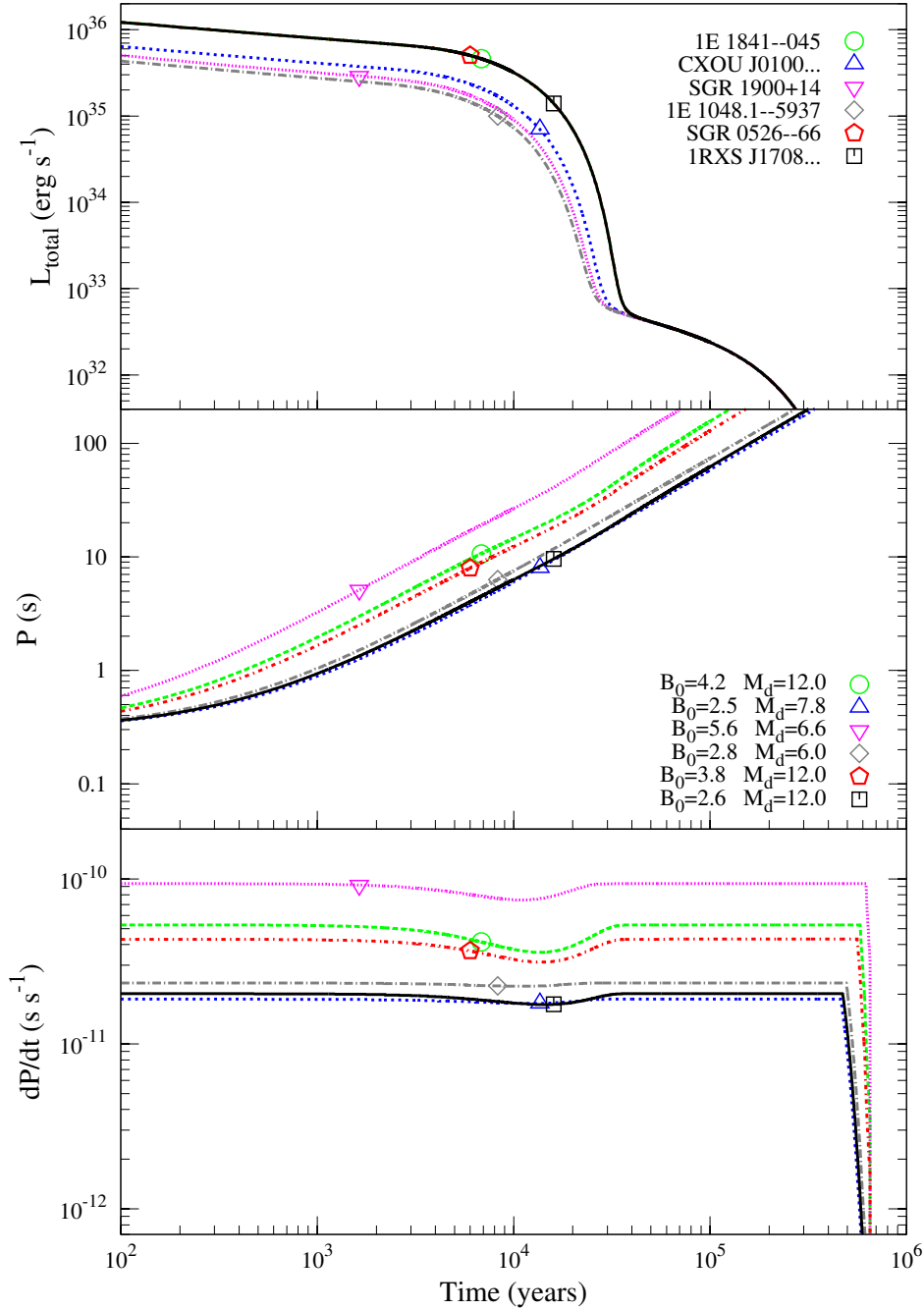


**Figure 5.2:** The long-term evolutionary model curves of six AXP/SGRs. For all these AXP/SGRs, both  $M_d$  and  $B_0$  are constrained to very narrow ranges with central values given in the middle panel. The names of the sources are shown in the top panel. For these models,  $T_p = 100$  K and  $C = 1 \times 10^{-4}$ .  $B_0$  and  $M_d$  values are given in units of  $10^{12}$  G and  $10^{-6} M_\odot$ . For these sources accretion goes on till  $t \sim 5 \times 10^5$  yr. But, the accretion luminosity remain below the cooling luminosity at  $t \sim$  a few  $10^4$  yr.

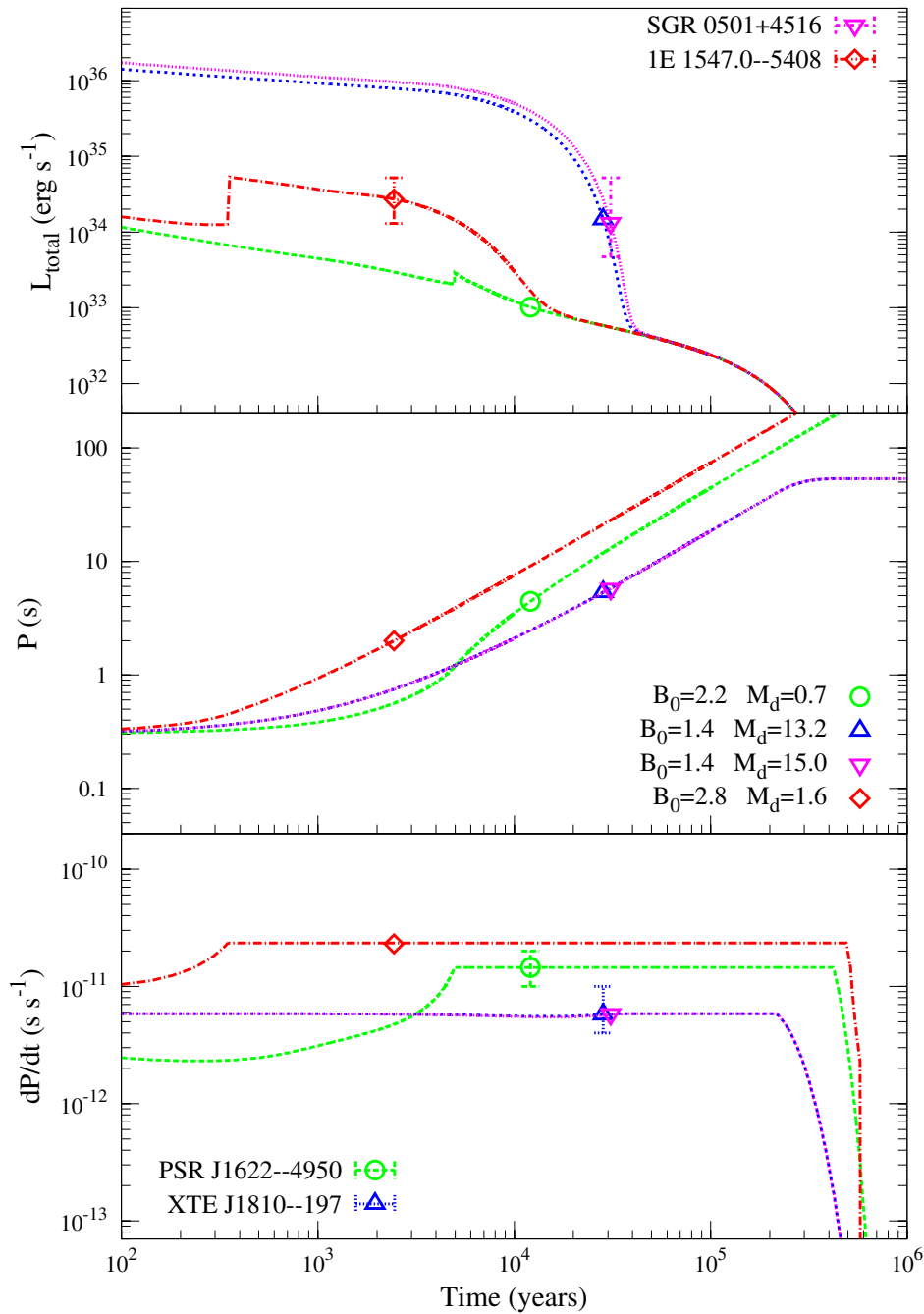


**Figure 5.3:** The illustrative model curves representing the long-term evolutions of the four AXP/SGRs which have uncertainties in either  $L_x$  or  $\dot{P}$  measurements. The error bars show the uncertainties in measurements. For these sources, unlike the six sources given in Fig. 5.2, our model cannot well constrain the  $M_d$  and  $B_0$  values.  $B_0$  and  $M_d$  values are given in units of  $10^{12}$  G and  $10^{-6} M_\odot$ . The model parameters are given in Table 5.1. The constant  $\dot{P}$  epochs correspond to accretion phases. 1E 1547.0–5408 and XTE J1810–197 enter the accretion phase at times  $\sim 3 \times 10^2$  and  $5 \times 10^3$  yr respectively.

**1E 1547.0–5408:**

This active transient source, also known as SGR J1550–5418, was discovered in 1980 by *Einstein* satellite in the X-ray band. Later, the source was also observed in the radio band with a pulsation period,  $P = 2.1$  s and  $\dot{P} = 2.3 \times 10^{-11}$  s s $^{-1}$  (Camilo et al., 2007b). From the analysis of more recent X-ray observations with *RXTE* and *Swift*, its average period derivative was estimated as  $\dot{P} \simeq 4.8 \times 10^{-11}$  s s $^{-1}$  after the burst (Dib et al., 2012). We adopt the  $\dot{P}$  value measured by Camilo et al. (2007b) in the quiescent state. The unabsorbed flux in 0.5–10 keV band is  $5.4 \times 10^{-12}$  erg s $^{-1}$  cm $^{-2}$  (Bernardini et al., 2011). The X-ray luminosity is estimated to be  $1.3 \times 10^{34}$  and  $5.2 \times 10^{34}$  erg s $^{-1}$  for distances,  $d = 4.5$  kpc (from the dust model by Tiengo et al. 2010) and  $d = 9$  kpc (derived from the dispersion measure by Camilo et al. 2007b). We adopt this X-ray luminosity range for 1E 1547.0–5408 in our model calculations.

**4U 0142+61:**

4U 0142+61 is one of the most extensively studied AXPs in different energy bands from optical to hard X-rays. It has  $P = 8.7$  s and  $\dot{P} = 2 \times 10^{-12}$  s s $^{-1}$  (Dib & Kaspi, 2014). The soft (< 10 keV) and the hard X-ray luminosity of the source are  $\sim 3.2 \times 10^{35}$  and  $1.4 \times 10^{35}$  erg s $^{-1}$  respectively (den Hartog et al., 2008). In the quiescent state, 0.8–160 keV luminosity of the source is  $\sim 4.6 \times 10^{35}$  erg s $^{-1}$  for a distance  $d = 3.6$  kpc (Durant & van Kerkwijk, 2006).

**1E 2259+586:**

This source has  $P = 7$  s and  $\dot{P} = 4.8 \times 10^{-13}$  s s $^{-1}$  (Dib & Kaspi, 2014; Morini et al., 1988). The unabsorbed flux of the source in 1–10 keV band is  $5 \times 10^{-11}$  erg s $^{-1}$  cm $^{-2}$  in the quiescent state. For  $d = 3.2$  kpc (Kothes, Uyaniker & Yar, 2002), the bolometric X-ray luminosity (including the hard x-ray emission) is assumed as  $\sim 2 \times 10^{35}$  erg s $^{-1}$  in the quiescent state (see Table 3 of Viganò et al. 2013).

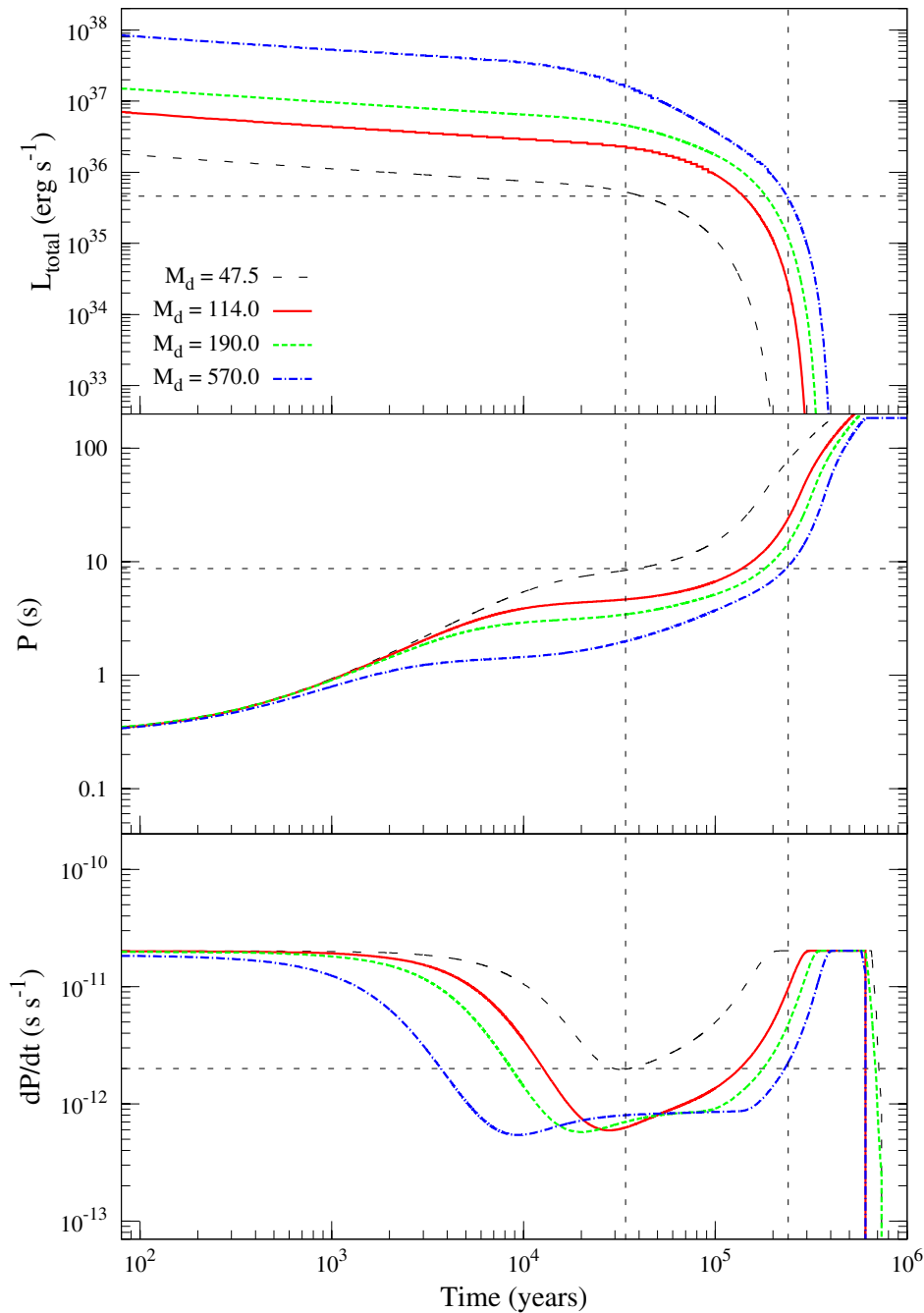


**Figure 5.4:** Illustrative model curves that could represent the long-term evolution of 4U 0142+61. Reasonable model fits could be obtained with a large range of disk mass, a narrow  $B_0$  range around  $2.6 \times 10^{12}$  G, and  $T_p \sim 50 - 60$  K. These models are obtained with  $T_p = 54$  K and  $M_d$  values (in units of  $10^{-6} M_\odot$ ) shown in the top panel. The model sources can acquire the source properties at the ages in the range limited by the vertical dashed lines shown in the figure ( $\sim 3 \times 10^4 - 2 \times 10^5$  y). The horizontal dashed lines show the observed properties of the source. For these model curves, accretion remains as the dominant source of luminosity.

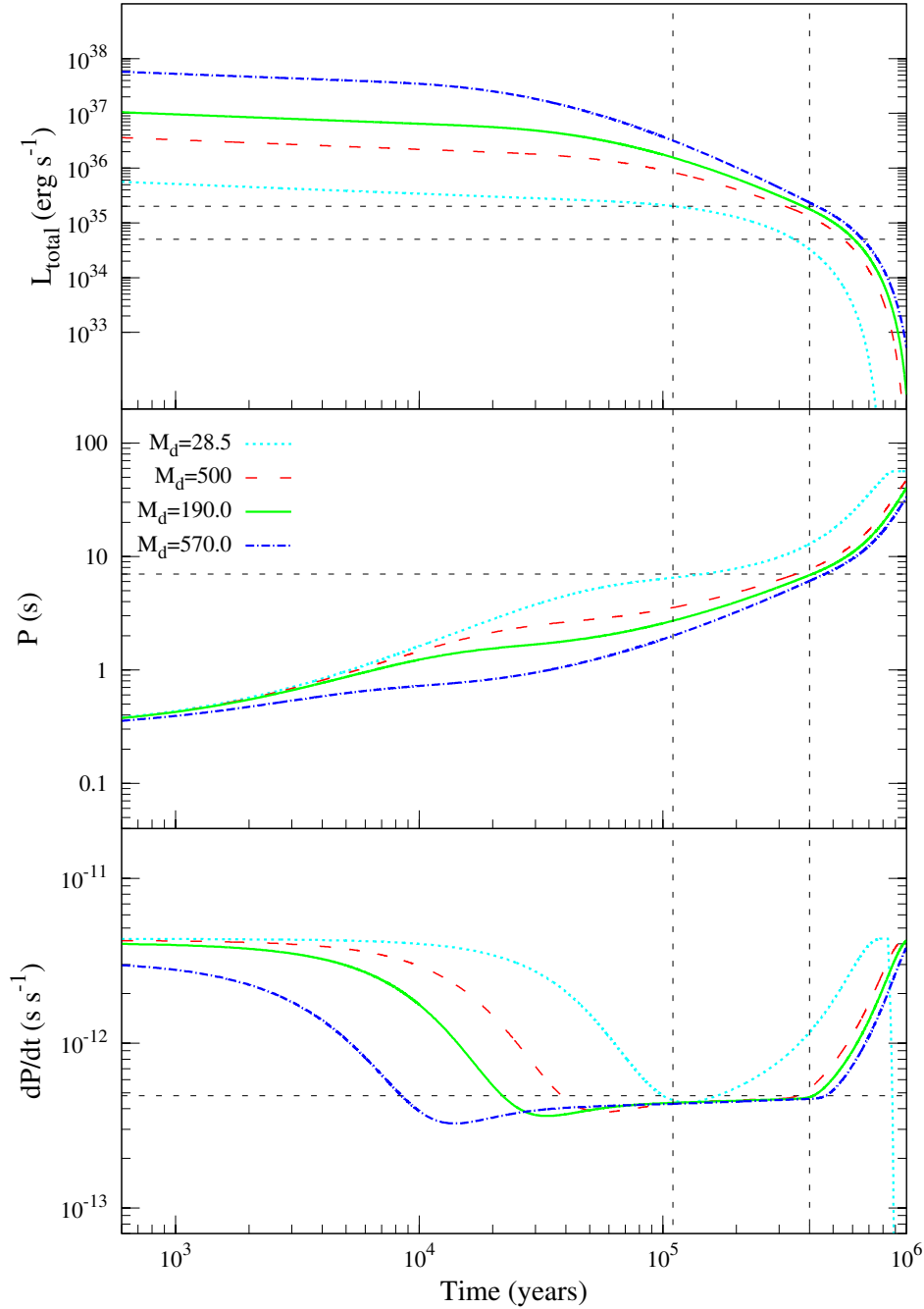


**Figure 5.5:** The same as Fig. 7, but for 1E 2259+586. For all these model curves,  $B_0 = 1.2 \times 10^{12}$  G,  $T_p = 30$  K and  $C = 1 \times 10^{-4}$ .  $M_d$  values are given in units of  $10^{-6} M_\odot$ . Reasonable model fits for this source could be obtained with  $T_p \sim 30\text{--}40$  K at the ages  $t \sim 1\text{--}4 \times 10^5$  yr (between the dashed vertical lines). These model sources, like those in Fig 5.4, remain in the accretion phase their births to the present ages.

**Table 5.1:** The initial disk mass ( $M_d$ ), dipole magnetic field strength at the pole of the star ( $B_0$ ), minimum active disk temperature ( $T_p$ ) and the current age of the sources found from the models with the evolutionary curves given in Fig 4., and the observed properties  $L_x$ ,  $P$  and  $\dot{P}$  of the sources. We take the irradiation parameter  $C = 10^{-4}$  and the viscosity parameter  $\alpha = 0.045$  for all of the sources.

Name	$M_d$ ( $10^{-6} M_\odot$ )	$B_0$ ( $10^{12}$ G)	$T_p$ (K)	age (yr)	$L_x$ ( $10^{33}$ erg s $^{-1}$ )	$P$ (s)	$\dot{P}$ ( $10^{-13}$ s s $^{-1}$ )
SGR 0526–66	12.0	3.8	100	$6 \times 10^3$	500	8	380
XTE J1810–197	6.0–24.0	1.2–1.8	100	$2\text{--}4 \times 10^4$	16	5.5	40–100
1E 1841–045	12.0	4.2	100	$7 \times 10^3$	$\sim 500$	11.8	410
1E 1048.1–5937	6.0	2.8	100	$8 \times 10^3$	100	6.5	225
PSR J1622–4950	0.7–1.2	1.8–2.2	100	$\sim 1 \times 10^4$	0.9	4.3	100–200
SGR 1900+14	6.6	5.6	100	$1.6 \times 10^3$	300	5.2	920
SGR 0501+4516	12.0–18.0	1.4	100	$3 \times 10^4$	4.7–52	5.76	58
CXOU J0100...	7.8	2.5	100	$1.3 \times 10^4$	65	8	190
1RXS J1708...	12.0	2.6	100	$1.4 \times 10^4$	150	11	190
1E 1547.0–5408	1.0–2.1	4.0	100	$2 \times 10^3$	13–52	2	230
4U 0142+61	47.5–570.0	2.4–2.6	54	$\sim 0.3\text{--}2 \times 10^5$	460	8.7	20
1E 2259+586	28.5–570.0	1.2	30	$\sim 1\text{--}4 \times 10^5$	$\sim 200$	7	4.8

**Table 5.2:** Observed properties of the six XDINs (see Ertan et al. 2014 and references therein for details).

	$P$ (s)	$\dot{P}$ ( $10^{-14}$ s s $^{-1}$ )	$L_x$ ( $10^{31}$ erg s $^{-1}$ )
RX J0720.4–3125	8.39	$\sim 7$	$\sim 16$
RX J1856.5–3754	7.06	2.97(7)	9.5
RX J2143.0+0654	9.43	4.1(18)	11
RX J1308.6+2127	10.31	11.2	7.9
RX J0806.4–4123	11.37	5.5(30)	2.5
RX J0420.0–5022	3.45	2.8(3)	2.6

**Table 5.3:** The disk parameters and the corresponding ages for the six XDINs. The viscosity parameter  $\alpha = 0.045$  for all the model sources. (Taken from Ertan et al. 2014).

	$B_0$ ( $10^{12}$ G)	$M_d$ ( $10^{-6} M_\odot$ )	$T_p$ (K)	$C$ ( $10^{-4}$ )	age ( $10^5$ y)
RX J0720.4–3125	1.1–1.3	0.8–12.0	106	1	1.45
RX J1856.5–3754	0.9–1.1	0.8–18.0	100	1	1.85
RX J2143.0+0654	1.0–1.2	1.0–11.6	100	1	1.9
RX J1308.6+2127	0.9–1.0	0.8–18.0	100	1.5	2.1
RX J0806.4–4123	0.8–0.9	0.5–18.0	100	2.3	3.1
RX J0420.0–5022	0.35–0.38	4.8–18.0	82	7	3.2

## 5.4 Results

We could reproduce the observed source properties ( $P$ ,  $\dot{P}$  and  $L_x$ ) of 12 AXP/SGRs in the frame of the fallback disk model (Figs. 5.2, 5.3, 5.4 and 5.5) using similar basic disk parameters ( $\alpha = 0.045$ ,  $C = 1 \times 10^{-4}$ ,  $T_p \sim 100$  K). We have chosen AXP/SGRs with relatively well-known quiescent-state properties for an investigation of the disk mass and magnetic field correlation. Our results indicate that the 12 AXP/SGRs that we have studied here are evolving in the accretion phase. Two sources, namely 4U 0142+61 and 1E 2259+586, seem to be the only AXP/SGRs that are currently evolving close to rotational equilibrium (see Figs 5.4 and 5.5). We have obtained the model curves that can fit the individual source properties with the model parameters given in Table 5.1. In the model, the dipole field strength,  $B_0$ , is well constrained for the accreting sources. Estimated  $B_0$  and  $M_d$  ranges given in Table 5.1 corresponds to the uncertainties in measured  $\dot{P}$  values (PSR J1622–4950, XTE J1810–197) and distances (SGR 0501+4516, 1E 1547.0–5408). Our earlier results indicate that SGR 0418+5729 completed its evolution in the accretion phase, and is now evolving in the final propeller phase (Alpar, Ertan & Çalışkan, 2011), Swift J1822.3–1606 could be in either accretion or in the final propeller phase depending on its actual X-ray luminosity in the quiescent state (Benli et al., 2013) and SGR 0501+4516 is found to be accreting from the fallback disk at present (Benli, Çalışkan & Ertan 2015).

Recently, Ertan et al. (2014) analysed the individual source properties of six XDINs using the same model as we employ in the present work. With almost the same basic disk parameters, current X-ray luminosity and rotational properties of XDINs can also be produced by this model. For comparison with AXP/SGRs properties, we also present the results obtained by Ertan et al. (2014) for XDINs in Table 5.3. The properties of the six XDINs could be achieved by the sources in the final propeller phase, unlike most of the AXP/SGRs which seem to be still accreting matter from the disk (Figs. 5.2 and 5.3). In the propeller phases, the surface emission of the sources are powered mainly by the cooling luminosity. In the final propeller phase, we obtain the properties of XDINs with a large range of  $M_d$ . Nevertheless,  $B_0$  values of these sources are well constrained despite the uncertainty in their initial disk masses. In Fig. 5.6, we plot the  $B_0$  and  $M_d$  values of both AXP/SGRs and XDINs, estimated from the model results. It is seen in Fig. 5.6 that

the magnitude of the dipole field on the pole of the star,  $B_0$ , ranges from  $\sim 3 \times 10^{11}$  G to  $\sim 6 \times 10^{12}$  G for all AXP/SGR and XDIN sources. In addition, it is clearly seen that the  $B_0$  values of XDINs ( $\sim 3 \times 10^{11}$ – $1 \times 10^{12}$  G) remains systematically below those of AXP/SGRs ( $\sim 1 \times 10^{12}$  –  $6 \times 10^{12}$  G). Due to large uncertainties in  $M_d$ , we could not determine whether there is a correlation between the disk mass and the dipole field strength of these sources.

## 5.5 Discussion and Conclusions

We have investigated the likely long-term evolutionary paths of individual AXP/SGR sources with relatively small uncertainties in distances and period derivatives in the quiescent state. Our results show that the observed  $P$ ,  $\dot{P}$  and  $L_x$  values of 14 sources, including the two low-B magnetars analyzed earlier (Alpar, Ertan & Çalışkan, 2011; Benli et al., 2013), could be achieved by neutron stars evolving with fallback disks and conventional dipole fields. Comparing Tables 5.1 and 5.3, it is seen that the basic disk parameters, namely the irradiation strength,  $C$ , the transition temperature between the active and passive disk state,  $T_p$ , and the  $\alpha$  parameter of the kinematic viscosity are all almost the same as the parameters used for XDINs in Ertan et al. (2014). The model can produce the individual source properties ( $P$ ,  $\dot{P}$ ,  $L_x$ ) simultaneously for each of AXP/SGR and XDIN sources.

Our results indicate that most AXP/SGRs are currently in the accretion phase. The two relatively old low-B magnetars seem to have completed the accretion epoch, and are currently spinning down by the disk torques without accretion on to the star, in the final propeller phase. Most of the accreting sources are not close to rotational equilibrium, with the exceptions 4U 0142+61 and 1E 2259+586 which seem to have initial disk masses greater than those of other AXP/SGR sources. We have obtained plausible model fits for these sources with relatively low  $T_p$  values (see Table 5.1), which might be due to unknown details of the disk-field interaction geometry and efficiency when the Alfvén radius approaches the co-rotation radius.

The birth rate of XDINs are estimated to be comparable to the radio pulsar birth rate and about an order of magnitude greater than that of AXP/SGRs (see e.g. Popov, Turolla & Possenti 2006). In other words, the number of currently known AXP/SGRs is

not sufficient for these sources to be the *only* progenitors of XDINs. Furthermore, our results imply that a fraction of AXP/SGRs have evolutionary paths not converging into the XDIN properties. In particular, some of AXP/SGRs could reach periods longer than the longest presently observed XDIN period,  $\sim 12$  s, but at late phases with very low luminosities. One basic difference between these populations seems to be the relatively weak dipole fields ( $\sim 10^{11}$ – $10^{12}$  G) of XDINs (see Tables 5.1 and 5.3). For this  $B_0$  range, the observed upper limit for periods of XDINs is likely to be due to physical constraints rather than the selection effects (see Fig. 3 of Ertan et al. 2014). Because, for given basic disk parameters, the dominant factor that determines the maximum period is the strength of the dipole field, rather than the disk mass. With the relatively weak dipole fields of XDINs, indicated by the model, the longest attainable periods are already close to the upper bound of observed periods. This result for the period upper limits needs more detailed investigation and should be taken with some caution due to our simplified condition for the transition between the accretion and propeller phases. The relation between  $B_0$  and the period upper limit will be investigated in detail in future work. In our model, the disk torque acting on the star is most efficient in the accretion epochs, and the increasing periods of the sources level off with termination of the accretion epoch. The results obtained by Ertan et al. (2014) imply that, unlike most AXP/SGRs, for the six XDIN sources<sup>1</sup> the accretion phase terminated long ago, and they are slowing down in the final propeller phase at present.

Since the model results do not well constrain the disk masses for XDINs, we are not able to determine whether there is a systematic relation between the actual disk masses and the dipole fields of the combined XDIN and AXP/SGR populations (see Fig. 5.6). Nevertheless, we estimate that XDINs are likely to be close to the lower bounds on their allowed disk masses seen in Fig. 5.6, since evolution with low disk masses leaves most of the young XDINs below the current detection limits. This picture is consistent with the lack of detections of many young XDINs in X-rays at the ages of AXP/SGRs. This might also imply that the disk masses of most XDINs could form the peak of the initial disk mass distribution of the young neutron star systems that have fallback disks. Among the neutron star systems that evolve with fallback disks and can enter the accretion phase, those with stronger fields are more likely to have greater initial disk masses. Because,

---

<sup>1</sup>The period derivative of seventh XDIN has not been confirmed yet.

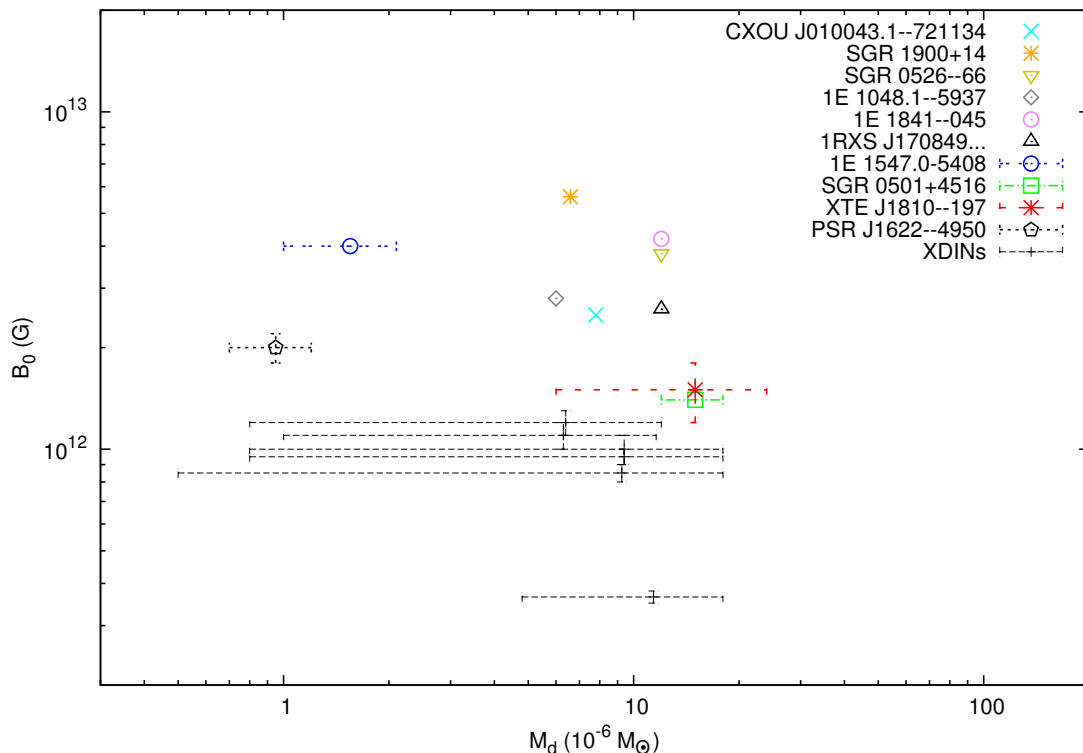


**Figure 5.6:** The  $B_0$  versus  $M_d$  distribution of some AXP/SGRs (present work) and the six XDINs (from Ertan et al. 2014). The error bars represent the  $B_0$  and  $M_d$  ranges for which the model sources acquire the observed source properties  $P$ ,  $\dot{P}$  and  $L_x$  simultaneously.

stronger fields require greater disk masses for the inner disk to enter the accretion phase. We could tentatively conclude that these systems that are located in the upper tails of both  $B_0$  and  $M_d$  distributions are likely to be the sources that are observed as X-ray luminous AXP/SGRs. In our model,  $\dot{P} \propto B_0^2$  in the accretion episode, and therefore among the accreting sources those with relatively high  $\dot{P}$  values have also stronger dipole fields. This conclusion cannot be generalized to the stars that are close to the rotational equilibrium, like 4U 0142+61 and 1E 2259+586 or the sources in the propeller phase, like XDINs.

As a final note, in our model, the sources in the first propeller phase could be observed as “high-B” radio pulsars. This is because the efficient disk torques increase  $\dot{P}$  significantly beyond the level that can be achieved by the magnetic dipole torques with the same field strength. A detailed population synthesis of these sources, which is beyond the scope of the present work, will be studied in a separate paper.

# **Chapter 6**

## **SUMMARY AND CONCLUSION**

In this thesis, we have investigated the long-term evolution, short-term X-ray enhancement/outburst, optical and infra-red disk emission properties and the radio properties of members of different young neutron star populations in the frame of the fallback disk model.

We have studied the long-term evolution of a source using a numerical code developed to investigate the evolution of magnetized neutron stars with fallback disks. In our applications, we have employed similar basic disk parameters (viscosity, irradiation efficiency and inactivation temperature of the disk), a requirement to remain self-consistent in testing the model and to have reliable set of results to be used for comparison of the properties of different populations. The different initial conditions (initial period and disk mass, the dipole magnetic field strength) are likely to be responsible for the emergence of different young neutron star populations. To constrain these properties, we have repeated our calculations many times tracing these properties. Finally, we have compared our results obtained for different populations.

We have also worked on the newly observed X-ray enhancement light curve of different sources, with the same model applied first to the enhancement light curve of SGR 1900+14. The detailed description of this model can be found in Çalışkan & Ertan (2012). Furthermore, we have examined the radio properties of XDINs indicated by our long-term evolution model, which provides an independent test for the predictions of the model. Finally, we have studied the broad-band optical-IR spectrum of the disk emitted from a large range of radii from inner to the outer disk.

In Chapter 2, we have analyzed both the long-term evolution and the X-ray enhancement of “low-B magnetar” Swift J1822–1606. We have shown that the rotational properties and the X-ray luminosity of the source can be explained in the fallback disk model. Our results imply that there are two possibilities for the long-term evolution of this source. At present, the source could be still in the accretion phase and powered by the accretion luminosity in the quiescent phase. The second possibility is that the source is in the final propeller phase in quiescence, and recently observed X-ray enhancement could have taken the source to the accretion phase. For both possibilities, it seems that Swift J1822–1606 is currently accreting. For the latter case, the star is expected to return back to the propeller phase at the end of the enhancement period. We have shown that this observed epoch of the enhancement light curve of Swift J1822–1606 could be produced by mass

flow from the inner disk onto the surface of the star with the initial conditions built up in the soft gamma burst episode, that is, after the burst energy pushed the inner disk back and formed a pile-up at the innermost disk.

In Chapter 3, we have applied the same model to the long-term evolution and short term X-ray enhancement of SGR 0501+4516. We have found that a neutron star with a fallback disk acquires the X-ray and the rotational properties of this typical AXP/SGR source. In this case, we could well constrain the dipole magnetic field strength. We have also shown that the X-ray enhancement light curve of the source can be reproduced by the same model employed for explaining the X-ray outburst of Swift J1822–1606. In addition, we have estimated the optical/IR data of the source. The results are in agreement with the emission from a disk explaining the evolution of the source. We do not expect radio pulses from SGR 0501+4516 because the source is currently in the accretion phase.

In Chapter 4, we have examined the long-term evolution of six individual XDIN sources with measured period, period derivative and X-ray luminosity and found that these sources slowed down to observed long periods (2–12 s) during the accretion phase. Our results showed that currently, all XDINs are in the final propeller phase where the X-ray luminosities are produced by the intrinsic cooling of the star and the disk torques acting on neutron stars are dropping off. The periods of XDINs will converge soon close to the current values. In this systematic study, we have constrained the strength of the dipole magnetic fields of XDINs into narrow range while initial disk masses producing the properties of these sources have been found to be in a wide range. These sources are not likely to produce pulsed radio emission, because the low magnetic fields that we have found places these sources below the so-called death-line on  $P - \dot{P}$  diagram. This result is consistent with none detection of radio pulse from XDINs yet.

Finally, in Chapter 5, we have investigated the long-term evolutionary paths of twelve AXP/SGR sources with well-known persistent properties. Properties of each individual source could be achieved by a neutron star with a conventional dipole field ( $\sim 10^{12}$ ), which evolves with the fallback disk with the similar basic disk parameters ( $C, T_p, \alpha$ ) to those of XDINs. Our results indicated that most AXP/SGRs are currently in the accretion phase. The two relatively old sources, namely 4U 0142+61 and 1E 2259+586, seem to have completed the accretion epoch, and are currently spinning down by the disk torques without accretion on to the star. In this study, we have constrained the magnetic fields

of AXP/SGRs into quite narrow ranges for each source. The initial disk masses which can produce the source properties are in wider ranges that makes it hard to understand the correlation between the disk mass and the dipole magnetic field strength of AXP/SGRs and XDINs. The possible correlation could be tested through further investigation of young neutron stars, e.g. “high-B radio pulsars”. This analysis will help us understand the differences in the initial conditions of different young neutron star populations.

The ultimate indication of our results in this thesis is that the fallback disk model that we employ is sufficiently successful in explaining the long-term properties of AXP/SGRs and XDINs, and also the optical/IR data of a typical AXP/SGR source, SGR 0501+4516. We could account for both the long-term evolutions and the X-ray enhancement data of “low-B magnetar”, Swift J1822–1606, and SGR 0501+4516 consistently. Through extensive investigation on the long-term evolutions of the sources in the AXP/SGR and XDIN populations, we have found that the fallback disk model provides reasonable explanations to the observed source properties and to the lack of radio pulse detections from these sources. Obviously, the further study of other young neutron star populations (e.g. HBRPs, RRATs, CCOs) similar to the works performed in this thesis, are of great importance in order to make a population synthesis of these groups within the same picture. Our future studies will be focused on the investigation of other populations. The priority will be given particularly to HBRPs.

## Bibliography

- Abdo A. A. et al., 2013, *ApJS*, 208, 17
- Alpar M. A., 2001, *ApJ*, 554, 1245
- Alpar M. A., 2007, *Ap&SS*, 308, 133
- Alpar M. A., Ankay A., Yazgan E., 2001, *ApJL*, 557, L61
- Alpar M. A., Ertan Ü., Çalışkan Ş., 2011, *ApJ*, 732, L4
- Anderson G. E. et al., 2012, *ApJ*, 751, 53
- Aptekar R. L., Cline T. L., Frederiks D. D., Golenetskii S. V., Mazets E. P., Pal'shin V. D., 2009, *ApJ*, 698, L82
- Archibald A. M., Kondratiev V. I., Hessels J. W. T., Stinebring D. R., 2014, *ApJL*, 790, L22
- Bachetti M. et al., 2014, *Nature*, 514, 202
- Balbus S. A., Hawley J. F., 1991, *ApJ*, 376, 214
- Barthelmy S. D. et al., 2008, *The Astronomer's Telegram*, 1676, 1
- Benli O., Çalışkan Ş., Ertan Ü., 2015, *MNRAS*, 447, 2282
- Benli O., Çalışkan Ş., Ertan Ü., Alpar M. A., Trümper J. E., Kylafis N. D., 2013, *ApJ*, 778, 119
- Benli O., Ertan Ü., 2016, *MNRAS*, 457, 4114
- Bernardini F. et al., 2009, *A&A*, 498, 195
- Bernardini F. et al., 2011, *A&A*, 529, A19
- Bondi H., Hoyle F., 1944, *MNRAS*, 104, 273

- Burwitz V., Haberl F., Neuhäuser R., Predehl P., Trümper J., Zavlin V. E., 2003, *A&A*, 399, 1109
- Çalışkan Ş., Ertan Ü., 2012, *ApJ*, 758, 98
- Çalışkan Ş., Ertan Ü., Alpar M. A., Trümper J. E., Kylafis N. D., 2013, *MNRAS*, 431, 1136
- Camero A. et al., 2014, *MNRAS*, 438, 3291
- Camilo F. et al., 2007a, *ApJ*, 663, 497
- Camilo F., Ransom S. M., Halpern J. P., Reynolds J., 2007b, *ApJ*, 666, L93
- Chatterjee P., Hernquist L., Narayan R., 2000, *ApJ*, 534, 373
- Chen K., Ruderman M., 1993, *ApJ*, 402, 264
- Chevalier R. A., 1989, *ApJ*, 346, 847
- Colgate S. A., 1971, *ApJ*, 163, 221
- Cummings J. R., Burrows D., Campana S., Kennea J. A., Krimm H. A., Palmer D. M., Sakamoto T., Zan S., 2011, *The Astronomer's Telegram*, 3488
- D'Angelo C. R., Spruit H. C., 2012, *MNRAS*, 420, 416
- Davidson K., Ostriker J. P., 1973, *ApJ*, 179, 585
- Davies B., Figer D. F., Kudritzki R.-P., Trombly C., Kouveliotou C., Wachter S., 2009, *ApJ*, 707, 844
- den Hartog P. R., Hermsen W., Kuiper L., Vink J., in't Zand J. J. M., Collmar W., 2006, *A&A*, 451, 587
- den Hartog P. R., Kuiper L., Hermsen W., Kaspi V. M., Dib R., Knödseder J., Gavriil F. P., 2008, *A&A*, 489, 245
- Dhillon V. S. et al., 2011, *MNRAS*, 416, L16
- Dib R., Kaspi V. M., 2014, *ApJ*, 784, 37

- Dib R., Kaspi V. M., Gavriil F. P., 2009, *ApJ*, 702, 614
- Dib R., Kaspi V. M., Scholz P., Gavriil F. P., 2012, *ApJ*, 748, 3
- Dickey J. M., Lockman F. J., 1990, *ARA&A*, 28, 215
- Drake J. J. et al., 2002, *ApJ*, 572, 996
- Dubus G., Lasota J.-P., Hameury J.-M., Charles P., 1999, *MNRAS*, 303, 139
- Duncan R. C., Thompson C., 1992, *ApJL*, 392, L9
- Durant M., van Kerkwijk M. H., 2006, *ApJ*, 650, 1070
- Ekşi K. Y., Alpar M. A., 2003, *ApJ*, 599, 450
- Ekşi K. Y., Alpar M. A., 2005, *ApJ*, 620, 390
- Ertan Ü., Alpar M. A., 2003, *ApJL*, 593, L93
- Ertan Ü., Çalışkan Ş., 2006, *ApJ*, 649, L87
- Ertan Ü., Çalışkan Ş., Benli O., Alpar M. A., 2014, *MNRAS*, 444, 1559
- Ertan Ü., Ekşi K. Y., Erkut M. H., Alpar M. A., 2009, *ApJ*, 702, 1309
- Ertan Ü., Erkut M. H., 2008, *ApJ*, 673, 1062
- Ertan Ü., Erkut M. H., Ekşi K. Y., Alpar M. A., 2007, *ApJ*, 657, 441
- Ertan Ü., Göğüş E., Alpar M. A., 2006, *ApJ*, 640, 435
- Faucher-Giguère C.-A., Kaspi V. M., 2006, *ApJ*, 643, 332
- Frank J., King A., Raine D. J., 2002, *Accretion Power in Astrophysics: Third Edition*
- Geppert U., Urpin V., Konenkov D., 1996, *A&A*, 307, 807
- Ghosh P., 2007, *Rotation and Accretion Powered Pulsars*. World Scientific Publishing Co
- Gogus E., Kouveliotou C., Strohmayer T., 2011, *The Astronomer's Telegram*, 3491
- Gotthelf E. V., Halpern J. P., Alford J., 2013, *ApJ*, 765, 58
- Göğüş E., Woods P., Kouveliotou C., 2008, *The Astronomer's Telegram*, 1677, 1

- Göğüş E., Woods P. M., Kouveliotou C., Kaneko Y., Gaensler B. M., Chatterjee S., 2010, *ApJ*, 722, 899
- Grenier I. A., 2000, *A&A*, 364, L93
- Haberl F., 2004, *Advances in Space Research*, 33, 638
- Haberl F., 2007, *Ap&SS*, 308, 181
- Haberl F., Motch C., Buckley D. A. H., Zickgraf F.-J., Pietsch W., 1997, *A&A*, 326, 662
- Haberl F. et al., 2004, *A&A*, 424, 635
- Halpern J. P., Gotthelf E. V., Becker R. H., Helfand D. J., White R. L., 2005, *ApJ*, 632, L29
- Hambaryan V., Suleimanov V., Schwobe A. D., Neuhäuser R., Werner K., Potekhin A. Y., 2011, *A&A*, 534, A74
- Hohle M. M., Haberl F., Vink J., Turolla R., Zane S., de Vries C. P., Méndez M., 2010, *A&A*, 521, A11
- Holland S. T. et al., 2008, *GRB Coordinates Network*, 8112, 1
- Hurley K. et al., 1999, *ApJ*, 510, L111
- Inutsuka S.-i., Sano T., 2005, *ApJ*, 628, L155
- Kaplan D. L., Kamble A., van Kerkwijk M. H., Ho W. C. G., 2011, *ApJ*, 736, 117
- Kaplan D. L., van Kerkwijk M. H., 2005, *ApJ*, 635, L65
- Kaplan D. L., van Kerkwijk M. H., 2009a, *ApJ*, 705, 798
- Kaplan D. L., van Kerkwijk M. H., 2009b, *ApJ*, 692, L62
- Kaplan D. L., van Kerkwijk M. H., 2011, *ApJ*, 740, L30
- Kaplan D. L., van Kerkwijk M. H., Anderson J., 2007, *ApJ*, 660, 1428
- Kaplan D. L., van Kerkwijk M. H., Marshall H. L., Jacoby B. A., Kulkarni S. R., Frail D. A., 2003, *ApJ*, 590, 1008

- Kaspi V. M., 2010, *Proceedings of the National Academy of Science*, 107, 7147
- Kaspi V. M., Gavriil F. P., Woods P. M., Jensen J. B., Roberts M. S. E., Chakrabarty D., 2003, *ApJL*, 588, L93
- Keane E. F., 2016, *MNRAS*, 459, 1360
- Keane E. F., Kramer M., 2008, *MNRAS*, 391, 2009
- Keane E. F., Kramer M., Lyne A. G., Stappers B. W., McLaughlin M. A., 2011, *MNRAS*, 415, 3065
- Konar S., Bhattacharya D., 1999, *MNRAS*, 303, 588
- Kothes R., Uyaniker B., Yar A., 2002, *ApJ*, 576, 169
- Kouveliotou C. et al., 1999, *ApJ*, 510, L115
- Kriss G. A., Becker R. H., Helfand D. J., Canizares C. R., 1985, *ApJ*, 288, 703
- Kuiper L., Hermsen W., den Hartog P. R., Collmar W., 2006, *ApJ*, 645, 556
- Kuiper L., Hermsen W., Mendez M., 2004, *ApJ*, 613, 1173
- Kumar H. S., Safi-Harb S., 2010, *ApJ*, 725, L191
- Lamb F. K., Pethick C. J., Pines D., 1973, *ApJ*, 184, 271
- Levin L. et al., 2010, *ApJ*, 721, L33
- Levin L. et al., 2012, *MNRAS*, 422, 2489
- Lewin W. H. G., van Paradijs J., van den Heuvel E. P. J., 1995, *Cambridge Astrophysics Series*, 26
- Livingstone M. A., Scholz P., Kaspi V. M., Ng C.-Y., Gavriil F. P., 2011, *ApJL*, 743, L38
- Malofeev V. M., Malov O. I., Teplykh D. A., 2007, *Ap&SS*, 308, 211
- Manchester R. N., Hobbs G. B., Teoh A., Hobbs M., 2005, *VizieR Online Data Catalog*, 7245
- Mazets E. P., Golenetskij S. V., Guryan Y. A., 1979, *Soviet Astronomy Letters*, 5, 641

- McGarry M. B., Gaensler B. M., Ransom S. M., Kaspi V. M., Veljkovic S., 2005, *ApJ*, 627, L137
- McLaughlin M. A. et al., 2006, *Nature*, 439, 817
- Mereghetti S., 2008, *A&Ar*, 15, 225
- Mereghetti S., 2011, *Advances in Space Research*, 47, 1317
- Mereghetti S., 2013, *Brazilian Journal of Physics*, 43, 356
- Mereghetti S. et al., 2006, *ApJ*, 653, 1423
- Mereghetti S., Stella L., 1995, *ApJL*, 442, L17
- Michel F. C., Dessler A. J., 1981, *ApJ*, 251, 654
- Mignani R. P. et al., 2013, *MNRAS*, 429, 3517
- Minter A. H., Camilo F., Ransom S. M., Halpern J. P., Zimmerman N., 2008, *ApJ*, 676, 1189
- Morini M., Robba N. R., Smith A., van der Klis M., 1988, *ApJ*, 333, 777
- Motch C., Pires A. M., Haberl F., Schwobe A., Zavlin V. E., 2009, *A&A*, 497, 423
- Nielbock M., Chini R., Jütte M., Manthey E., 2001, *A&A*, 377, 273
- Norris J. P., Hertz P., Wood K. S., Kouveliotou C., 1991, *ApJ*, 366, 240
- Olausen S. A., Kaspi V. M., 2014, *ApJs*, 212, 6
- Paczynski B., 1992, *Acta Astronomica*, 42, 145
- Page D., 2009, in *Astrophysics and Space Science Library*, Vol. 357, *Astrophysics and Space Science Library*, Becker W., ed., p. 247
- Page D., Geppert U., Weber F., 2006, *Nuclear Physics A*, 777, 497
- Papitto A., de Martino D., Belloni T. M., Burgay M., Pellizzoni A., Possenti A., Torres D. F., 2015, *MNRAS*, 449, L26
- Park S., Hughes J. P., Slane P. O., Burrows D. N., Lee J.-J., Mori K., 2012, *ApJ*, 748, 117

- Pavlov G. G., Kargaltsev O. Y., Sanwal D., Garmire G. P., 2001, *ApJL*, 554, L189
- Pires A. M., Haberl F., Zavlin V. E., Motch C., Zane S., Hohle M. M., 2014, *A&A*, 563, A50
- Pons J. A., Rea N., 2012, *ApJ*, 750, L6
- Pons J. A., Walter F. M., Lattimer J. M., Prakash M., Neuhäuser R., An P., 2002, *ApJ*, 564, 981
- Popov S. B., Pons J. A., Miralles J. A., Boldin P. A., Posselt B., 2010, *MNRAS*, 401, 2675
- Popov S. B., Turolla R., Possenti A., 2006, *MNRAS*, 369, L23
- Posselt B., Neuhäuser R., Haberl F., 2009, *A&A*, 496, 533
- Posselt B., Popov S. B., Haberl F., Trümper J., Turolla R., Neuhäuser R., 2007, *Ap&SS*, 308, 171
- Rappaport S. A., Fregeau J. M., Spruit H., 2004, *ApJ*, 606, 436
- Rea N. et al., 2013, *ApJ*, 775, L34
- Rea N. et al., 2012, *ApJ*, 754, 27
- Rea N. et al., 2007a, *Ap&SS*, 308, 505
- Rea N. et al., 2009, *MNRAS*, 396, 2419
- Rea N. et al., 2007b, *MNRAS*, 379, 1484
- Scholz P., Ng C.-Y., Livingstone M. A., Kaspi V. M., Cumming A., Archibald R. F., 2012, *ApJ*, 761, 66
- Schwope A. D., Hambaryan V., Haberl F., Motch C., 2005, *A&A*, 441, 597
- Schwope A. D., Schwarz R., Greiner J., 1999, *A&A*, 348, 861
- Shakura N. I., Sunyaev R. A., 1973, *A&A*, 24, 337
- Sterne T. E., 1933, *MNRAS*, 93, 117

- Tam C. R., Gavriil F. P., Dib R., Kaspi V. M., Woods P. M., Bassa C., 2008, *ApJ*, 677, 503
- Tetzlaff N., Neuhäuser R., Hohle M. M., Maciejewski G., 2010, *MNRAS*, 402, 2369
- Thompson C., Duncan R. C., 1995, *MNRAS*, 275, 255
- Tian W. W., Leahy D. A., 2008, *ApJ*, 677, 292
- Tiengo A., Esposito P., Mereghetti S., 2008, *ApJ*, 680, L133
- Tiengo A. et al., 2009, *MNRAS*, 399, L74
- Tiengo A., Mereghetti S., 2007, *ApJ*, 657, L101
- Tiengo A. et al., 2010, *ApJ*, 710, 227
- Turolla R., 2009, in *Astrophysics and Space Science Library*, Vol. 357, *Astrophysics and Space Science Library*, Becker W., ed., p. 141
- Turolla R., Zane S., Pons J. A., Esposito P., Rea N., 2011, *ApJ*, 740, 105
- van den Heuvel E. P. J., Heise J., 1972, *Nature Physical Science*, 239, 67
- van Kerkwijk M. H., Kaplan D. L., 2008, *ApJ*, 673, L163
- van Kerkwijk M. H., Kaplan D. L., Pavlov G. G., Mori K., 2007, *ApJ*, 659, L149
- Vasisht G., Gotthelf E. V., 1997, *ApJ*, 486, L129
- Viganò D., Pons J. A., 2012, *MNRAS*, 425, 2487
- Viganò D., Rea N., Pons J. A., Perna R., Aguilera D. N., Miralles J. A., 2013, *MNRAS*, 434, 123
- Vrba F. J. et al., 1996, *ApJ*, 468, 225
- Walter F. M., Eisenbeiß T., Lattimer J. M., Kim B., Hambaryan V., Neuhäuser R., 2010, *ApJ*, 724, 669
- Walter F. M., Lattimer J. M., 2002, *ApJ*, 576, L145
- Wang Z., Chakrabarty D., Kaplan D. L., 2006, *Nature*, 440, 772

Zane S., Cropper M., Turolla R., Zampieri L., Chierigato M., Drake J. J., Treves A., 2005, *ApJ*, 627, 397

Zeldovich Y. B., Guseynov O. H., 1966, *ApJ*, 144, 840

Zel'dovich Y. B., Novikov I. D., 1965, *Soviet Physics Uspekhi*, 7, 763